

THESIS ON CHEMISTRY AND CHEMICAL ENGINEERING G40

Modification of Ammonium Nitrate Fertilizer

IRINA KLIMOVA

TUT
PRESS

TALLINN UNIVERSITY OF TECHNOLOGY
Faculty of Chemical and Materials Technology
Laboratory of Inorganic Materials

This dissertation was accepted for the defense of the degree of Doctor of Philosophy in Chemistry and Materials Technology on October 13, 2014

Supervisor: Senior Research Scientist, Tiit Kaljuvee, Laboratory of Inorganic Materials, Tallinn University of Technology

Co-Supervisor: Senior Research Scientist, Professor Andres Triikkel, Laboratory of Inorganic Materials, Tallinn University of Technology

Opponents: Professor Vilma Petkova, Department "Natural Science", New Bulgarian University, Bulgaria

Senior Research Scientist, PhD Valli Loide, Estonian Crop Research Institute, Estonia

Defense of the thesis: December 4, 2014, at 10:30 Lecture hall: U04-307
Tallinn University of Technology, Ehitajate tee 5,
Tallinn

Declaration:

I hereby declare that this doctoral thesis, my original investigation and achievement, submitted for the doctoral degree at Tallinn University of Technology, has not previously been submitted for doctoral or equivalent academic degree.

Irina Klimova



This work has been partially supported by graduate school "Functional materials and technologies" receiving funding from the European Social Fund under project 1.2.0401.09-0079 in Estonia.

Copyright: Irina Klimova, 2014
ISSN 1406-4774
ISBN 978-9949-23-689-3 (publication)
ISBN 978-9949-23-690-9 (PDF)

KEEMIA JA KEEMIASTEHNIIKA G40

Ammooniumnitraatväetise modifitseerimine

IRINA KLIMOVA

TABLE OF CONTENTS

LIST OF PUBLICATIONS.....	7
THE AUTHOR'S CONTRIBUTION.....	8
LIST OF ABBREVIATIONS AND SYMBOLS.....	9
INTRODUCTION.....	10
1. LITERATURE REVIEW.....	12
1.1. Ammonium nitrate (AN).....	12
1.1.1. Problems related to soil fertilization with AN.....	12
1.1.2. Crystal structures and transitions of solid phase modifications of AN.....	12
1.1.3. Thermal decomposition of AN.....	13
1.1.4. Stabilization of AN with additives.....	15
1.2. Limestones (L) and dolomites (D).....	16
1.3. Granulation.....	17
1.4. Summary of the literature review.....	19
2. OBJECTIVES OF THE THESIS.....	20
3. MATERIALS AND METHODS.....	21
3.1. Thermodynamic calculations.....	21
3.2. Thermal analysis.....	21
3.3. Granulation.....	22
3.4. Agrochemical tests.....	24
4. RESULTS AND DISCUSSION.....	25
4.1. Reactions between AN and $\text{CaCO}_3/\text{CaMg}(\text{CO}_3)_2$	25
4.1.1. Equilibrium in the multi-component system based on AN and CaCO_3	25
4.1.2. Equilibrium in the multi-component system based on AN and $\text{CaMg}(\text{CO}_3)_2$	25
4.1.3. Impact of CuSO_4 , H_3BO_4 and MnO_2 on the reactions between AN and CaCO_3 or $\text{CaMg}(\text{CO}_3)_2$	28
4.1.4. Summary of the thermodynamic analysis.....	30
4.2. Thermal behavior of AN + L/ D systems.....	32
4.2.1. Thermal behavior of ground and prilled AN.....	32
4.2.2. The effect of L/ D on the thermal behavior of AN.....	36
4.2.3. Effect of H_3BO_3 , CuO and MnO_2 on the thermal behavior of blends of AN and L/ D.....	41
4.2.4. Summary of the thermal analysis.....	42
4.3. Covering of AN prill with L/ D powder in the disk granulator.....	43
4.3.1. Granules growth.....	43
4.3.2. Granules strength.....	46
4.3.3. Resistance of the covered granules to temperature fluctuations.....	48
4.3.4. Summary of the covering process.....	48
4.3.5. Recommendations for design of the covering process.....	48
4.4. Agrochemical testing of the designed fertilizer granules.....	49

5. CONCLUSIONS	51
REFERENCES	52
ABSTRACT	60
KOKKUVÕTE	61
APPENDIX A: ORIGINAL PUBLICATIONS	63
APPENDIX B: CURRICULUM VITAE	109

LIST OF PUBLICATIONS

The thesis is based on four original articles published in peer-reviewed international research journals (hereafter referred to as *Paper I – Paper IV*).

- I **I. Klimova**, T. Kaljuvee, L. Törn, V. Bender, A. Trikkel and R. Kuusik, "Interactions of ammonium nitrate with different additives: thermodynamic analysis," *Journal of Thermal Analysis and Calorimetry*, vol. 105, no. 1, pp. 13-26, 2011.
- II T. Kaljuvee, **I. Rudjak**, E. Edro and A. Trikkel, "Heating rate effect on the thermal behavior of ammonium nitrate and its blends with limestone and dolomite," *Journal of Thermal Analysis and Calorimetry*, vol. 97, no. 1, pp. 215-221, 2009.
- III **I. Rudjak**, T. Kaljuvee, A. Trikkel and V. Mikli, "Thermal behaviour of ammonium nitrate prills coated with limestone and dolomite powder," *Journal of Thermal Analysis and Calorimetry*, vol. 99, no. 3, pp. 749-754, 2010.
- IV **I. Klimova**, T. Kaljuvee and R. Kuusik, "Investigation of Limestone Powder Layering onto Ammonium Nitrate Prills in Disc Granulator," *Journal of Materials Science and Engineering*, vol. 5A, pp. 151-159, 2014.

Copies of these publications are included in APPENDIX A.

Other closely related publications by the author

I. Klimova, T. Kaljuvee, V. Mikli and A. Trikkel, "Influence of some lime-containing additives on the thermal behavior of urea," *Journal of Thermal Analysis and Calorimetry*, vol. 111, no. 1, pp. 253-258, 2013.

I. Klimova, V. Mikli and T. Kaljuvee, "Upgrading the crush strength of ammonium nitrate prills by coating with limestone or dolomite powder," *Proceedings of the 6th International Granulation Workshop & Conference*, Sheffield, UK, no. 75, 2013.

THE AUTHOR'S CONTRIBUTION

- I** The author conducted part of the thermodynamic calculations, participated in interpreting the data, wrote part of the manuscript and presented the results at the 21st International Conference on Chemical Thermodynamics (ICCT-2010).

- II** The author participated in experimental work, data processing and in the discussion of the results.

- III** The author participated in the planning of experiments, conducted part of the experimental work, and participated in the analysis of results and manuscript writing.

- IV** The author planned the experimental work, conducted the experiments and analysis of samples, interpreted the data obtained and wrote the manuscript.

LIST OF ABBREVIATIONS AND SYMBOLS

Abbreviations

AN	Ammonium nitrate
AN _I	The AN solid phase modification with cubic crystalline lattice
AN _{II}	The AN solid phase modification with tetragonal crystalline lattice
AN _{III}	The AN solid phase modification with α -rhombohedral crystalline lattice
AN _{IV}	The AN solid phase modification with β -rhombohedral crystalline lattice
AN _V	The AN solid phase modification with tetragonal crystalline lattice
AN _{VI}	The AN sixth solid phase modification
B/P	Binder to powder mass ratio in %
CRH	Critical relative humidity
D	Dolomite
DSC	Differential scanning calorimetry
DTA	Differential thermal analysis
DTG	Differential thermogravimetry
FTIR	Fourier Transform Infrared Spectroscopy
L	Limestone
P/S	Powder to seeds (AN prills) mass ratio, [-]
R	Reaction
RH	Relative humidity in %
SEM	Scanning electron microscope
SSA	Specific surface area in $\text{m}^2 \cdot \text{g}^{-1}$
TG	Thermogravimetry

Symbols

A	Pre-exponent factor in s^{-1}
E	Activation energy in $\text{kJ} \cdot \text{mol}^{-1}$
$N\%$	Nitrogen content of fertilizer granules in %
ΔH	Heat of reaction in $\text{kJ} \cdot \text{mol}^{-1}$
ΔG_T	Gibbs free energy changes in $\text{kJ} \cdot \text{mol}^{-1}$
α	The degree of conversion, [-]
γ	Inclination angle of the disk to the horizontal plane in $^\circ$
d	Inner diameter of the disk in m
n, n_{cr}	Speed and critical speed of disk rotation in rpm

INTRODUCTION

Ammonium nitrate (AN) is used in agriculture as a source of nitrogen for crop production. Advantages of this fertilizer are a high nitrogen content (~35%) and a relatively simple manufacturing technology. Disadvantages of AN are caking of fertilizer particles/ granules due to the high hygroscopicity of the salt and transitions between the α -rhombohedral (AN_{III}) and the β -rhombohedral (AN_{IV}) modifications of its solid phase at close to the ambient temperature during storage, and acidification of the fertilized soil due to the high solubility of the salt. Also AN is a strong oxidizer, which can spontaneously decompose in the absence of a heat sink and ventilation during storage and transport, and in the presence of organic substances, which can lead to an explosion. For this reason, fertilizers containing a high percentage of AN are classified as dangerous in many national and international regulations. Restrictions on the use of pure AN as a fertilizer are imposed in a number of countries. The problem of obtaining AN and the products based on it with increased thermal stability is very relevant in the world today.

One possible way to increase the thermal stability of AN is to reduce the total nitrogen content of the fertilizer by introducing an inert additive, internal or external. This can be done by prilling of premixed melted AN and the additive or by covering AN prills with a powdered substance in a drum or disk granulator. The latter method allows wide variation of the content of the nitrogen in the fertilizer. Also, covering of the fertilizer granules should strengthen these.

As excessive nitrogen fertilization causes soil mineralization and acidification, and also over 40% of Estonian soils are acidic [1] and require continuous liming for preservation of their cultivation value, it is reasonable to use limestone (L) and/ or dolomite (D), deposits of which are abundant in Estonia, as well as in many other countries, as a modification additive to AN.

In this thesis, the possibility of obtaining an eco-friendly and thermally stable AN and L/ D based fertilizer is considered. The work begins with a theoretical justification of the compatibility of these materials and ends with the development of the technology for producing the developed fertilizer granules.

ACKNOWLEDGMENTS

First of all I would like to express my sincere gratitude to my supervisors, Senior Research Scientist Tiit Kaljuvee and Professor Andres Trikkel, for their excellent supervision, constant guidance, support, invaluable comments and contribution to this work, as well as their encouragement and patience throughout the course of this research, which helped in my personal development.

I wish to thank my colleagues at the Laboratory of Inorganic Materials for their valuable assistance and consultations, especially leading research scientist Rein Kuusik and Helle Ehala. I am also grateful to Dr. Mai Uibu for SSA measurements

and her help with the performance of porosity measurements and Dr. Valdek Mikli for the performance of SEM measurements.

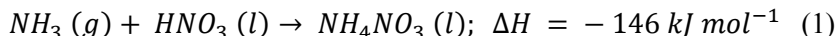
Financial support for the research was provided by the Estonian Ministry of Education and Research (SF0140082s08) and the Estonian Science Foundation (G7548). This work has been partially supported by graduate school “Functional materials and technologies” receiving funding from the European Social Fund under project 1.2.0401.09-0079 in Estonia. Additionally, this research was supported by the DoRa and Kristjan Jaak programs.

Finally, I owe great gratitude to my family and friends, whose support and encouragement has helped me greatly throughout my studies.

1. LITERATURE REVIEW

1.1. Ammonium nitrate (AN)

Ammonium nitrate (AN) is a compound with the chemical formula NH_4NO_3 and is a white crystalline solid at room temperature and standard pressure. It is produced by the neutralization of nitric acid with ammonia, as shown in reaction (1) [2, 3, 4]:



1.1.1. Problems related to soil fertilization with AN

Nitrogen fertilizers are absolute leaders in the use of the mineral fertilizers in agriculture all over the world, and the consumption in 2011 was on the level of 108 million tons [5]. Nitrogen (N) plays the main role in the metabolic and genetic processes of plants and is therefore required in greater amounts than any other mineral nutrient [6, 7, 8, 9]. Consumption of AN in the agricultural sector is second only to the consumption of urea.

The main problem with soil fertilization with AN is its high solubility in water (118 g AN/ 100 g H_2O at 0 °C [10]). As shown in [6, 7, 11, 12, 13, 14], only 20-70% of the applied N, depending on the N fertilizing rates and time, crop type, climate conditions, tillage practices, etc., are taken up by the plant. A high level of applied N fertilizers leads to massive losses of nitrogen through the various mechanisms, including leaching, volatilization of ammonia (NH_3), denitrification leading to gaseous emissions of nitrogen dioxide (N_2O), nitric oxide (NO), and dinitrogen (N_2), and fixation in soil organic matter [6, 7, 15]. Excessive use of N fertilizers in crop production can cause degradation of water quality. The agricultural sector is the largest contributor to the non-point source nitrate (NO_3^-) pollution of surface and ground waters [12, 16]. N fertilization has been shown to have a significant decreasing effect on soil pH and on the concentration of microelements in soil and in crops [17]. Long-term N additions also have an impact on the composition and function of the soil microbial community by decreasing active fungal biomass and fungal/bacterial ratios [18, 19].

The demand for nitrogen fertilizers is forecast to grow annually [20]; therefore redoubling of the above-mentioned negative effects is inevitable in the coming years.

1.1.2. Crystal structures and transitions of solid phase modifications of AN

AN has seven temperature-dependent solid state phases at normal pressure [21, 22, 23, 24, 25, 26, 27, 28, 29]. The cubic (AN_I), tetragonal (AN_{II}), α -rhombohedral (AN_{III}), β -rhombohedral (AN_{IV}) and tetragonal (AN_V) forms of AN are stable in the temperature ranges from 125.2 to 169 °C, 84.2 to 125.2 °C, 32.3 to 84.2 °C, -16.8 to 32.3 °C and -103 to -16.8 °C, respectively. The crystal structure of the sixth and seventh solid states of AN (AN_{VI} is stable at -170 to -103 °C) is unknown.

Problems of granulated AN fertilizer storage are associated with the solid phase transition $AN_{IV} \leftrightarrow AN_{III}$ [30, 31], which occurs at close to ambient temperature

(32°C–55°C), because it involves significant reorganization in the AN crystalline lattice and density ($\rho(\text{AN}_{\text{IV}}) = 1.72 \text{ g cm}^{-3}$ to $\rho(\text{AN}_{\text{III}}) = 1.66 \text{ g cm}^{-3}$, *Fig. 1*) and a drastic change of crystal volume ($\sim 3.84\%$). Repeated cycling between these phases leads to cracking and caking of AN granules [32, 31], and to subsequent decreases in the thermal stability of AN, because of better access to the oxygen from the air [21, 28]. From the technological point of view, avoiding the $\text{AN}_{\text{IV}} \leftrightarrow \text{AN}_{\text{III}}$ transition in the manufacturing, storing and handling of AN has a great importance considering the practical applications. There is a preference for the metastable transition $\text{AN}_{\text{IV}} \leftrightarrow \text{AN}_{\text{II}}$, that can occur at 50 °C [28, 29]. The transition temperatures of AN depend on several factors as well as on their interrelationships [33, 34, 35, 36, 37, 38, 39]. Repeated heating–cooling cycles cause significant unpredictable changes to the transition paths [24, 28, 35, 36].

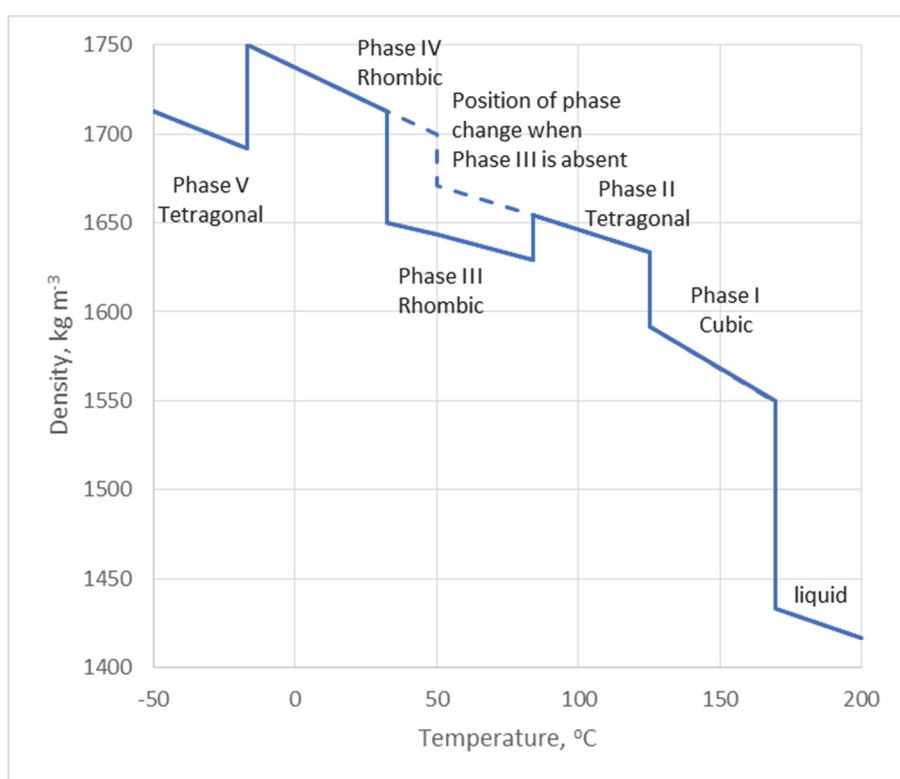


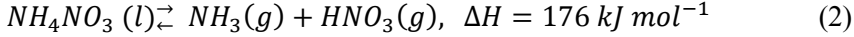
Figure 1. Density of AN as a function of temperature [40]

1.1.3. Thermal decomposition of AN

AN melts at 169.6 °C and immediately begins to decompose. The path of thermolysis of AN depends on various factors such as the size of the substance particles and the purity of the substance, rate of heating, and the presence of foreign substances [21, 22, 24, 23, 25, 26, 27, 28, 29, 33]. During the thermal decomposition

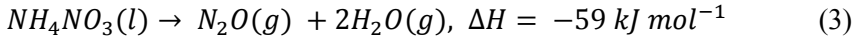
of AN, four chemical species (NH_3 , HNO_3 , N_2O and H_2O) are formed in the gas phase, as shown in reactions (2) and (3). In an open system, the decomposition process of AN is endothermic. These gases may further react with one another to form water, N_2 , and NO in a closed system, and the complete decomposition process is an exothermic process [41].

It is generally accepted that the thermolysis of AN is initiated by the vaporization of melted AN accompanied by an endothermic proton transfer reaction, leading to the formation of ammonia and nitric acid, as shown in reaction (2) [37, 38, 39]:

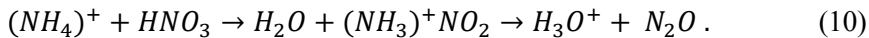
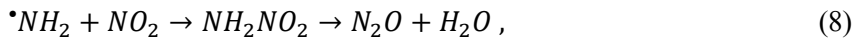
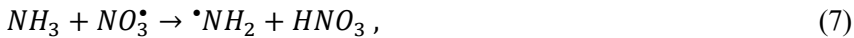
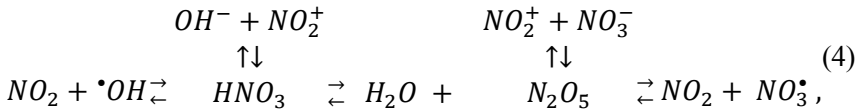


Reaction (2) is reversible; AN can be detected in a gas phase or in the form of crystals on a cold surface [42].

Simultaneously with reaction (2) in the temperature range from 200 to 300 °C, irreversible decomposition of AN to water and nitrous oxide occurs (R. 3) [21]:



Transition pathways from reaction (2) to (3) follow an ionic mechanism (R. 4 – 10 [43]) and the rate-determining factor of this process is the formation rate of nitronium ions (NO_2^+) [44, 45], which depends on the rate of HNO_3 decomposition, and on the features of the secondary reactions with the participation of NH_3 and HNO_3 .



Acidic species, such as ammonium ion, hydronium ion or nitric acid, increase the rate of AN decomposition dramatically (R. 4). Above 290 °C, a free radical decomposition mechanism dominates and homolysis of nitric acid forming N_2O and hydroxyl radical (HO^\bullet) is the rate-controlling step (R. 5, 8) [44, 45].

The kinetics of the thermolysis of AN has also been extensively studied, using a variety of techniques under different experimental conditions [46, 47, 48, 49]. It is generally accepted that the overall decomposition reaction of AN is described by the first order reaction kinetics. Activation energies ranging widely from 83.8 to 206.9 kJ mol^{-1} are suggested in the literature.

1.1.4. Stabilization of AN with additives

While designing granules of AN-containing fertilizers, it is necessary to take into account the strong oxidation properties, risks of an explosion, $AN_{III} \leftrightarrow AN_{IV}$ phase transition at a close to ambient temperature, high hygroscopicity, and low mechanical resistance of pure granules.

1.1.4.1. Additives for reducing the hygroscopicity of AN

AN is a highly hygroscopic salt (the critical relative humidity (CRH) of pure AN is 62.7% at 25 °C [50]), and its hygroscopicity increases with temperature, as the CRH of pure AN decreases from 75.8% at 10 °C to 48.4% with increase of the ambient temperature to 50 °C [50]. The salt moistens and deliquesces in summer storage conditions of 25–40 °C and 40–90% of relative humidity (RH) [51]. This tends to cause the fertilizer to consolidate into hard masses or cakes, which are unusable for mechanical distribution devices.

Slackening of the atmospheric water vapor absorption can be achieved by using internal additives or by covering the granules of AN with hydrophobic materials [52, 53, 54].

External additives include finely divided powders such as talc, kaolin, L and D, which cover the AN granules uniformly, reducing the incidence and extent of the coalescence of the fertilizer granules. Another external group of additives is surfactants, which form a hydrophobic film around the fertilizer granules. For example, AN may be provided with a thin surface covering of a sulfonated aromatic dye. Paraffin wax, polyolefin wax and mineral oils also tend to form a hydrophobic film [51, 55, 56].

Mixes of AN with Na^+ , PO_4^{3-} and Mg^{2+} ions in the form of salts are less hygroscopic than pure AN [55]. Combinations of AN with $CO(NH_2)_2$, $Ca(NO_3)_2$, $NaNO_3$, NH_4Cl , $NH_4H_2PO_4$ are more hygroscopic [50]. The value of the CRH is independent of the weight ratio of solid components in equilibrium with the saturated solution of a multicomponent fertilizer [50, 52]. But the presence in the mixture of small amounts of highly soluble components that form an eutectic can alter the CRH appreciably when slight variations occur in moisture content or temperature [50, 52]. The CRH of AN – L/ D mixture is not influenced by $CaCO_3$ due to the insolubility of the latter in water, but as Latham and Geissler [52] showed, the CRH of AN – L mixture decreases with increase of the concentration of $Ca(NO_3)_2$.

1.1.4.2. Phase stabilizing additives

Laboratory studies of the $AN_{IV} \leftrightarrow AN_{III}$ and $AN_{IV} \leftrightarrow AN_{II}$ phase transitions have indicated that the transition path and temperature depend strongly on the thermal history [57, 58, 59], moisture content [60, 61], method of crystallization [31, 36, 57, 62], grain size [57] and presence of impurities [21, 63, 64, 65].

The inclusion of some impurities such as K^+ ions (in the form of salts) [66] or some metal oxides (CuO , ZnO and Al_2O_3 [25, 32]) in AN particles can lead to

suppression of $\text{AN}_{\text{IV}} \leftrightarrow \text{AN}_{\text{III}}$ transition or to an increase of the temperature of this transition.

1.1.4.3. Additives for decreasing the explosive potential of AN

Pure AN is stable and relatively safe at ambient temperature and pressure. However, it is a strong oxidizer and supports and accelerates combustion, providing oxygen in the process. Contact of AN with combustible materials, or the presence of such impurities (even in fairly low percentages), and the presence of a source of heat lead to the hazard of an auto-ignition and explosion.

Several catastrophic explosions (attributed to both careless handling and criminal intent or terrorist bombings) that have led to a serious loss of life have raised widespread calls for AN to be banned in Europe [3]. On September 21, 2001, an explosion of 390–450 tons of substandard AN in Toulouse, France produced a seismic wave of 3.4 on the Richter scale and cost over 30 lives [3]. Most recently, on April 17, 2013, a fire at a fertilizer storage and distribution facility in West, Texas, resulted in the detonation of AN fertilizer stored at the facility, killing 15 people [67]. Several countries (e.g. Germany and the Republic of Ireland) have already banned the use of AN outright and stipulate the addition of other chemicals to try to reduce its explosive potential [21, 23, 68].

As a fertilizer, AN is often mixed with a number of additives. A low temperature, ionic decomposition pathway for AN suggests acidic additives to destabilize and basic ones to stabilize the thermal decomposition [21, 23, 45].

The following impurities destabilize AN and are therefore incompatible with it: chlorates, hypochlorites, chlorides, permanganates, sulfur and several finely divided metal powders, such as zinc (Zn), cadmium (Cd), copper (Cu), magnesium (Mg), and lead (Pb), organic substances, such as oils, fats and waxes, hay and straw, paper and finely divided wood material [3, 21, 23, 29, 68].

In [21] sodium (Na^+), potassium (K^+), ammonium (NH_4^+), magnesium (Mg^{2+}) and calcium (Ca^{2+}) sulfates (SO_4^{2-}), phosphates (PO_4^{3-}) and carbonates (CO_3^{2-}), plus some high N-content organic compounds such as carbamide (H_2NCONH_2) were studied as possible additives to enhance AN's thermal stability. Most of these additives shifted the maximum decomposition exotherm of the AN towards higher temperatures. The best stabilizing effect on AN was obtained with carbonate additives and of these CaCO_3 stabilized AN better than Na_2CO_3 , K_2CO_3 or MgCO_3 .

1.2. Limestones (L) and dolomites (D)

The best natural sources of CaCO_3 and MgCO_3 are L and D. Calcite and aragonite, which are different crystal forms of CaCO_3 , are the main minerals of L. Dolomite is composed of $\text{CaMg}(\text{CO}_3)_2$. Both are quite soft rocks, with a hardness of 3.5–4.

L and D, formed in different geological epochs, are found on almost all continents except Australia. The seam thickness varies from a few centimeters to hundreds of meters. Estonia is also rich in L and D resources, with over 660 million

m³ of active and passive L deposits, and about 280 million m³ of active and passive D deposits [69]. These resources vary, depending on the deposit, in their content of the main components – calcite and dolomite, and also in the content of mineral impurities.

Due to their wide distribution, ease of processing and chemical properties, L and D are mined and used in larger amounts than other minerals, second only to sand and gravel deposits. In the agricultural sector, mixes of L and D powder are usually applied to raise the soil pH to the ideal range for crop production, create an environment for healthy functioning of microbes, and increase the levels of Ca²⁺ and Mg²⁺ in the soil.

1.3. Granulation

Solid mineral fertilizers can be powdered, granular or prilled. Compared to powder, granular and prilled fertilizer has better flowability and it is non-caking.

Prilling is a method of producing spherical particles from molten solids, strong solutions or slurries. Liquid drops cool and solidify as they fall through a rising ambient air stream. There is no agglomeration, so the size distribution of the drops determines that of the product. The process is widely used in the fertilizer industry for making AN, Ca(NO₃)₂, urea and compound NPK fertilizers.

Granulation is the set of physical and physico-chemical processes of converting small particles into larger agglomerates or granules of a certain spectrum of size, form and structure [70]. Granulation methods can be divided into two subcategories: dry granulation and wet granulation. Dry granulation relies on the physical forces of pressure and compaction to produce granules [71], whereas wet granulation makes use of a liquid binder to bind the particles together.

In wet granulation, the agglomeration is initiated by the wetting action of the binder, which acts as a bonding agent and leads to the formation of physical-mechanical boundaries between particles. Coalescence of the particles results in the growth of granules. This process is also called layering in the case where small particles coalesce with much larger particles [72]. The compacting of a structure of a granule in time occurs under the influence of the forces of interaction between particles and in their movement in a dense tumbling layer [70].

The forces acting on the particles in the growth and formation of granules are [70, 73, 74, 75]:

- Capillary and surface tension forces at the interface between the solid and liquid phases;
- Adhesion forces arising from surface tension forces at the liquid/ air interface and hydrostatic suction pressure in the liquid bridge;
- Attractive forces between the solid particles (van der Waals, magnetic and electrostatic forces);

- Bonding forces, caused by the formation of solid bridges formed through chemical reactions, crystallization, binder solidification and sintering during drying;
- Forces due to mechanical interlocking between solid particles.

The intensity of the compaction of the granule structure can be defined as the sum of all kinds of bonds between particles.

The relative importance of these bonding forces in determining the strength of a granule will vary from case to case. In some types of granules, some of these forces will not exist. For the layering process, the tension strength of the bonds in a granule is caused by the action of capillary adsorption cohesive forces and tension in the film contacts [70]. This fact can be explained by the existence of liquid binder and the formation of crystal bridges.

The main stages of granule formation through wet granulation are [75, 76, 77, 78, 79, 80, 81, 82]:

- *Nucleation*, where the liquid binder disperses as a film on the particle surfaces and nuclei are formed as a result of successful collision and bridging of the wetted fine particles;
- *Consolidation and growth*, where collisions between two granules, granules and feed powder, or a granule and the equipment lead to granule compaction and growth, through the coalescence or layering mechanism. The layering of powder particles onto a sphere-shaped granule is similar to the process of snowball formation, i.e. rolling about a larger particle in a slightly wetted mass;
- *Breakage*, where granules break due to impact, wear or compaction in the granulator.

During granulation, the domination of the stages changes until equilibrium between them is reached. In the case of the granules covering, the homogeneity of the covered granule size can be obtained by suppression of the nucleation stage, and by the elimination of the granule growth by coalescence.

The amount of liquid added needs to be very well controlled in the wet granulation process as over-wetting will cause over-granulation, producing large and hard granules that are not compressible, whilst under-wetting will lead to soft and fragile granules.

The wet granulation process can be performed in many types of equipment, such as a high shear mixer, fluidised bed and rotating drum and disks. Enlargement of the granule size through the layering of fine particles can be conducted in tumbling granulators, such as a disk or a drum.

Particles are set in motion by the tumbling actions caused by the balance between gravity and the centrifugal forces in both kinds of granulator [83]. In contrast to a drum granulator, the use of a disk granulator allows the granulation process to be observed visually.

A typical disk granulator consists of an inclined rotating disk with a rim to hold the tumbling granules. Powder is continuously fed to the disk and wetted by the continuously sprayed binder liquid. A covering of feed powder builds up on the disk to form the base on which the mass rolls. The thickness of this layer is controlled by a scraper. Disk granulators are extensively used in fertilizer granulation, because the construction and size (up to a few meters in diameter) of the device is suitable for continuous granulation and very high throughputs (up to tens of tons per hour). In contrast to the drum granulator, there is a size classification at the output, therefore recycling of undersize and crushed oversize granules is at a minimum level.

A key operating parameter for the disk granulator is the critical speed (speed at which a granule is just held stationary on the rim of the disk by centripetal force alone) [83], which can be calculated by Eq. 11:

$$n_{cr} = \sqrt{\frac{g \sin \gamma}{2 \pi^2 d}}, \quad (11)$$

where g is free-fall acceleration, γ is the inclination angle of the disk to the horizontal plane and d is the disk inner diameter.

Optimum operating conditions for granulation of any powder depend on the physical and chemical properties of the material, liquid and solid phases feeding intensities, etc.

1.4. Summary of the literature review

The main problems related to the use of AN fertilizer are its thermal instability, tendency to caking and the negative impact on the environment.

Considering the positive influence of reactive-grade Ca- and Mg-carbonates on the thermal characteristics of AN, natural L and D would be suitable minerals for mixing with AN in order to get eco-friendly and thermally stable AN-based fertilizer with good storage properties.

Covering of AN prills on the disk granulator is the most convenient for the production of AN – L/ D based fertilizer granules, because this method allows a very high throughput capacity and convenient control of the process.

2. OBJECTIVES OF THE THESIS

Considering the results of the literature review, the objectives of the current study have been formulated as follows:

- To justify the compatibility of AN and L/ D of the main Estonian deposits, and to clarify the effect of L/ D additive on the thermal stability of AN.
- To develop the basics of the process and recommendations for control of the main technological parameters for the production of AN – L/ D based fertilizer granules at a pilot scale installation.

In order to achieve these tasks, the following steps will be taken.

- Thermodynamic analysis of the different reactions between AN and Ca and Mg carbonates will be carried out to elucidate the influence of the main components of L/ D on the thermal decomposition of AN and to elucidate the influence of some micronutrient additives (Cu, B and Mn-containing substances can be added to the granules to enrich the fertilizer with microelements that are in deficit in Estonian soils [84]) on the reactions between AN(s) and CaCO₃(s) or AN(s) and CaMg(CO₃)₂(s).
- Thermal analysis of the systems of AN and L/ D, in which the latter is applied as both an internal and an external additive to AN, will be performed to clarify the influence of the additives on the temperatures and the pathway of the phase changes, as well as the mechanism and kinetics of the decomposition of AN. Also, the influence of some additives on the thermal characteristics of the blends of AN with L/ D will be analyzed.
- Developed granules of the fertilizer will be tested for their suitability for use in soil fertilization.
- The AN prills covering process in the disk granulator will be investigated in order to develop recommendations for the design of the production process of AN – L/ D based fertilizer granules.

3. MATERIALS AND METHODS

3.1. Thermodynamic calculations

Thermodynamic analysis of different reactions between AN and CaCO_3 , MgCO_3 and $\text{CaMg}(\text{CO}_3)_2$, with or without the presence of $\text{CuSO}_4(\text{s})$, $\text{H}_3\text{BO}_3(\text{s})$ and $\text{MnO}_2(\text{s})$, was carried out to elucidate the influence of the main components of L/ D on the thermal decomposition of AN (*Paper I*). The temperature dependency of Gibbs free energy changes ΔG_T and the equilibrium composition of the reaction products were calculated for a set of reactions (*Paper I: Table 1*) in the temperature range of 273–2073 K. Calculations were based on the initial amount of 2 moles of AN. Initial amounts of $\text{CaCO}_3/\text{CaMg}(\text{CO}_3)_2$ varied from 0.2 to 2.1 mol. The initial amounts of $\text{CuSO}_4(\text{s})$, $\text{H}_3\text{BO}_3(\text{s})$ and $\text{MnO}_2(\text{s})$ were 0.01, 0.05 and 0.5 mol. Thermodynamic analysis was performed using the HSC Chemistry for Windows software package [85].

3.2. Thermal analysis

Thermal analysis of the samples consisting of AN and L/ D (from different Estonian deposits) was performed to clarify the influence of the additives on the temperatures and the pathway of the phase changes, as well as the mechanism and kinetics of decomposition of AN (*Paper II, III*). The chemical composition of the L and D samples is presented in Table 1.

Table 1. Chemical composition and specific surface area (SSA) of the L and D samples

Sample	Chemical composition [mass %]							SSA, $\text{m}^2 \text{g}^{-1}$
	CaO	MgO	CO ₂	I. R.	Al ₂ O ₃	Fe ₂ O ₃	Ssulphate	
Karinu (L)	52.92	2.76	38.98	0.80	1.72	0.08	0.04	0.74
Võhmuta (L)	53.17	1.50	39.87	1.33	1.81	0.04	0.06	1.56
Vasalemma (L)	54.22	1.14	40.45	0.75	1.50	0.09	0.09	0.89
Kurevere (D)	29.04	24.40	41.87	3.17	0.64	0.21	0.09	1.70
Anelema (D)	28.85	26.63	40.81	5.83	0.84	0.14	0.10	2.44

In order to obtain the influence of L/ D as an internal additive on the thermal behavior of AN (*Paper II*), samples of blends of ground AN prills with 5, 10 and 20 mass% of L/ D powder were prepared. Blends of AN, L/ D and $\text{CuO}/\text{H}_3\text{BO}_3/\text{MnO}_2$ with the mol ratio of the components $\text{AN}:\text{CaCO}_3/\text{CaMg}(\text{CO}_3)_2:\text{CuO}/\text{H}_3\text{BO}_3/\text{MnO}_2$ of 2:1:0.05 and 2:1:0.5 were prepared to obtain the effects of CuO , H_3BO_3 and MnO_2 (purified reagents) on the thermal behavior of AN blends with L/ D.

In order to obtain the influence of L/ D as an external additive on the thermal behavior of AN (*Paper III*), samples of AN prills covered with the L/ D powder were prepared (Figs. 2, 3). The mole ratio of components $\text{AN}:\text{CaCO}_3/\text{CaMg}(\text{CO}_3)_2$ in covered granule was 2:1.

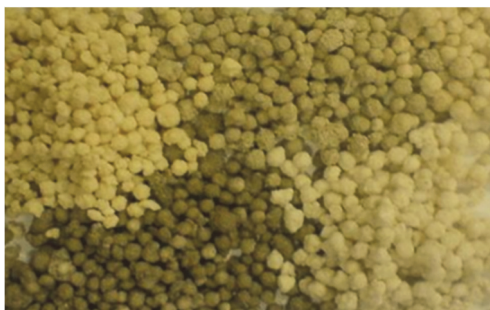


Figure 2. AN prills covered with L (light) and D (dark) powder

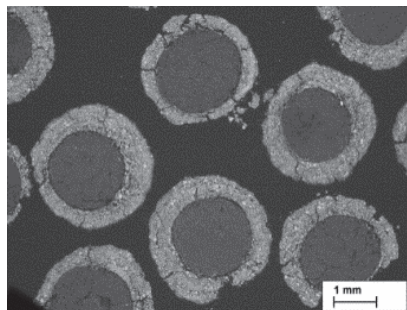


Figure 3. SEM pictures of the cross-sections of AN prills covered with L powder

The thermal behavior of the prepared samples was studied using Setaram Labsys 2000 equipment (capable of simultaneously recording mass loss (TG), differential mass loss (DTG) and a differential thermal analysis curve (DTA)) coupled to an Interspec 2020 Fourier Transform Infrared Spectrometer (FTIR) by a transfer line for identification of the compounds emitted during thermal treatment of the samples.

Experiments were carried out under dynamic heating conditions from 30 °C to 900 °C at heating rates of 2, 5, 10, or 20 °C min⁻¹ in a stream of synthetic air (80% of Ar and 20% of O₂) with a flow rate of 120 mL min⁻¹.

FTIR measurements were recorded in the 4000–600 cm⁻¹ region with a resolution of 4 cm⁻¹ and the average of four scans was registered. To identify gaseous compounds, the Bio-Rad (Sadler) KnowItAll search program and Gases & Vapours Database (code GS) and The Aldrich Library of FTIR Spectra were used.

Calculations of the kinetic parameters (activation energy $E(\alpha)$ and pre-exponential factor $A(\alpha)$) of the decomposition of the samples (*Paper II, III*) were based on the differential isoconversional method of Friedman [86]. After baseline correction and normalization, the TG signals obtained by different heating rates were processed with the AKTS Advanced Thermokinetics software [87].

3.3. Granulation

Investigation of AN prills covering with L/ D powder was carried out in a lab-scale disk granulator (*Paper IV*). It was equipped with a scraper bar and a pin (*Fig. 4*) for removing excessive build-up on the disk walls and for providing better mixing of the tumbling mass. The diameter of the disk was 0.5 meters and the rim height was 0.1 m.

To observe the effect of the variables of the granulation process (time, binder to powder and powder to seeds mass ratios) and equipment (rotation speed and angle of inclination of the disk) on the layering effectiveness and on the quality of the produced granules, a set of experiments designed to study one factor at a time were carried out (for details see *Paper IV, Materials and Methods Section*).



Figure 4. Photo of the disk granulator

For greater clarity, the close-cut fraction (2.00–2.24 mm) of AN prills was used in the experiments. L and D samples were ground to a particle size $<160 \mu\text{m}$ ($\text{SSA} = 1.93 \text{ m}^2 \text{ g}^{-1}$). To prevent dissolution of AN prills during the granulation process, a saturated solution of AN (47.3 wt%, density = 1.086 g cm^3) was used as a binder liquid.

Sieve analysis of the dried (3 hours in an oven at $60 \text{ }^\circ\text{C}$) granulate of each set of experiments was performed. The weight mean diameter (d_w) of the 2.0–5.0 mm fraction in each sample was calculated as follows:

$$d_w = \sum_{i=1}^{k-1} \left[\frac{w_i \times d_i}{w_t} \right], \quad (12)$$

where k is the number of sieves with the aperture size between 5.0 and 2.0 mm, w_i is the mass of granules remaining on each sieve, w_t is the total mass of the dried granulate, and d_i is the mean diameter of the collecting sieve and the one above.

The effectiveness of powdered material consumption was calculated as follows:

$$\eta = \left(1 - \frac{w_1}{P} \right) \times 100, \quad (13)$$

where w_1 is the mass of particles smaller than 1.0 mm and P is the mass of powder feed.

At least 30 granules in the size range of 3.0–4.0 mm from each set of experiments were tested for crush strength by applying slowly increasing pressure (0.10 mm s^{-1}) on the individual granule placed on a scale. The average strength and the coefficient of its variation, i.e. the ratio of standard deviation and mean value, were calculated.

To investigate the resistance of the granules produced to daily temperature fluctuations, hermetically packed granules were placed in a climate chamber, where the temperature was changed every 2 hours from $15 \text{ }^\circ\text{C}$ to $35 \text{ }^\circ\text{C}$ and vice versa. The change in the granules crush strength was checked at stated time intervals.

3.4. Agrochemical tests

Outdoor pot-experiments were performed to test the suitability of the produced granules (AN prills covered with L/ D) for use in soil fertilization. The impact of the fertilizer on soil acidity and on the yield of rye-grass was investigated.

Pots were filled with field-moist soil and the seeds of one-year rye-grass 'Barspectria' were planted in the soil. When the plants were three weeks old, nitrogen fertilizer was added as a surface fertilizer. Three types of fertilizer were used in this test: pure AN (34%N), AN covered with L powder (20%N), and AN covered with D powder (20%N). The norm 80 kgN ha⁻¹ of fertilizer was added onto the first and second meadow.

To determine the influence of the first fertilizing on each sample, one was left without refertilization. In order to determine the effect of the second fertilization, the crops were collected from all three samples. Because of the small amount of rainfall and high temperature in 2010, the plants were additionally watered from under the pot during the period from the end of June until the middle of August, in order to prevent the plants withering.

Crops were collected once every three weeks and dried inside the thermostat. After the crops were collected, the pH_{KCl} of the soil was measured in the Agricultural Research Centre of Estonia.

4. RESULTS AND DISCUSSION

4.1. Reactions between AN and CaCO₃/ CaMg(CO₃)₂

4.1.1. Equilibrium in the multi-component system based on AN and CaCO₃

Considering the thermodynamic calculations (*Paper I*), in the equilibrium system based on AN and CaCO₃ the most probable Ca-containing compounds are CaO(s), CaO₂(s), Ca(OH)₂(s), and Ca(NO₃)₂(s), while N-containing gases are NO, NO₂, N₂O and N₂, and C-containing gas is CO₂ (*Fig. 5a*). At constant temperature and while keeping the amount of AN at the level of 2 moles, the equilibrium amount of gaseous compounds does not depend on the amounts of CaCO₃/ CaMg(CO₃)₂, which varied from 0.2 to 2.1 mol. The content of NO₂(g) and N₂O(g) differs by 6–7% compared to their content in the equilibrium system based only on AN; thereby, the NO(g) content does not differ at all (*Paper I: Table 2*).

Comparison of the temperature dependence of Gibbs free energy changes ΔG_T calculated for a set of reactions (*Paper I: Table 1: R. 1-25*) in the temperature range of 273–2073 K shows that reactions between AN and CaCO₃ with the simultaneous formation of NO(g) and N₂(g) are more probable than those where only NO(g) is formed. The formation of NO₂(g) or N₂O(g) becomes more probable at a higher content of the simultaneous formation of N₂(g) in the system. Most of these reactions are already probable at room temperature or over 373–473 K (*Fig. 6*).

For example, if simultaneous formation of NO(g) and N₂(g) is assumed (*Paper I: Table 1: R. 5, 7, 9*), the formation of Ca(OH)₂(s), CaO(s) and CaO₂(s) is already probable at room temperature, but if only the formation of NO(g) is assumed (*Paper I: Table 1: R. 4, 6, 8*), the Ca(OH)₂(s) and CaO(s) formation becomes probable at temperatures over 600–620 K and CaO₂(s) over 850 K. The formation of N₂O(g) (with or without N₂(g)) and the solid phases like Ca(OH)₂, CaO and CaO₂ is already probable at room temperature and is definitely more probable than the explosive decomposition of AN. The formation of Ca(NO₃)₂(s) together with NO(g)/ NO₂(g)/ N₂O(g) and N₂(g) (*Paper I: Table 1: R. 3, 11, 19*) is probable at temperatures over 1000 K, but with N₂(g) alone (*Paper I: Table 1: R. 2*), over 473 K (*Fig. 6*).

4.1.2. Equilibrium in the multi-component system based on AN and CaMg(CO₃)₂

In comparison to equilibrium systems based on AN and CaCO₃, in equilibrium systems based on AN and CaMg(CO₃)₂ there are also Mg-containing compounds, such as MgO(s), MgO₂(s), Mg(OH)₂(s), and Mg(NO₃)₂(s) (*Fig. 5b*). The reaction between AN and CaMg(CO₃)₂ with formation of Ca(OH)₂(s) and Mg(OH)₂(s) (*Paper I: Table 1: R. 64*) and with simultaneous formation of NO(g), becomes probable at $T > 590$ K; with simultaneous formation of NO₂(g) and N₂(g) (*Paper I: Table 1: R. 82*) it becomes probable at temperatures over 373 K; and with simultaneous formation of N₂O(g) (with or without N₂(g)) (*Paper I: Table 1: R. 99, 100*) it is also probable at room temperature, in the same way as the respective reactions between AN and CaCO₃.

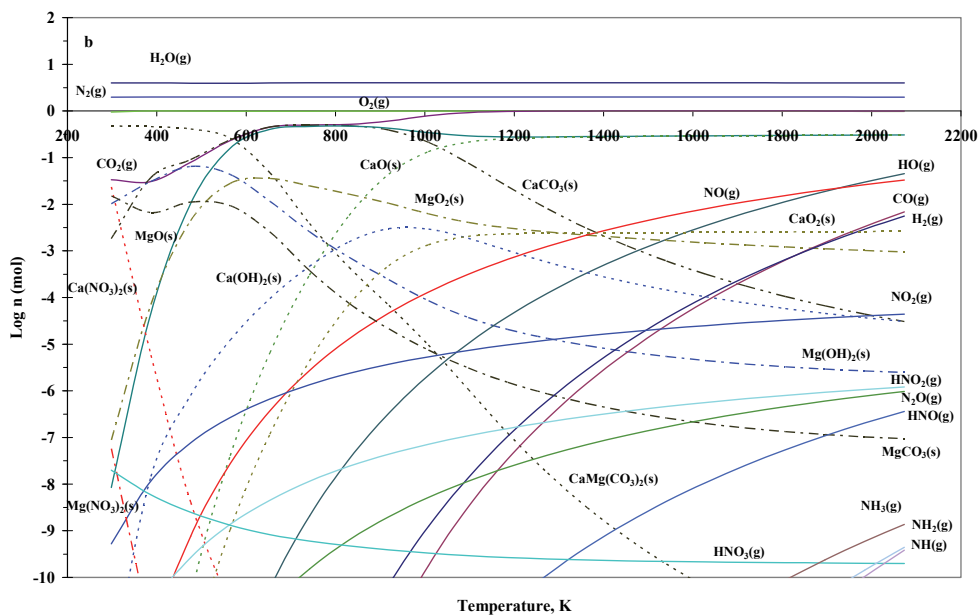
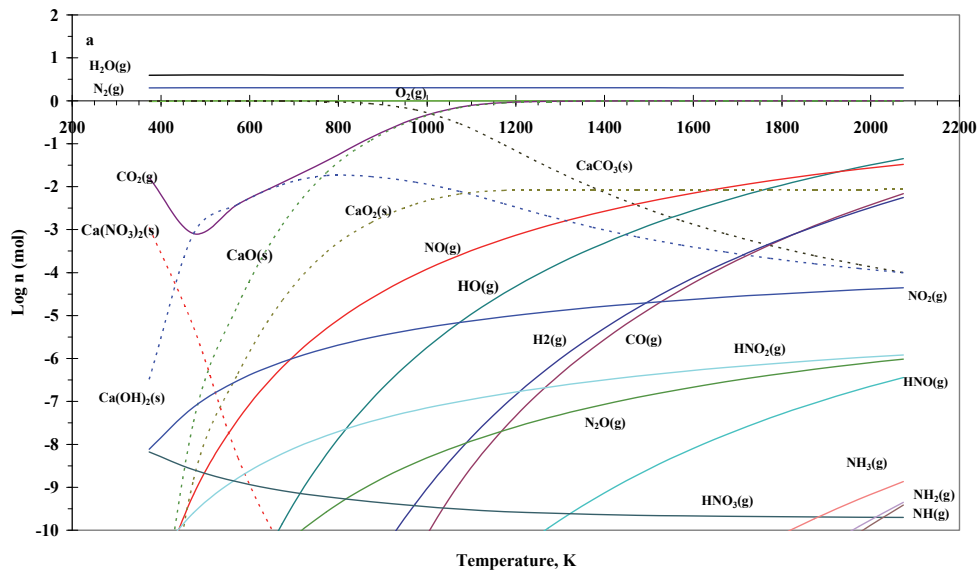


Figure 5. Temperature dependencies of equilibrium amounts of compounds in the system (a) $2\text{NH}_4\text{NO}_3 - \text{CaCO}_3$ and (b) $2\text{NH}_4\text{NO}_3 - 0.5\text{CaMg(CO}_3)_2$

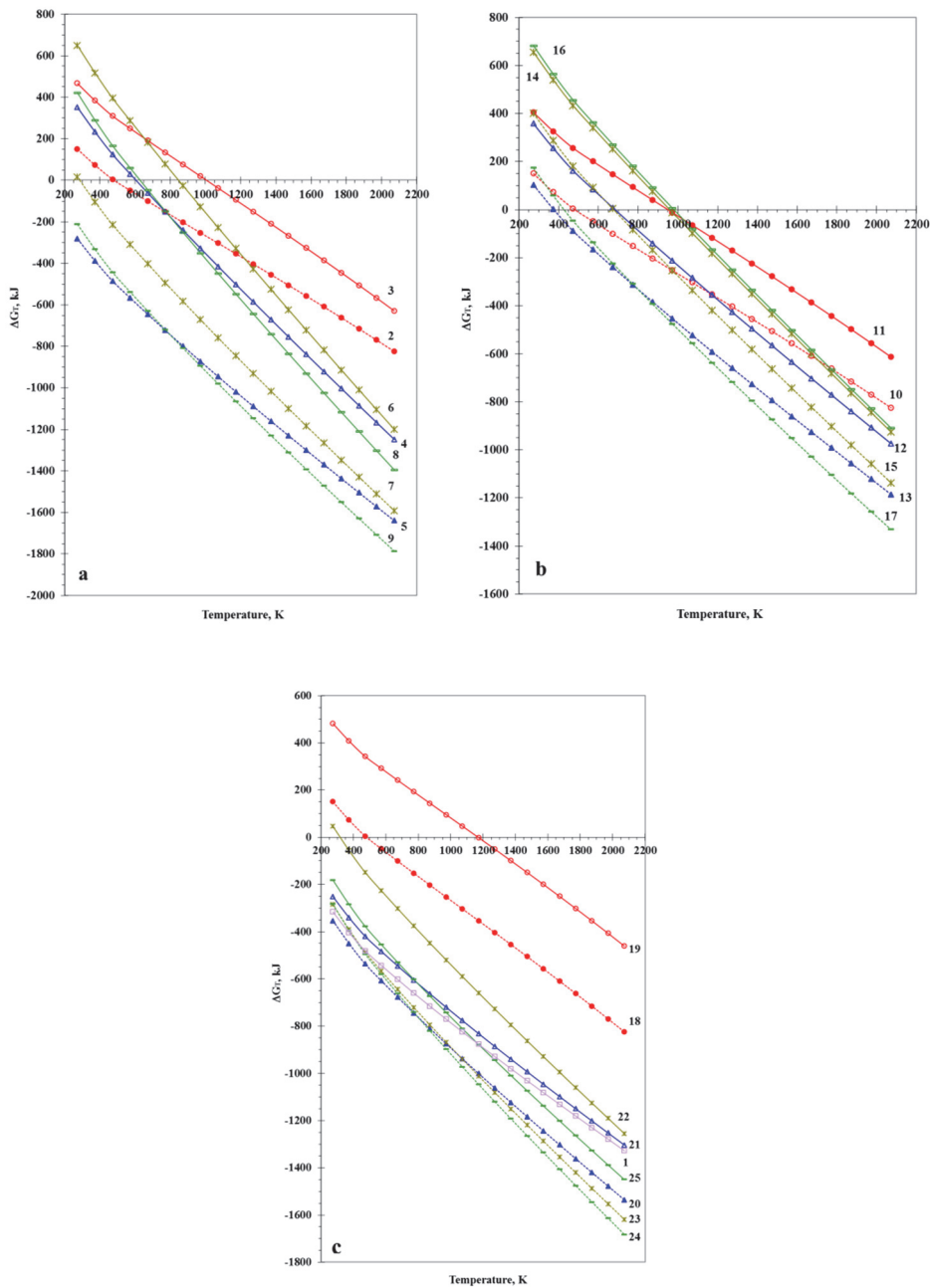


Figure 6. Temperature dependence of Gibbs free energy changes ΔG_T in the $2\text{NH}_4\text{NO}_3 - \text{CaCO}_3$ system with the formation of (a) NO (Paper I: Table 1: R. 2–9), (b) NO_2 (Paper I: Table 1: R. 10–17), and (c) N_2O (Paper I: Table 1: R. 1, 18–25)

The formation of CaO(s)/ CaO₂(s) and MgO(s)/ MgO₂(s) with simultaneous formation of NO(g) (*Paper I: Table 1: R. 65, 66*) or with simultaneous formation of NO₂(g) and N₂(g) (*Paper I: Table 1: R. 83, 84*) or with formation of N₂O(g) (*Paper I: Table 1: R. 101, 104*) or N₂O(g) and N₂(g) (*Paper I: Table 1: R. 102, 103*) becomes probable at temperatures that are 20–50 K lower compared with the respective reactions between AN and CaCO₃.

The formation of Ca(NO₃)₂(s) and Mg(NO₃)₂(s) with simultaneous formation of some or a combination of NO(g)/ NO₂(g)/ N₂O(g)/ N₂(g) (*Paper I: Table 1: R. 63, 67, 80, 81, 97, 99*) is probable at temperatures that are 30–60 K higher than in the case of the respective reactions between AN and CaCO₃ (*Paper I: Fig. 4*).

4.1.3. Impact of CuSO₄, H₃BO₄ and MnO₂ on the reactions between AN and CaCO₃ or CaMg(CO₃)₂

The influence of CuSO₄(s), H₃BO₃(s) and MnO₂(s) additives in the initial amount ≤ 0.05 mol/ 2 mol of AN on the reactions between AN(s) and CaCO₃(s) or AN(s) and CaMg(CO₃)₂(s) is very slight. In the amounts ≥ 0.5 mol/ 2 mol of AN, these additives have a significant effect on the above-mentioned reactions. In the studied systems with CuSO₄(s) additive, the compounds that are most likely to form are SO₂(s) and CuO(s). In the case of the studied systems with H₃BO₃(s) or MnO₂(s) additives – HBO(g) or MnO(s) are most probable, respectively (*Paper I: Table 3, Fig. 2*).

CuSO₄(s) additive in an amount of 0.5 mol in the 2AN + CaCO₃ and 2AN + 0.5CaMg(CO₃)₂ systems shifted the probability of the formation of NO(g), Ca(NO₃)₂(s) and Mg(NO₃)₂(s) (*Paper I: Table 1: R. 26, 68*) 70–80 K towards higher temperatures (*Paper I: Table 1: R. 3, 63*), but the formation of Ca(OH)₂(s) and Mg(OH)₂(s), CaO₂(s) and MgO₂(s), CaO(s) and MgO(s) and NO(g) (*Paper I: Table 1: R. 27–29, 69–71*) shifted 20–50 K towards lower temperatures (*Table 2*).

The temperature of the probable NO₂(g) formation is increased, depending on the solid compound formed, by 40–100 K towards higher temperatures (*Table 2, Paper I: Table 1: R. 30–33, R 85–88*).

Formation of N₂O(g) together with Ca(OH)₂(s) and Mg(OH)₂(s), CaO₂(s) and MgO₂(s), and CaO(s) and MgO(s) (*Paper I: Table 1: R. 35–37; 106–108*) is probable at room temperature. However, these reactions are less probable (ΔG_T values are higher) compared to those in the system without the CuSO₄ additive (*Table 2, Paper I: Table 1: R. 21, 22, 25; 99, 101, 104*). The temperature at which the reactions of the formation of Ca- and Mg-nitrates in the additive-containing system become probable is moved in the 2AN–0.5CaMg(CO₃)₂ system by 130 K (*Paper I: Table 1: R. 98, 105*) and in the 2AN–CaCO₃ system by 170 K (*R. 19, 34*) towards lower temperatures—respectively, to 1050 K and 1000 K (*Table 2*).

H₃BO₃(s) additive in an amount of 0.5 mol in the 2AN–CaCO₃ and 2AN–0.5CaMg(CO₃)₂ systems practically does not influence the temperature dependencies of ΔG_T of the reactions between AN and CaCO₃(s) or CaMg(CO₃)₂(s) with the formation of solid Ca- and Mg-nitrates and NO(g) (*Table 2, Paper I: Table*

1: R. 3, 38, 63; 72), but in the cases of formation of $\text{Ca(OH)}_2(\text{s})$ and $\text{Mg(OH)}_2(\text{s})$, $\text{CaO}_2(\text{s})$ and $\text{MgO}_2(\text{s})$, and $\text{CaO}(\text{s})$ and $\text{MgO}(\text{s})$ (Paper I: Table I: R. 4, 6, 8, 40–42, 64–66, 73–75), the temperatures at which these reactions become probable decrease by 170–260 K (Table 2).

Table 2. The influence of CuSO_4 , H_3BO_3 and MnO_2 additive on the change in temperature ($\pm \Delta T$, K) at which reactions in the $2\text{AN}-\text{CaCO}_3$ and $2\text{AN}-0.5\text{CaMg}(\text{CO}_3)_2$ system become thermodynamically probable

System	N-containing gaseous compound		
	NO	NO ₂	N ₂ O
2AN + CaCO₃ + 0.5CuSO₄			
Ca(NO ₃) ₃	+80	+80	-170
Ca(OH) ₂	-30	+90	At room temperature, but less probable than without the additive
CaO ₂	-50	+50	
CaO	-30	+50	
2AN + 0.5CaMg(CO₃)₂ + 0.5CuSO₄			
Ca(NO ₃) ₃ , Mg(NO ₃) ₃	+70	+90	-130
Ca(OH) ₂ , Mg(OH) ₂	-20	+100	At room temperature, but less probable than without the additive
CaO ₂ , MgO ₂	-40	+70	
CaO, MgO	-30	+40	
2AN + CaCO₃ + 0.5H₃BO₃			
Ca(NO ₃) ₃	+10	-30	-470
Ca(OH) ₂	-190	+30	At room temperature, but less probable than without the additive
CaO ₂	-260	-20	
CaO	-180	-20	
2AN + 0.5CaMg(CO₃)₂ + 0.5H₃BO₃			
Ca(NO ₃) ₃ , Mg(NO ₃) ₃	0	-30	-460
Ca(OH) ₂ , Mg(OH) ₂	-180	+20	At room temperature, but less probable than without the additive
CaO ₂ , MgO ₂	-210	0	
CaO, MgO	-170	-20	
2AN + CaCO₃ + 0.5MnO₂			
Ca(NO ₃) ₃	+80	+320	-200
Ca(OH) ₂	-70	+70	At room temperature, but less probable than without the additive
CaO ₂	-70	+50	
CaO	-60	+40	
2AN + 0.5CaMg(CO₃)₂ + 0.5MnO₂			
Ca(NO ₃) ₃ , Mg(NO ₃) ₃	+70	+70	-160
Ca(OH) ₂ , Mg(OH) ₂	-70	+40	At room temperature, but less probable than without the additive
CaO ₂ , MgO ₂	-60	+60	
CaO, MgO	-70	+50	

The formation temperatures of $\text{NO}_2(\text{g})$ are decreased by 20–30 K (*Paper I: Table I: R. 11, 14, 16, 43, 45–46, 80, 83–84, 89, 91, 92*) except for the reactions with Ca- and Mg-hydroxides formation (*Paper I: Table I: R. 12, 40, 82, 90*), in which case these are shifted 20–30 K towards higher temperatures (*Table 2*).

The $\text{N}_2\text{O}(\text{g})$, and $\text{Ca}(\text{NO}_3)_2(\text{s})$, and $\text{Mg}(\text{NO}_3)_2(\text{s})$ formation in the presence of $\text{H}_3\text{BO}_3(\text{s})$ can take place at 700 K (*Paper I: Table I: R. 47*) instead of 1170 K (*Paper I: Table I: R. 19*) in the 2AN– CaCO_3 system and at 750 K (*Paper I: Table I: R. 109*) instead of 1210 K (*Paper I: Table I: R. 98*) in the 2AN–0.5CaMg(CO_3)₂ system (*Table 2*). The formation of the other solid phases studied can occur at room temperature (*Paper I: Table I: R. 48–50; 110–112*), but these reactions are less probable compared to those in the system without the boron additive (*Table 2, Paper I: Table I: R. 21–22, 25; 99, 101, 104*).

MnO₂(s) additive in an amount of 0.5 mol in the 2AN– CaCO_3 and 2AN–0.5CaMg(CO_3)₂ systems moves the temperatures of $\text{NO}(\text{g})$ formation together with $\text{Ca}(\text{NO}_3)_2(\text{s})$ and $\text{Mg}(\text{NO}_3)_2(\text{s})$ 70–80 K in the direction of higher temperatures (*Paper I: Table I: R. 3, 51, 63; 76*) and with $\text{Ca}(\text{OH})_2(\text{s})$ and $\text{Mg}(\text{OH})_2(\text{s})$; $\text{CaO}_2(\text{s})$ and $\text{MgO}_2(\text{s})$; $\text{CaO}(\text{s})$ and $\text{MgO}(\text{s})$ 60–70 K towards lower temperatures (*Paper I: Table I: R. 52–54; 77–79*) compared to the temperatures without manganese dioxide additive in the system (*Table 2, Paper I: Table I: R. 4, 6, 8; 64–66*).

The temperature of the probable formation of $\text{NO}_2(\text{g})$ simultaneously with $\text{Ca}(\text{NO}_3)_2(\text{s})$ and $\text{Mg}(\text{NO}_3)_2(\text{s})$ as the solid products is increased by up to 320 K and 70 K, respectively, (*Paper I: Table I: R. 11, 55, 80, 93*) and with the formation of the other solid phases under consideration by 40–70 K towards higher temperatures (*Table 2, Paper I: Table I: R. 12, 14, 16, 56–58, 82–84, 94–96*).

In the presence of the additive, the temperature of the probable formation of $\text{N}_2\text{O}(\text{g})$ and Ca- and Mg-nitrates(s) is shifted by 160 K in the 2AN–0.5CaMg(CO_3)₂ system (*Paper I: Table I: R. 98, 113*) and by 200 K in the 2AN– CaCO_3 system (*Paper I: Table I: R. 19, 59*) in the direction of lower temperatures—from 1170 to 970 K and from 1210 to 1050 K, respectively (*Table 2*). $\text{Ca}(\text{OH})_2(\text{s})$ and $\text{Mg}(\text{OH})_2(\text{s})$; $\text{CaO}_2(\text{s})$ and $\text{MgO}_2(\text{s})$; $\text{CaO}(\text{s})$ and $\text{MgO}(\text{s})$ can form at room temperature (*Paper I: Table I: R. 60–62, 114–116*), but these reactions are also less probable compared to those in the system without MnO_2 additive (*Table 2, Paper I: Table I: R. 21–22, 25; 99, 101, 104*).

4.1.4. Summary of the thermodynamic analysis

- The main compounds that form in the reactions between AN and $\text{CaCO}_3/\text{CaMg}(\text{CO}_3)_2$ are $\text{Ca}(\text{NO}_3)_2(\text{s})/\text{Mg}(\text{NO}_3)_2(\text{s})$, $\text{Ca}(\text{OH})_2(\text{s})/\text{Mg}(\text{OH})_2(\text{s})$, $\text{CaO}_2(\text{s})/\text{MgO}_2(\text{s})$, $\text{CaO}(\text{s})/\text{MgO}(\text{s})$, $\text{NO}(\text{g})$, $\text{N}_2\text{O}(\text{g})$, $\text{NO}_2(\text{g})$, $\text{N}_2(\text{g})$, $\text{CO}_2(\text{g})$, $\text{H}_2\text{O}(\text{g})$ and $\text{H}_2(\text{g})$. In the case of the existence in these systems of $\text{CuSO}_4(\text{s})$, $\text{H}_3\text{BO}_3(\text{s})$ or $\text{MnO}_2(\text{s})$, in addition to the above listed compounds, the formation of $\text{SO}_2(\text{g})$, $\text{CuO}(\text{s})$, $\text{HBO}(\text{g})$ or $\text{MnO}(\text{s})$, respectively, is also highly probable.
- The reactions between AN and $\text{CaCO}_3(\text{s})/\text{CaMg}(\text{CO}_3)_2(\text{s})$ with the formation of $\text{NO}(\text{g})$, $\text{NO}_2(\text{g})$ or $\text{N}_2\text{O}(\text{g})$ with the simultaneous formation of $\text{N}_2(\text{g})$ are more

probable than those without $N_2(g)$ formation and most of these reactions are probable at room temperature or in the temperature region of AN decomposition.

- $CaMg(CO_3)_2(s)$ is more reactive towards AN compared to $CaCO_3$, and the temperatures at which reactions between AN and $CaMg(CO_3)_2(s)$ become probable are lower by 20–50 K compared with reactions between AN and $CaCO_3(s)$.
- $CuSO_4(s)$, $H_3BO_3(s)$ or $MnO_2(s)$ additives in the amount ≤ 0.05 mol in the $2AN + CaCO_3$ and $2AN + 0.5CaMg(CO_3)_2$ systems do not influence the temperature dependencies of ΔG_T of the reactions between AN and $CaCO_3(s)$ or $CaMg(CO_3)_2(s)$. In amounts ≥ 0.5 mol, these additives change the equilibrium and the mechanisms of the reactions between components in the AN – Ca-, Mg-carbonates system, and shift significantly the temperatures at which these reactions are probable.

4.2. Thermal behavior of AN + L/ D systems

4.2.1. Thermal behavior of ground and prilled AN

4.2.1.1. Temperatures of transitions of solid phase modifications of AN

On the DTA curves of the thermal treatment of ground or prilled AN, four endotherms (accompanied with no mass loss on the TG curve) between 30 and 180 °C corresponding to the $AN_{IV} \leftrightarrow AN_{III} \leftrightarrow AN_{II} \leftrightarrow AN_I \leftrightarrow AN_{melt}$ solid phase modifications transitions can be observed (Figure 7, Table 3, Paper III: Fig. 2a).

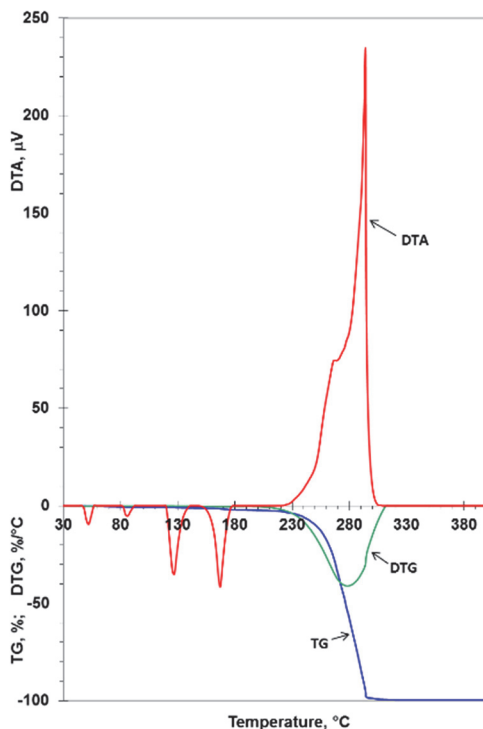


Figure 7. Thermal analysis curves of ground AN at a heating rate of 20 °C min⁻¹

Thermal treatments of AN samples at different heating rates showed that prilled AN is more resistant than ground AN to temperature fluctuations. The increase of the heating rate of ground samples from 2 to 20 °C min⁻¹ has very slight effects (1–4 °C) on the temperatures of the transitions of the solid phases modifications of AN, but in the case of the thermal treatment of prilled samples this effect is significant (16–19 °C), with only the melting point as an exception (Table 3, Paper III: Fig. 2a). At heating rates above 10 °C min⁻¹, the $AN_{IV} \leftrightarrow AN_{III}$ transition in prilled samples occurs at about 10 °C higher temperatures than the temperature of the same transition of ground samples.

Table 3. Temperatures of endoeffects minimums and exoeffects maximums on DTA curves corresponding to the principal transitions of $AN_{IV} \leftrightarrow AN_{III} \leftrightarrow AN_{II} \leftrightarrow AN_I \leftrightarrow AN_{melt}$ and to the decomposition of AN

AN sample	Heating rate [°C/min]	$AN_{IV} \leftrightarrow$ AN_{III} [°C]	$AN_{III} \leftrightarrow$ AN_{II} [°C]	$AN_{II} \leftrightarrow$ AN_I [°C]	$AN_I \leftrightarrow$ AN_{melt} [°C]	AN decompo- sition [°C]	AN decompo- sition [°C]
		Endo- effect	Endo- effect	Endo- effect	Endo- effect	Exo- effect	Endo- effect
Ground	2	53.7	90.4	126.1	165.2	239.6	-
Ground	5	53.6	88.1	126.6	165.9	258.8	-
Ground	10	53.0	86.5	127.1	166.8	262.9	-
Ground	20	52.2	86.4	127.1	167.2	282.9	-
Prilled	2	52.1	90.8	131.4	167.8	226.1	280.1
Prilled	5	55.9	93.5	136.3	168.2	235.4	298.7
Prilled	10	62.7	99.1	140.8	168.4	245.3	308.5
Prilled	20	70.6	106.6	150.3	169.9	257.8	324.3

4.2.1.2. Decomposition of AN

With the thermal treatment of the samples, the decomposition (the thermoeffects on DTA curves are accompanied by almost 100% mass loss on TG curves) of AN follows after its melting. For both kinds of samples the temperatures of the exotherms maximums, corresponding to the exothermic decomposition of AN, are influenced significantly by the heating rate – the higher the heating rate, the higher the temperatures of the extremums of the DTA curves in the decomposition region (Table 3, Paper II: Fig. 2a, Paper III: Fig. 2a). Compared to the ground sample, the maximum of the exotherm of the DTA curve of the prilled sample is at 14–24 °C lower temperatures and the peak of this exotherm is much smaller. But this exotherm of decomposition is followed by a massive endoeffect with a minimum between 280 and 324 °C (Table 3, Paper III: Fig. 2a). Besides, the endoeffect also has two shoulders between 259–290 °C and 273–307 °C, indicating the complicated multi-step character of the decomposition pathway of prilled AN.

FTIR spectra of gaseous compounds that evolved with the thermal treatment of AN prills showed peaks characteristic of NH_3 (967 and 932 cm^{-1}), N_2O (2235 and 2215 cm^{-1}), NO_2 (1630 and 1595 cm^{-1}) and H_2O (bands in the broad ranges 3900–3500 and 1900–1300 cm^{-1}), having the maximum intensity at 250, 280, 300 and 300 °C, respectively (Figs. 8, 9).

The peaks characteristic of NO_2 and NH_3 were 1.5–2 times more intensive than those obtained with thermal treatment of previously ground AN prills. This is in good correlation with the results obtained by Brower *et al.* [44] and Oxley *et al.* [45]

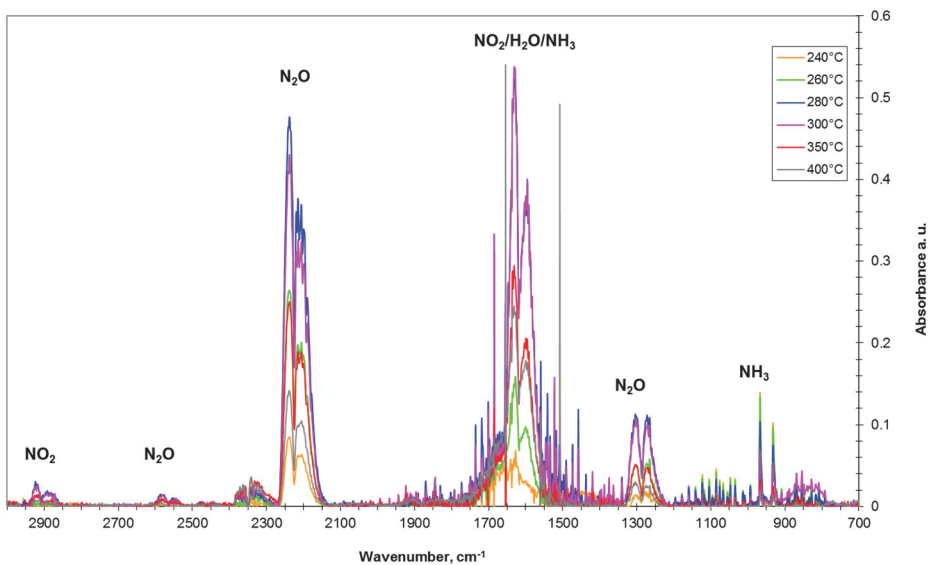


Figure 8. FTIR spectra of gaseous compounds evolved with thermal treatment of neat AN prill at a heating rate of $10\text{ }^{\circ}\text{C min}^{-1}$

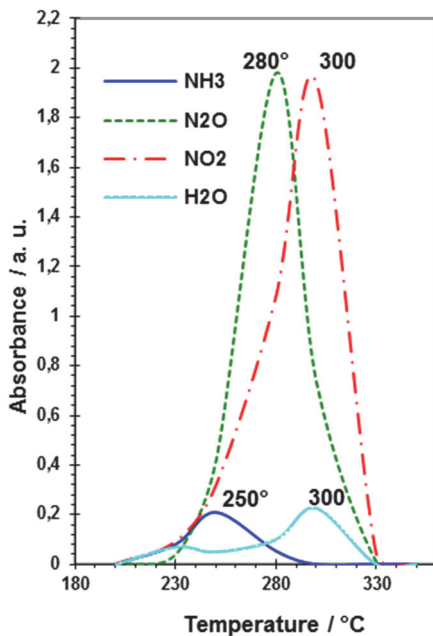
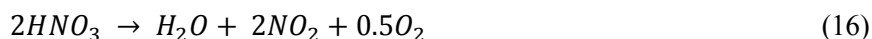


Figure 9. Absorbance profiles of gaseous compounds evolved with thermal treatment of neat AN prill at a heating rate of $10\text{ }^{\circ}\text{C min}^{-1}$

– the decomposition of AN, after dissociation into NH_3 and HNO_3 in the first step, can follow different pathways with the formation of N_2O at lower temperatures ($<280\text{ °C}$) and NO_2 at higher temperatures. AN prills follow preferentially a high-temperature route of AN decomposition. So, the decomposition pathway of AN with thermal treatment can be presented by the following simplified reactions:



The reaction rates and the kinetic parameters $A(\alpha)$ and $E(\alpha)$ for the decomposition of ground and prilled neat AN are presented in *Figures 10* and *11*, respectively.

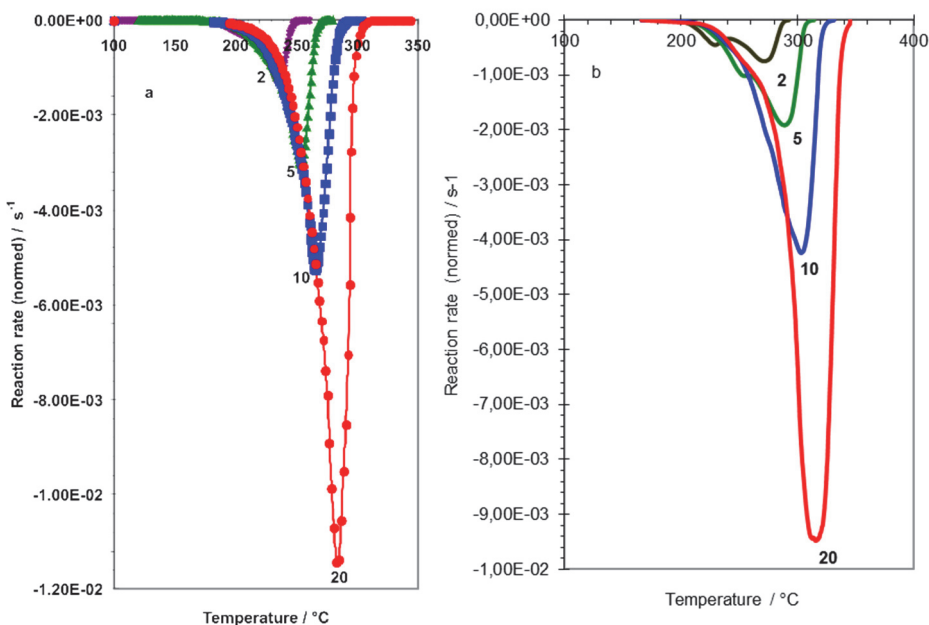


Figure 10. Reaction rate da/dt (DTG, normalized signals) for the decomposition of neat ground AN (a) and for neat AN prills (b) as a function of temperature for different heating rates (The values of the heating rate in °C min^{-1} are marked on the curves)

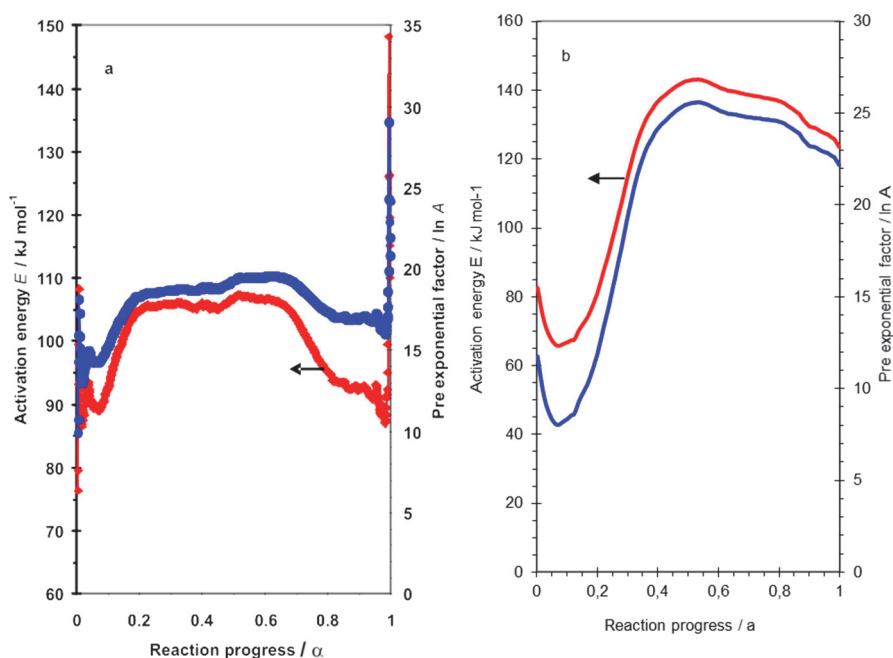


Figure 11. Activation energy E and pre-exponential factor A determined by Friedman analysis as a function of the reaction progress for the decomposition of (a) neat ground AN and (b) neat AN prills

Activation energy $E(\alpha)$ in the range of a conversion (decomposition) degree of $0.1 < \alpha < 0.9$ for ground neat AN varies between 92.4 and 106.8 kJ mole⁻¹ (pre-exponential factor $A(\alpha)$ – from 4.41×10^6 to 2.94×10^8 s⁻¹) (Fig. 11a), this being 0.9–12.9 kJ mole⁻¹ higher than that calculated in [88] by DSC signals ($E(\alpha) = 92.7 \pm 1.2$ kJ mole⁻¹, sample mass ~1 mg) using the isoconversional method for non-isothermal gasification of AN. The $E(\alpha)$ of the decomposition of AN prill varies from 66.7 to 142.7 kJ mole⁻¹ ($A(\alpha)$ – from 4.0×10^3 to 1.2×10^{11} s⁻¹) (Fig. 11b), indicating the more complicated character of the decomposition of AN in prills than in powdered form.

4.2.2. The effect of L/ D on the thermal behavior of AN

4.2.2.1. L/ D powder as an internal additive

- With thermal treatment of the blends of AN with L/ D powder, the temperatures of the minimums of the endotherms on DTA curves, corresponding to the temperatures of the $AN_{IV} \leftrightarrow AN_{III} \leftrightarrow AN_{II} \leftrightarrow AN_I \leftrightarrow AN_{melt}$ phase changes, do not differ from the corresponding temperatures for the neat ground AN samples.
- But, with thermal treatment of the blends (even if the amount of L/ D additives is 5 mass%), an endotherm is observed on the DTA curves in the

temperature interval of 180–280 °C, characterizing the interaction of the AN with CaCO_3 and $\text{CaMg}(\text{CO}_3)_2$ from natural L and D, leading to the formation of $\text{Ca}(\text{NO}_3)_2$ and $\text{Mg}(\text{NO}_3)_2$ (Fig. 12).

- This endoeffect is followed, as a rule, by a more or less intensive exoeffect, which characterizes the decomposition of residual AN (Fig. 12).
- The decomposition exotherm of the AN is shifted towards higher temperatures and the intensities of the exotherms in this case are much smaller than with neat AN (Paper II: Fig. 2). At a heating rate of 2 °C min^{-1} , it is especially weak or indeed absent.
- The endotherms in the temperature range of 350–600 °C characterize the decomposition of the previously formed $\text{Mg}(\text{NO}_3)_2$ and $\text{Ca}(\text{NO}_3)_2$, and the endotherms between 600 and 700 °C – the decomposition of residual carbonates.

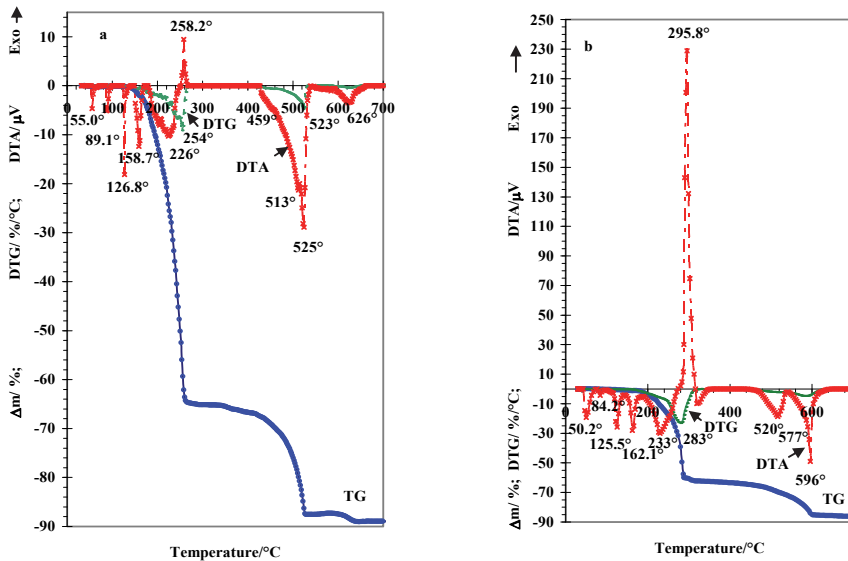


Figure 12. Thermal analysis curves of AN blend with Vasalemma limestone (20 mass%) at a heating rate of (a) 2 °C min^{-1} and (b) 20 °C min^{-1}

4.2.2.2. L/ D powder as external additive

The thermograms of AN prills covered with L/ D powder show quite similar pathways of interactions compared to the thermal behavior of AN blends with L/ D additives (Fig. 13, Table 4):

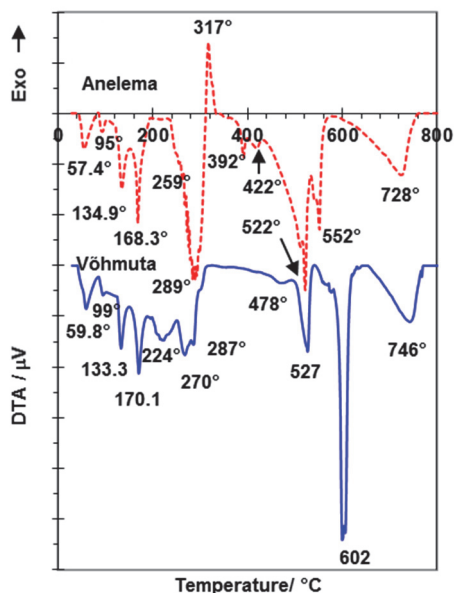


Figure 13. DTA curves of AN prills covered with Anelema dolomite and Vöhmuta limestone powder at a heating rate of $10\text{ }^{\circ}\text{C min}^{-1}$

Table 4. Mass losses of samples (AN prills covered with L/ D, the mole ratio of AN:CaCO₃/ CaMg(CO₃)₂ is 2:1) at thermal treatment (2 and 20 °C min⁻¹, 30 °C - 900 °C)

Sample	T ₁ [°C]	Δm ₁ [%]	T ₂ [°C]	Δm ₂ [%]	T ₃ [°C]	Δm ₃ [%]	T ₄ [°C]	Δm ₄ [%]
AN+Karinu (L) 2 °C min ⁻¹	266.7	-55.0			560.3	-86.0	742.0	-88.1
AN+Karinu (L) 20 °C min ⁻¹	325.8	-61.9			565.1	-68.6	753.0	-89.4
AN+Vöhmuta (L) 2 °C min ⁻¹	280.3	-42.9			528.6	-77.2	731.0	-81.3
AN+Vöhmuta (L) 20 °C min ⁻¹	308.3	-56.0			544.4	-64.3	754.6	-86.9
AN+Vasalema (L) 2 °C min ⁻¹	287.0	-59.0			556.2	-88.4	753.5	-89.3
AN+Vasalema (L) 20 °C min ⁻¹	331.3	-59.9			566.8	-66.7	761.2	-88.0
AN+Kurevere (D) 2 °C min ⁻¹	292.1	-66.5	407.4	-69.7	540.2	-84.0	752.4	-90.0
AN+Kurevere (D) 20 °C min ⁻¹	314.2	-77.0	440.3	-80.8	545.1	-85.4	809.4	-93.6
AN+Anelema (D) 2 °C min ⁻¹	277.7	-65.6	394.2	-68.4	525.9	-79.4	752.0	-88.1
AN+Anelema (D) 20 °C min ⁻¹	308.7	-74.1	436.9	-77.5	544.9	-82.8	797.7	-90.2

- An endothermic peak in the temperature region of 190–340 °C characterizes the interactions between AN and Ca- and Mg-carbonates with the formation of Ca- and Mg-nitrates;
- The subsequent exothermic peak characterizes the decomposition of residual AN;
- Endothermic peaks in the temperature region of 350–650 °C characterize the decomposition of previously formed $\text{Mg}(\text{NO}_3)_2$ and $\text{Ca}(\text{NO}_3)_2$ [89, 90];
- Endothermic peaks on the DTA curves with minimums at 700 and 800 °C correspond to the decomposition of MgCO_3 and CaCO_3 .

FTIR spectra of gaseous compounds that evolved with the thermal treatment of AN prills covered with L/D powder showed peaks characteristic of NH_3 , N_2O , NO_2 , NO , CO_2 and H_2O . The temperatures of the maximum emission of these gases depend on whether the sample contains L or D (Fig. 14, Table 4).

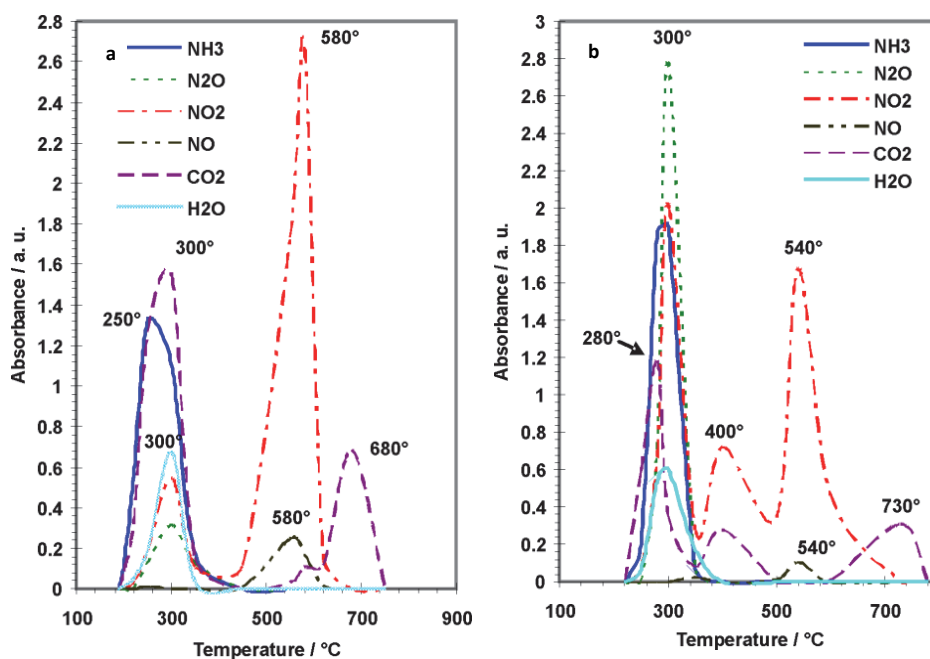
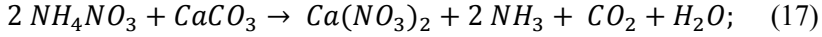


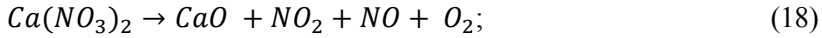
Figure 14. Absorbance profiles of gaseous compounds evolved with thermal treatment of AN prills covered with (a) L and (b) D powder at a heating rate of $10\text{ }^\circ\text{C min}^{-1}$

The decomposition pathway of the thermally treated sample composed of AN and L can be represented by R. 17–19:

- The formation of $\text{Ca}(\text{NO}_3)_2$ at 200–300 °C:



- The decomposition of $\text{Ca}(\text{NO}_3)_2$ at 400–600 °C:

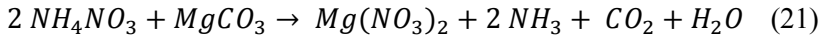
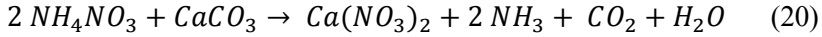


- The decomposition of residual CaCO_3 at 600–800 °C:

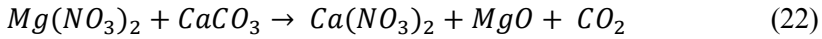


The decomposition pathway of the thermally treated sample composed from AN and D can be represented by R. 20–26:

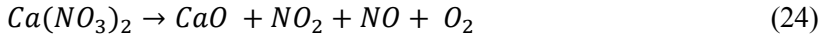
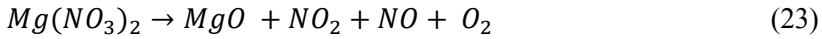
- The formation of $\text{Ca}(\text{NO}_3)_2$ and $\text{Mg}(\text{NO}_3)_2$ at 200–300 °C:



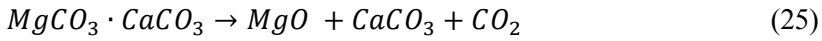
- The interaction of formed $\text{Mg}(\text{NO}_3)_2$ with CaCO_3 at 300–400 °C:



- The decomposition of $\text{Ca}(\text{NO}_3)_2$ and $\text{Mg}(\text{NO}_3)_2$ at 400–600 °C:



- The decomposition of residual MgCO_3 and CaCO_3 at 600–800 °C:



Interactions between AN and Ca- and Mg-carbonates follow a complex reaction mechanism, including steps with both lower and higher activation energies, compared to the decomposition of neat AN.

- Step I – interactions between AN and carbonates with the formation of Ca- and Mg-nitrates and decomposition of unreacted AN, occurring in the low temperature region (depending on the heating rate between 150 and 350 °C).
- Step II – decomposition of nitrates formed in step I. In the case of mixes of AN with D, step II is divided into step IIA (reactions occurring with $\text{Mg}(\text{NO}_3)_2$ in the temperature region of 310–450 °C) and step IIB (decomposition of $\text{Ca}(\text{NO}_3)_2$ in the temperature region of 420–620 °C).

For AN blends with L/ D, as well as for AN prills covered with L/ D powder, the values of $E(\alpha)$ in step I varied much more than for neat AN (*Paper II: Table 2; Paper III: Table 2*).

- For example, the $E(\alpha)$ of step I for AN blended with Vasalemma L varied from 74.7 to 148.8 kJ mole⁻¹ (A in between 4.4×10^4 and 2.6×10^{12} s⁻¹) (*Fig.*

- 15), for AN prills covered with Vasalemma L – from 85.5 to 119.2 kJ mole⁻¹ (A in between 2.4×10^8 and 8.0×10^8 s⁻¹).
- The $E(\alpha)$ of step I for AN blended with Kurevere D varied from 30.2 to 125.5 kJ mole⁻¹ (A in between 5.5×10^9 and 9.7×10^9 s⁻¹) and for AN prills covered with Kurevere D – from 111.3 to 154.8 kJ mole⁻¹ (A in between 2.0×10^8 and 2.9×10^{12} s⁻¹).

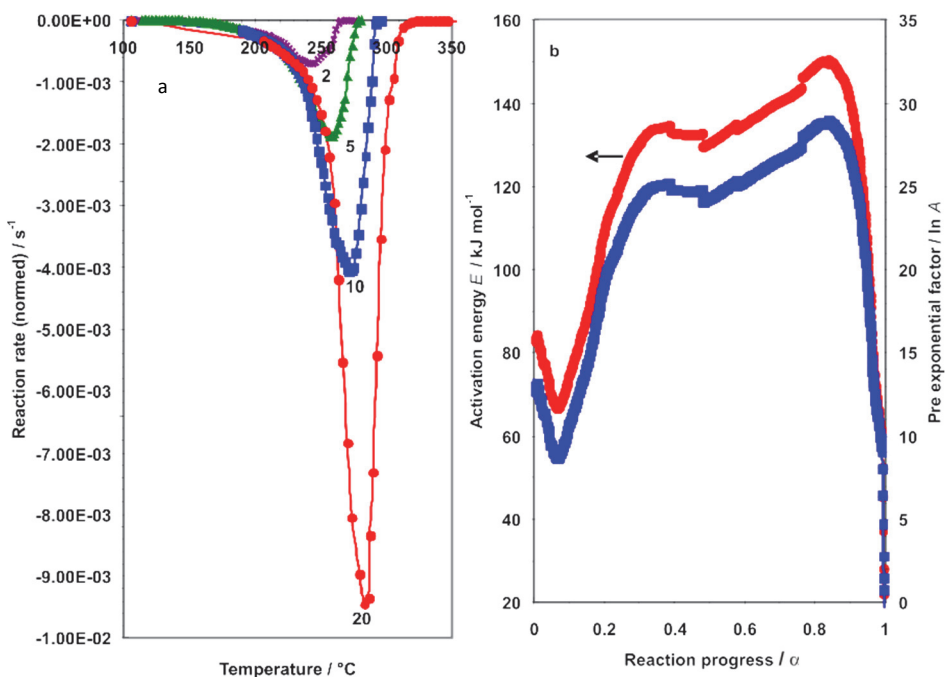


Figure 15. (a) Reaction rate $d\alpha/dt$ (DTG, normalized signals) as a function of temperature for different heating rates, and (b) activation energy E and pre-exponential factor A determined by Friedman analysis as a function of the reaction progress for step I of decomposition of AN blended with Vasalemma L

4.2.3. Effect of H_3BO_3 , CuO and MnO_2 on the thermal behavior of blends of AN and L/D

Since the efficiency of N uptake by plants decreases with even a relatively short-term deficit of Mn, Cu and B in the soil [91, 92], these microelements could be added to the fertilizer in micro amounts.

H_3BO_3 , CuO and MnO_2 in amounts of 0.05 mol in the $2AN + CaCO_3$ and $2AN + 0.5CaMg(CO_3)_2$ systems do not show a destabilizing effect on blends of AN with L/D (Table 5).

Table 5. Temperatures of the endoeffects minimums on DTA curves corresponding to the principal transitions of $AN_{IV} \leftrightarrow AN_{III} \leftrightarrow AN_{II} \leftrightarrow AN_I$ and exoeffect maximum/ endoeffect minimum corresponding to the decomposition of residual AN in blends of AN + L/ D + CuO/ H₃BO₃/ MnO₂ in mol ratio 2:1:0.05 (heating rate 10 °C min⁻¹, 30 °C – 900 °C)

Compounds	AN _{IV} ↔ AN _{III} / AN _{IV} ↔ AN _{II} phase change [°C]	AN _{III} ↔ AN _{II} phase change [°C]	AN _{II} ↔ AN _I phase change [°C]	AN _I ↔ AN _{melt} phase change [°C]	Endotherm minimum [°C]
AN	53.0	86.5	127.1	166.8	262.9 (exotherm maximum)
AN + Karinu (L)	57.2	90.2	131.0	166.9	242.4
AN + L + H ₃ BO ₃	55.6	90.9	128.6	167.3	242.1
AN + L + CuO	54.9	91.2	128.0	157.94	247.8
AN + L + MnO ₂	57.6	94.3	131.8	166.7	205.1
AN + Anelema (D)	55.4	91.9	128.4	166.8	289.0
AN + D + H ₃ BO ₃	58.5	93.2	116.3	163.9	278.3
AN + D + CuO	56.6	90.0	127.7	166.0	282.0
AN + D + MnO ₂	56.5	90.0	128.4	166.3	259.7

4.2.4. Summary of the thermal analysis

- The L/ D addition to AN in amounts ≤20 mass% has no systematic influence on the temperatures of the transitions of the solid phase modification $AN_{IV} \leftrightarrow AN_{III} \leftrightarrow AN_{II} \leftrightarrow AN_I$.
- With thermal treatment, AN prills covered with L/ D powder predominantly follow the same complicated but safe behavior as AN blends with L/ D. Interactions between AN and Ca- and Mg-carbonates with the formation of Ca- and Mg-nitrates prevent the exothermic explosive decomposition of AN. Variation of the value of the activation energy during progress of the reaction shows the complex character of the decomposition of the samples.
- H₃BO₃, CuO and MnO₂ additives in amounts of 0.05 mol in the 2AN + CaCO₃ and 2AN + 0.5CaMg(CO₃)₂ systems showed no destabilizing effect on the blends of AN and L/ D.
- The results of the experiments carried out confirm the suitability of L and D for use as an additive in the production of AN-based fertilizer.

4.3. Covering of AN prill with L/ D powder in the disk granulator

4.3.1. Granules growth

Nitrogen content (N%) of the fertilizer granules can be controlled through the mean granule diameter (d_m) (Fig. 16, Eq. 27). The P/S ratio has the main effect on the mean size of the produced granules, but it can also be corrected through the correct selection of the size range of the product granules.

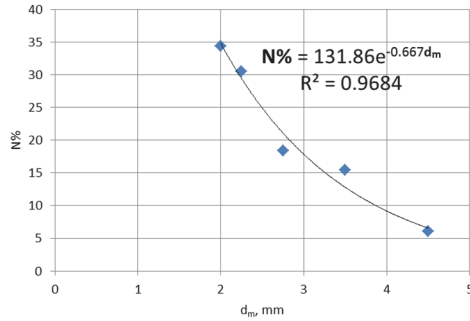


Figure 16. Nitrogen content of the fertilizer versus the mean granule size (granule core is 2.00 – 2.24 mm AN prill)

$$N\% = 131.86e^{-0.667d_m}, R^2 = 0.9684 \quad (27)$$

The mixture of AN prills and L powder in the granulator is not subjected to heating, so the risk of ammonia loss and the formation of highly hygroscopic calcium nitrate during the granulation process via interaction of AN with CaCO_3 is eliminated.

Granulate particles can be divided into four groups according to their nature: non layered powder (0–1.0 mm); fragments of broken seeds and their nuclei (1.0–2.0 mm); AN prills fully or partly covered with L powder (2.0–5.0 mm); oversize particles – agglomerates of several granules (> 5.0 mm).

The fractions of 0–1.0 mm and 1.0–2.0 mm contain 2.648% and 19.43% nitrogen, respectively. The formation of the 1.0–2.0 mm fraction leads to a serious loss of nitrogen and should therefore be suppressed. On the other hand, considering the high content of nitrogen in the fraction of broken seeds and nuclei (1–2 mm) allows this fraction to be used as a conventional fertilizer.

In the initiation stage of granulation, the tumbling of seeds leads to their attrition and breakage, as they are rather fragile particles (mean crush strength (CS) is 3.0 N per AN prill). The increase of the ratios of P/S and B/P during granulation leads to suppression of the breakage phenomenon. Granule growth occurs through the

layering and consolidation mechanisms until oversaturation of the granules is reached, which leads to over-wetting of the tumbling mass.

4.3.1.1. Optimum granulation duration

The optimum granulation time regarding granule growth through the powder layering is 4 min. The yield of covered granules is upwards of 80% and does not change with increase in the granulation duration beyond 4 min, as well as the mean granule size (*Paper IV: Fig. 4*). This is consistent with the results obtained by other researchers [93, 94] in the sense that the optimum granulation time is quite short, at just a few minutes.

4.3.1.2. Optimum inclination angle and rotation speed of the disk

Fig. 6 in *Paper IV* shows the effect of the inclination angle of the disk on the cumulative size distribution of the granulate particles. Breakage of the seeds and granules is not affected by the disk's angle of inclination. But the effectiveness of the powder layering increases from 67% to 77% with the increase of the disk angle of inclination from 30° to 45°. Usually granulators are operated at up to a 55° disk inclination, because of construction limits.

Fig. 5 in *Paper IV* shows the effect of the disk's rotation speed on the cumulative size distribution of the granulate particles. The optimum rotation speed for the disk with $d = 0.5$ m is 23 rpm. The optimum rotation speed for the disk with any other diameter can be calculated through n_{cr} (*Eq. 11*) specifically for it keeping constant $n/n_{cr} = 0.46$ (*Table 6*).

Table 6. Optimum rotation speeds for disks with different diameters

Inner diameter of disk, m	Angle of disk inclination, °	n_{cr} , rpm (Eq. 11)	n/n_{cr}	Optimum n , rpm
0.5	45	50.28	0.46	23
1.0	45	35.55	0.46	16
2.0	45	25.14	0.46	12
3.0	45	20.52	0.46	9
4.0	45	17.78	0.46	8

4.3.1.3. Effect of P/S and B/P ratios

Breakage of granules and seeds can be suppressed only by increasing the rate of binder liquid delivery (*Fig. 17*). The optimum B/P ratio is 15–20% considering the layering effectiveness. A greater quantity of powder and binder liquid in the granulation process improves the powder particle packing (*Fig. 18*). The most obvious effect of B/P on the layering of powder can be seen with granules in the size range of 2.0–2.5 mm. A characteristic feature of such granules prepared with a low amount of binder is the irregular covering layer (*Fig. 19*). Independently of the

P/S and B/P ratios used, granules produced in the size range of 2.5–5.0 mm have a well-formed covering layer (Fig. 3).

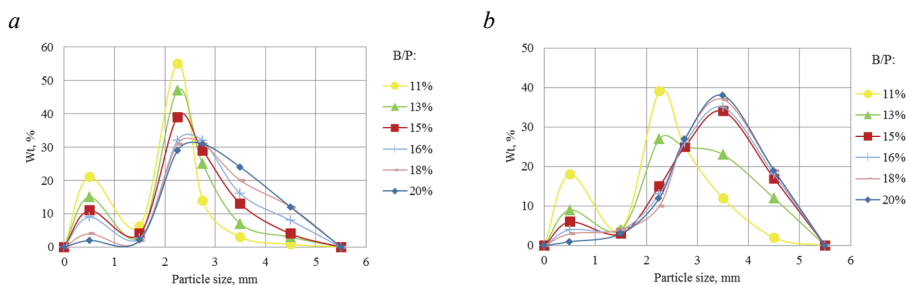


Figure 17. Differential size distribution of granulate obtained at (a) $P/S=0.5$ and (b) $P/S=2.0$ at different B/P ratios

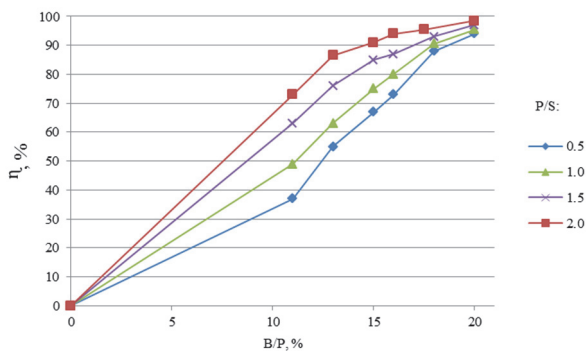


Figure 18. Effectiveness of powder consumption

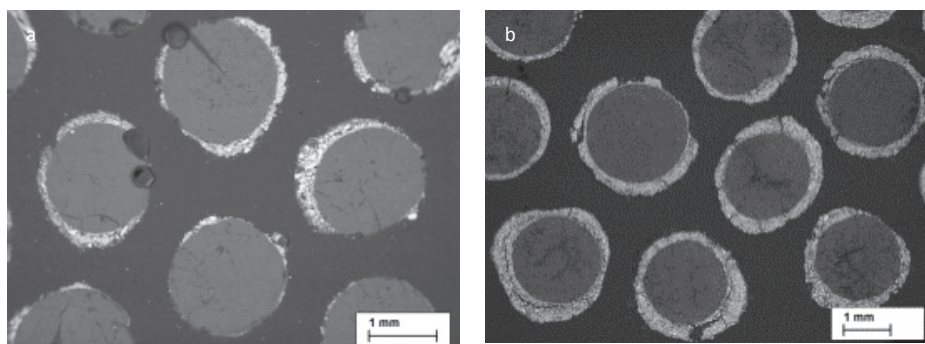


Figure 19. SEM images of cross-sections of granules in the size range of 2.0–2.5 mm produced with (a) $B/P = 11\%$ and $P/S = 0.5$ and (b) $B/P = 18\%$ and $P/S = 2.0$

4.3.2. Granules strength

4.3.2.1. Effect of granulation time

The effect of granulation time on the mean strength of the covering layer of the granules produced is shown in *Fig. 20*. The most durable layer was obtained in 3–4 minutes of granulation. A further increase in the granulation time reduces the strength of the covering layer. This fact confirms that the process of the powder particle layering and the process of destruction of the top layer reach equilibrium in the 4th minute. An increase in the quantity of defects in the top layer of granules leads to a decrease in its strength. When the amount of binder liquid is sufficient for maximum granule saturation ($B/P = 20\%$), the decrease in strength is less obvious, but the coefficient of variation of strength (the ratio of standard deviation to mean crush strength) decreases from 0.23 to 0.16 with an increase in granulation time from 4 to 16 min. This indicates that by increasing the residence time of granules in the tumbling layer, a narrower strength distribution of the granules covering layer can be obtained.

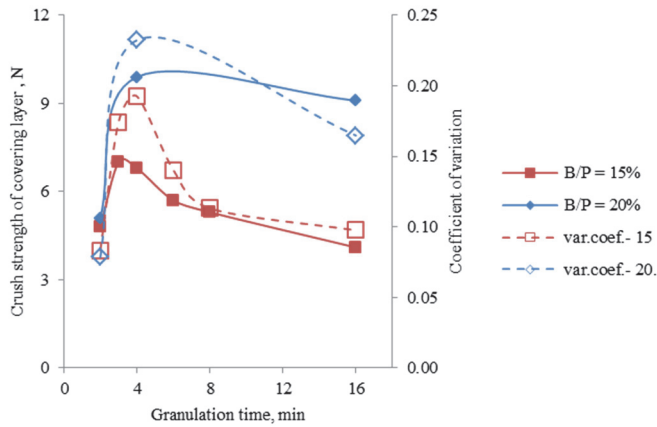


Figure 20. Effect of granulation time on the strength of granule covering layer

4.3.2.2. Effect of inclination angle and rotation speed of disk

The crush strength of the covering layer increases with the increase of the disk rotation speed to the critical speed ratio (n/n_{cr}) from 0.38 to 0.46 rpm (*Eq. 11, Paper IV: Table 2*). As shown in [95], the probability of a successful coalescence and densification rate of particles increases with an increase in the collision velocity of the particles. The greater consolidation leads to lower porosity and hence higher strength [94]. This correlation between the mean crush strength of the covering layer and the porosity of covered AN prills is well seen in *Fig. 21*. The results of the granule strength at higher ratios of the rotation speed to the critical speed (from 0.46

to 0.56) suggest that the maximum strength of the covering layer for the B/P ratio used has been achieved.

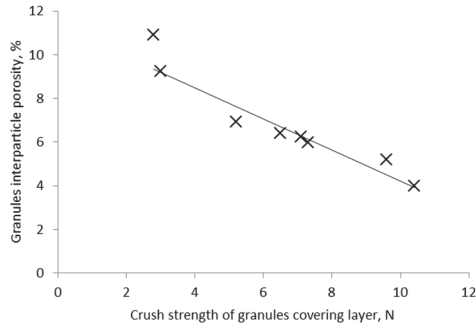


Figure 21. Trend of granule strength versus porosity

4.3.2.3. Effect of P/S and B/P ratios

It is shown in [96] that the parameter with the greatest influence on the granulation mechanism and on the properties of granules is liquid saturation. Granulation with high liquid to solid phase ratios and therefore high fractional saturation produces granules with more binder liquid in the bonds between particles. These lead to the formation of large and strong crystal bridges and therefore serve to decrease porosity and increase the strength of the granules. The results show that the strength of the covering layer of the granules is independent of the P/S ratio, but it increases from 4.3 to 9.9 N with increase of the B/P ratio from 11% to 20% (Fig. 22). A further increase of this parameter leads to over-wetting of the tumbling mass. The maximum strength of granules is achieved with this.

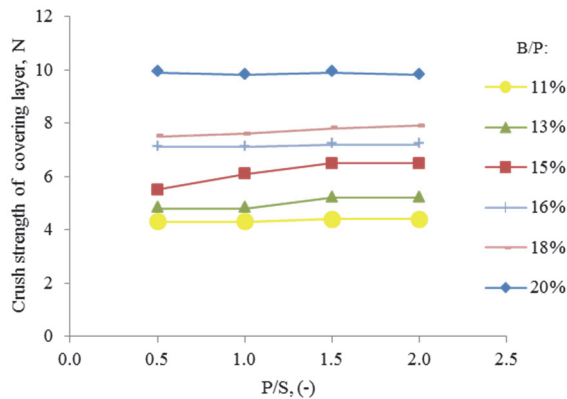


Figure 22. Effect of B/P and P/S on the strength of the granules covering layer

4.3.3. Resistance of the covered granules to temperature fluctuations

The durability under compression of AN prills decreased twofold after heating to 35 °C degrees (from 3.0 N to 1.5 N) and become friable with repeated heating until the prills were scattered after 8 cycles. The durability of the AN prills covered with L or D powder, under the influence of the temperature fluctuations (36 cycles), did not change, and remained at the level of 9–10 N. Thus covered prills showed good resistance to temperature fluctuations (15–35 °C), conducted in a climate chamber, which suggests that the strength of covered granules is less influenced by the density fluctuations of its core, caused by the AN_{IV}↔AN_{III} transition of the solid-phase modifications.

4.3.4. Summary of the covering process

The prospects for the strengthening of AN prills by forming a covering layer on their surface have been proven. The maximum obtained crush strength of covered granules exceeded the strength of the pure AN prills just over three times, and is almost 10 N per granule. Covered granules showed good resistance to ambient temperature fluctuations, and the strength of the covered granules was not influenced by density fluctuations of its core, i.e. AN prill.

4.3.5. Recommendations for design of the covering process

Recommendations for the covering of AN prills on the disk granulator are as follows:

- Four minutes is sufficient residence time for granules in the tumbling layer for granule growth through the layering of powder particles and for obtaining the maximum strength of covered granules.
- The inclination angle of the disk should be 45°.
- The optimal rotation speed of the disk can be calculated through the critical rotation speed, as shown in Section 4.3.1.2. The optimal ratio of the disk rotation speed to the critical rotation speed is 0.46 (for a disk angle of inclination of 45°).
- The B/P ratio should be 18–20% to obtain high yields of strong covered granules. The tumbling mass reaches saturation with a B/P ratio higher than 20%, and further binder addition leads to over-wetting of the tumbling mass.
- When the B/P is at the recommended level, the effectiveness of the powder layering practically does not depend on the P/S ratio, and can be selected according to the desired nitrogen content of the covered granules. The P/S ratio has the greatest effect on the mean size of the fertilizer granules produced, but it can also be corrected through correct selection of the size range of the granules produced.
- The correlation between the granules' diameter and nitrogen content is as follows: $N\% = 131.86EXP(-0.667d_m)$.

4.4. Agrochemical testing of the designed fertilizer granules

Intensive usage of grassland requires fertilization with nitrogen several times during the vegetative period, which in turn has a considerable acidifying impact on the soil. The availability of nutrients for plants deteriorates if the soil pH is less than 6. Improving the availability of nutrients is important not only from an economic point of view, but also for preservation of the environment.

The tests conducted showed that L and D as a covering material do not affect the digestibility of AN by plants. Variations in the yield of the rye-grass obtained after the first and second fertilization with different kinds of granules did not exceed a statistical test error limit (PD 95%) (Fig. 23). Measurements of the percentage of chlorophyll in the grass with the N-tester did not show any difference between the samples.

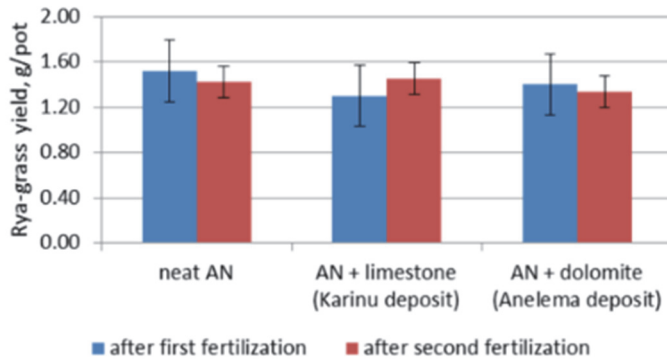


Figure 23. Effect of fertilization ($80 \text{ kg N} \cdot \text{ha}^{-1}$) on hay yield

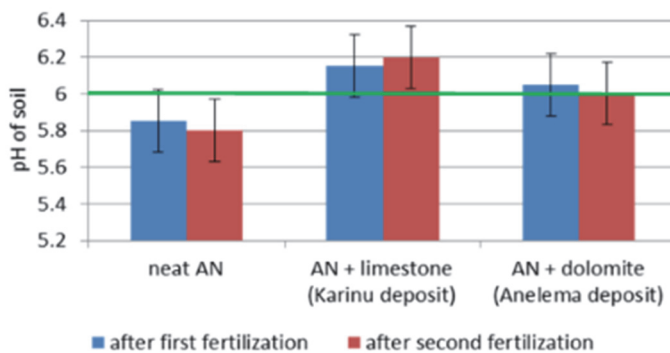


Figure 24. Effect of fertilization ($80 \text{ kg N} \cdot \text{ha}^{-1}$) on soil pH

At the same time, tests showed that the L/ D contained in the designed granules neutralizes the excessive AN introduced into the soil (*Fig. 24*). The soil pH was the lowest after the second fertilization with pure AN (acidification of the soil occurred) and the highest after the second fertilization with AN prills covered with L. The neutralizing effect of D powder is somewhat lower. But the soil pH was left at the optimal level for plant growth after fertilization with granules containing L as well as D.

Summarizing the data above, we can say that

- The L/ D covering does not affect the solubility of the fertilizer. Granules of both fertilizers completely dissolve in soil solution.
- The L/ D covering does not affect the digestibility of AN by plants. The covering of AN prills with L/ D powder had no significant effect on the one-year rye-grass yield.
- The presence of L/ D in AN-based fertilizer granules prevents the degradation of the soil. Calcium-enriched nitrogen fertilizer is needed, especially during intensive use of grassland and fertilization of non-carbonate soils.
- Since the research was relatively short-term, potentially greater changes did not have time to occur.

5. CONCLUSIONS

On the basis of the fulfilled investigation and the development of AN-based fertilizer with advanced properties, the following main conclusions can be outlined:

- AN in the form of prills is more thermally stable than AN in the ground form.
- L/ D has no systematic influence on the pathways and on the temperatures of transitions of the solid phase modification $AN_{IV} \leftrightarrow AN_{III} \leftrightarrow AN_{II}$. L/ D does not promote $AN_{IV} \leftrightarrow AN_{II}$ transition and does not inhibit $AN_{IV} \leftrightarrow AN_{III}$ transition.
- However, AN prill covered with L/ D powder is three times more durable and is many times more resistant to daily temperature fluctuations compared with the neat AN prill.
- Data obtained from the thermodynamic analysis of different reactions between AN and Ca- and Mg-carbonates with and without the presence of Cu, B and Mn-containing substances was confirmed by the data obtained in thermal analysis of the systems of AN + L/ D with and without the presence of Cu, B and Mn-containing substances.
- $CaCO_3/ MgCO_3$ contained in L/ D has a stabilizing effect on AN. Interactions between AN and Ca- and Mg-carbonates with the formation of Ca- and Mg-nitrates prevent the exothermic explosive decomposition of AN.
- H_3BO_3 , CuO and MnO_2 in amounts of ≤ 0.05 mol have no destabilizing effect on the systems containing 2 mol of AN and 1 mol of Ca- and Mg-carbonate, i.e., they have no destabilizing effect on the fertilizer granules developed.
- L/ D covering does not constrain the dissolution of AN contained in the fertilizer granules.
- In contrast to fertilization of soil with pure AN, which leads to soil acidification, fertilization of soil with AN – L/ D based granules allows to keep the acidity of the soil at the optimal level.
- The suitability of some Estonian L and D for use as an additive in the production of secure and eco-friendly AN-based fertilizer is justified in this thesis.
- The production process of the developed AN – L/ D granules in the disk granulator should be carried out at the optimal ratio of the disk rotation speed to the critical rotation speed, and at a binder to powder ratio close to the saturation level (20% of the binder to powder ratio). The residence time of granules in the tumbling layer should be quite short – 4 minutes. The mixture of AN prills and L/ D powder in the granulator is not subjected to heating, so the risk of highly hygroscopic Ca- and Mg-nitrates forming during the production process of the fertilizer granules is eliminated.

REFERENCES

- [1] M. Järvan and U. Järvan, "Muldade lupjamise ajaloost Eestis [in Estonian, Soil liming in Estonia]," in *Muldade lupjamine*, Saku, Eesti Maaviljeluse Instituut, 2010, pp. 12-14.
- [2] T. J. Weerden and S. C. Jarvis, "Ammonia emission factors for N fertilizers applied to two contrasting grassland soils," *Environmental Pollution*, vol. 95, pp. 205-211, 1997.
- [3] N. Dechy, T. Bourdeaux, N. Ayrault, M. A. Kordek and J. C. L. Coze, "First lessons of the Toulouse ammonium nitrate disaster, 21st September, AZF plant, France," *Journal of Hazardous Materials*, vol. 111, pp. 131-138, 2004.
- [4] "Process of producing concentrated solutions of ammonium nitrate". Patent 4927617, 1990.
- [5] "International Fertilizer Industry Association's Public Statistics. Fertilizer supply statistics," 2012. [Online]. Available: Available at <http://www.fertilizer.org/ifa/ifadata/results>. [Accessed 31 October 2013].
- [6] R. Fernández-Escobar, M. Benlloch, E. Herrera and J. M. García-Novelo, "Effect of traditional and slow-release N fertilizers on growth of olive nursery plants and N losses by leaching," *Scientia Horticulturae*, vol. 101, pp. 37-39, 2004.
- [7] B. Eickhout, A. F. Bouwman and H. Zeijts, "The role of nitrogen in the world food production and environmental sustainability," *Agriculture, Ecosystems and Environment*, vol. 116, pp. 4-14, 2006.
- [8] T. Salo and E. Turtola, "Nitrogen balance as an indicator of nitrogen leaching in Finland," *Agriculture, Ecosystems and Environment*, vol. 113, pp. 98-107, 2006.
- [9] F. Moldan, O. J. Kjønaas, A. O. Stuanes and R. F. Wright, "Increased nitrogen in runoff and soil following 13 years of experimentally increased nitrogen decomposition to a coniferous-forested catchment at Gårdsjön, Sweden," *Environmental Pollution*, vol. 144, pp. 610-620, 2006.
- [10] P. Patnaik, *Handbook of Inorganic Chemicals*, McGraw-Hill, 2002.
- [11] P. Angás, J. Lampurlanés and C. Cantero-Martínez, "Tillage and N fertilization effects on N dynamics and barley yield under semiarid Mediterranean conditions," *Soil & Tillage Research*, vol. 87, pp. 59-71, 2006.
- [12] M. G. Pilkington, S. J. M. Caporn, J. A. Carroll, N. Cresswell, J. A. Lee, T. W. Ashenden, S. A. Brittain, B. Reynolds and B. A. Emmett, "Effects of increased deposition of atmospheric nitrogen on an upland moor:

- leaching of N species and soil solution chemistry," *Environmental Pollution*, vol. 135, pp. 29-40, 2005.
- [13] J. R. Martínez, V. H. D. Francia Zuazo and A. M. Raya, "Environmental impact from mountainous olive orchards under different soil-management systems," *Science of the Total Environment*, vol. 358, pp. 46-60, 2006.
- [14] R. Papini, G. Valboa, C. Piovanelli and G. Brandi, "Nitrogen and phosphorus in a loam of soil of central Italy as affected by 6 years of different tillage systems," *Soil & Tillage Research*, vol. 92, pp. 175-180, 2006.
- [15] G. Kutra and R. Aksomaitiene, "Use of nutrient balances for environmental impact calculations on experimental field scale," *European Journal of Agronomy*, vol. 20, pp. 127-135, 2003.
- [16] R. P. Udawatta, P. P. Motavalli, H. E. Garret and J. J. Krstansky, "Nitrogen losses in runoff from three adjacent agricultural watersheds with claypan soils," *Agriculture, Ecosystems and Environment*, vol. 117, pp. 39-48, 2006.
- [17] S. S. Malhi, M. Nyborg and J. T. Harapiak, "Effects of long-term N fertilizer-induced acidification and liming on micronutrients in soil and in bromegrass hay," *Soil and Tillage Research*, vol. 48, pp. 91-101, 1998.
- [18] S. D. Frey, M. Knorr, J. L. Parrent and R. T. Simpson, "Chronic nitrogen enrichment affects the structure and function of the soil microbial community in temperate hardwood and pine forests," *Forest Ecology and Management*, vol. 196, pp. 159-171, 2004.
- [19] A. H. Magill, J. D. Aber, W. S. Currie, K. J. Nadelhoffer, M. E. Martin, W. H. McDowell, J. M. Melillo and P. Steudler, "Ecosystem response to 15 years of chronic nitrogen addition to Harvard Forest LTER, Massachusetts, USA," *Forest Ecology and Management*, vol. 196, pp. 7-28, 2004.
- [20] "Food and Agriculture Organization of the United Nations. Current world fertilizer trends and outlook to 2016," 2012. [Online]. Available: Available at <ftp://ftp.fao.org/ag/agp/docs/cwfto16.pdf>. [Accessed 31 October 2013].
- [21] J. C. Oxley, J. L. Smith, E. Rogers and M. Yu, "Ammonium nitrate: thermal stability and explosivity modifiers," *Thermochimica Acta*, vol. 384, pp. 23-45, 2002.
- [22] M. Olszak-Humienik, "On the thermal stability of some ammonium salts," *Thermochimica Acta*, vol. 378, pp. 107-120, 2001.
- [23] J. Sun, Z. Sun, Q. Wang, H. Ding, T. Wang and C. Jiang, "Catalytic effects of inorganic acids on the decomposition of ammonium nitrate," *Journal of Hazardous Materials*, vol. 127, pp. 204-210, 2005.

- [24] M. Harju, "Solid state transition mechanisms of ammonium nitrate phases IV, III, II investigated by simultaneous Raman spectrometry and differential scanning calorimetry," *Applied Spectroscopy*, vol. 47, pp. 19-26, 1993.
- [25] A. O. R. Sudhakar and F. Mathew, "Thermal behaviour of CuO doped phase-stabilised ammonium nitrate," *Thermochimica Acta*, vol. 451, pp. 5-9, 2006.
- [26] H. B. Wu and C. K. Chan, "Effects of potassium nitrate on the solid phase transitions of ammonium nitrate particles," *Atmospheric Environment*, vol. 42, pp. 313-322, 2008.
- [27] C. S. Skordilis and P. J. Pomonis, "The influence of Mn, Co and Cu cations on the thermal decomposition of NH_4NO_3 in pure form and supported on alumina," *Thermochimica Acta*, vol. 216, pp. 137-146, 1993.
- [28] E. Kestilä, M. E. E. Harju and J. Valkonen, "Differential scanning calorimetric and Raman studies of phase transition V - IV of ammonium nitrate," *Thermochimica Acta*, vol. 214, pp. 67-70, 1993.
- [29] P. N. Simões, L. M. Pedroso, A. A. Portugal and J. L. Campos, "Study of the decomposition of phase stabilized ammonium nitrate (PSAN) by simultaneous thermal analysis: determination of kinetic parameters," *Thermochimica Acta*, vol. 319, pp. 55-65, 1998.
- [30] A. Lafci, K. Guruz and H. Yucel, "Investigation of factors affecting caking tendency of calcium ammonium nitrate fertilizer and coating experiments," *Fertilizer Research*, vol. 18, pp. 63-70, 1988.
- [31] H. B. Wu, M. N. Chan and C. K. Chan, "FTIR characterization of polymorphic transformation of ammonium nitrate," *Aerosol Science and Technology*, vol. 41, pp. 581-588, 2007.
- [32] C. Oommen and S. R. Jain, "Ammonium nitrate: a promising rocket propellant oxidizer," *Journal of Hazardous Materials*, vol. 67, pp. 253-281, 1999.
- [33] G. F. Velardez, S. Alavi and D. L. Thompson, "Molecular dynamics studies of melting and solid-state transitions of ammonium nitrate," *Journal of Chemical Physics*, vol. 120, pp. 9151-9159, 2004.
- [34] L. Filipescu, D. Fatu, T. Coseac, M. Mocioi and E. Segal, "On the chemical and thermal stabilization of ammonium nitrate (IV)," *Thermochimica Acta*, vol. 97, pp. 229-241, 1986.
- [35] C. A. van Driel, A. E. D. M. van der Heijden, S. de Boer and G. M. van Rosmalen, "The III-IV phase transition in ammonium nitrate: mechanisms," *Journal of Crystal Growth*, vol. 141, pp. 404-418, 1994.

- [36] E. Kestila and J. Valkonen, "Effect of crystallization on the phase transition IV–III and IV–II of ammonium nitrate," *Thermochimica Acta*, vol. 214, pp. 305-314, 1993.
- [37] I. Dellien, "A DSC study of the phase transformations of ammonium nitrate," *Thermochimica Acta*, vol. 55, pp. 181-191, 1982.
- [38] H. Langfelderova and P. Ambrovic, "Study of the influence of experimental conditions on the course of the DSC curve of ammonium nitrate (20–140 °C)," *Thermochimica Acta*, vol. 56, pp. 385-389, 1982.
- [39] R. N. Brown and A. C. McLaren, "On the mechanism of the thermal transformations in solid ammonium nitrate," *Proceedings of the Royal Society of London*, vol. 266, pp. 329-343, 1962.
- [40] K. D. Shah and A. G. Roberts, "Properties of ammonium nitrate in nitric acid and fertilizer nitrates," C. Keleti, Ed., New York, Dekker Inc, 1985, p. 173.
- [41] L. A. Medard, "Types of Explosives Substances," in *Accidental Explosions*, J. Wiley, Ed., New York, Chichester: Ellis Horwood, 1989, pp. 545-590.
- [42] T. P. Russel and T. B. Brill, "Thermal decomposition of energetic materials 31—fast thermolysis of ammonium nitrate, ethylenediammonium dinitrate and hydrazinium nitrate and the relationship to the burning rate," *Combustion and Flame*, vol. 76, pp. 393-401, 1989.
- [43] B. A. Lurie and C. Lianshen, "Kinetics and Mechanism of Thermal Decomposition of Ammonium Nitrate Powder under the Action of Carbon Black," *Combustion, Explosion, and Shock Waves*, vol. 36/5, pp. 607-617, 2000.
- [44] K. R. Brower, J. C. Oxley and M. P. Tewari, "Evidence of homolytic decomposition of ammonium nitrate at high temperature," *Journal of Physical Chemistry*, vol. 93, pp. 4029-4033, 1989.
- [45] J. C. Oxley, S. M. Kaushik and N. S. Gilson, "Thermal decomposition of ammonium nitrate-based composites," *Thermochemica Acta*, vol. 153, pp. 269-286, 1989.
- [46] K. S. Barclay and J. M. Crewe, "The thermal decomposition of ammonium nitrate in the fused salt solution and in the presence of added salts," *Journal of Applied Chemistry*, vol. 17, pp. 21-26, 1967.
- [47] D. Bennet, "A study of the thermal decomposition of ammonium nitrate using a gas chromatography technique," *Journal of Applied Chemistry*, vol. 22, pp. 973-982, 1972.
- [48] N. Koga and H. Tanaka, "Effect of sample mass on the kinetics of thermal decomposition of a solid. Part 3. Non-isothermal mass loss

- process of molten NH_4NO_3 ," *Thermochimica Acta*, vol. 240, pp. 141-151, 1994.
- [49] N. Koga and H. Tanaka, "Effect of sample mass on the kinetics of thermal decomposition of a solid. Part 1. Isothermal mass-loss process of molten NH_4NO_3 ," *Thermochimica Acta*, vol. 209, pp. 127-134, 1992.
- [50] J. R. Adams and A. R. Merz, "Hygroscopicity of Fertilizer Materials and Mixtures," *Industrial and Engineering Chemistry*, vol. April, pp. 305-307, 1929.
- [51] P. Kirilov, "Non-caking fertilizers from ammonium nitrate and supplementary nutrients," *Journal of the University of Chemical Technology and Metallurgy*, vol. 40/3, pp. 209-212, 2005.
- [52] R. L. Latham and P. R. Geissler, "Hygroscopicity of complex fertilizers: Effect of Calcium Nitrate and water concentrations on critical relative humidity of Ammonium Nitrate-Limestone," *Journal of Agricultural and Food Chemistry*, vol. 16/3, pp. 384-387, 1968.
- [53] B. Svenningsson, J. Rissler, E. Swietlicki, M. Mircea, M. Bilde, M. C. Facchin, S. Decesari, S. Fuzzi, J. Zhou, J. Mønster and T. Rosenørn, "Hygroscopic growth and critical supersaturations for mixed aerosol particles of inorganic and organic compounds of atmospheric relevance," *Atmospheric Chemistry and Physics*, vol. 6, pp. 1937-1952, 2006.
- [54] L. Komunjer and C. Affolter, "Absorption-evaporation kinetics of water vapour on highly hygroscopic powder: Case of ammonium nitrate," *Powder Technology*, vol. 157, pp. 67-71, 2005.
- [55] "Process for the production of ammonium nitrate of low hygroscopicity and high bulk density". Patent 3171716, 2 March 1965.
- [56] "Materials containing anti-caking powders". Patent 3880641, 29 April 1975.
- [57] A. A. Vargeese, S. S. Joshi and V. N. Krishnamurthy, "Effect of method of crystallization on the IV–III and IV–II polymorphic transitions of ammonium nitrate," *Journal of Hazardous Materials*, vol. 161/1, pp. 373-379, 2009.
- [58] T. Sramko and E. Jona, "Thermal properties of ammonium nitrate. II. Study of modification transformations and their completeness by the change of heating mode," *Thermochimica Acta*, vol. 92, pp. 731-734, 1985.
- [59] R. N. Brown and A. C. McLaren, "On the mechanism of the thermal transformations in solid ammonium nitrate," *Proceedings of the Royal Society of London Series A*, vol. 266, pp. 329-343, 1962.
- [60] C. Sjölin, "The influence of moisture on the structure and quality of NH_4NO_3 -prills," *Journal of Agriculture and Food Chemistry*, vol. 19, pp. 83-95, 1971.

- [61] E. J. Griffith, "Phase transitions of the ammonium nitrate–magnesium nitrate system," *Journal of Chemical & Engineering Data*, vol. 8, pp. 22-25, 1963.
- [62] K. Menke, J. Böhnlein-Mauß and H. Schubert, "Characteristic properties of AN/GAP-propellants," *Propellants, Explosives, Pyrotechnics*, vol. 21, pp. 139-145, 1996.
- [63] A. N. Campbell and A. J. R. Campbell, "The effect of a foreign substance on the transition: NH_4NO_3 IV \leftrightarrow NH_4NO_3 III," *Canadian Journal of Research*, vol. 24, pp. 93-108, 1946.
- [64] A. Deimling, W. Engel and N. Eisenreich, "Phase transitions of ammonium nitrate doped with alkali nitrate studied with fast X-ray diffraction," *Journal of Thermal Analysis and Calorimetry*, vol. 38, pp. 843-853, 1992.
- [65] M. E. E. Harju and J. Valkonen, "Effect of sample treatment on the phase transition paths of ammonium nitrate solid state phases IV, III and II," *Journal of Thermal Analysis*, vol. 39, pp. 681-693, 1993.
- [66] C. Oommen and S. R. Jain, "Phase modification of ammonium nitrate by potassium salts," *Journal of Thermal Analysis and Calorimetry*, vol. 55, pp. 903-918, 1999.
- [67] "Chemical Advisory: Safe Storage, Handling, and Management of Ammonium Nitrate. EPA 550-S-13-001," [Online]. Available: http://www.epa.gov/oem/docs/chem/AN_advisory.pdf. [Accessed 20 November 2013].
- [68] S. Zeman, P. Kohlíček and A. Maranda, "A study of chemical micromechanism governing detonation initiation of condensed explosive mixtures by means of differential thermal analyses," *Thermochimica Acta*, vol. 398, pp. 185-194, 2003.
- [69] "Eesti maavarade koondbilanss 2012 [in Estonian, The consolidated balance of mineral resources of Estonia 2012]," [Online]. Available: http://geoportaal.maaamet.ee/docs/koondbilanss_2012.pdf?t=20130614161639. [Accessed 9 October 2014].
- [70] И. Г. а. И. Ш. П. Классен, Гранулирование [in Russian, Granulation], Москва, СССР: Химия, 1991, p. 240.
- [71] M. G. Herting and P. Kleinebudde, "Studies on the reduction of tensile strength of tablets after roll compaction/dry granulation," *European Journal of Pharmaceutics and Biopharmaceutics*, vol. 70, no. 1, pp. 372-379, 2008.
- [72] A. Braumann, M. Kraft and P. R. Mort, "Parameter estimation in a multidimensional granulation model," *Powder Technology*, vol. 197, pp. 196-210, 2010.

- [73] H. Rumpf, "The strength of granules and agglomerates," in *Agglomeration*, W. Knepper, Ed., New York, AIME, Interscience, 1962, pp. 379-418.
- [74] H. Schubert, "Tensile strength of agglomerates," *Powder Technology*, vol. 11, pp. 107-119, 1975.
- [75] P. R. Mort, "Scale-up of binder agglomeration processes," *Powder Technology*, vol. 150, pp. 86-103, 2005.
- [76] S. H. Schaafsma, P. Vonk, P. Segers and N. W. F. Kossen, "Description of agglomerate growth," *Powder Technology*, vol. 97, pp. 183-190, 1998.
- [77] N. Ouchiyama and T. Tanaka, "The probability of coalescence in granulation kinetics," *Industrial & Engineering Chemistry Process Design and Development*, vol. 14, pp. 286-289, 1975.
- [78] H. G. Kristensen, P. Holm and T. Schaefer, "Granulation in high-speed mixers, Part VI. Effects of process conditions on power consumption and granule growth," *Powder Technology*, vol. 43, no. 3, pp. 225-233, 1985.
- [79] S. M. Iveson, J. D. Litster and B. J. Ennis, "Fundamental studies of granule consolidation, Part 1: Effects of binder content and binder viscosity," *Powder Technology*, vol. 88, no. 1, pp. 15-20, 1996.
- [80] S. M. Iveson and J. D. Litster, "Growth regime map for liquid-bound granules," *AIChE Journal*, vol. 44, no. 7, pp. 1510-1518, 1998.
- [81] P. Roy, M. Vashishtha, R. Khanna and D. Subbarao, "Size-dependent coalescence kernel in fertilizer granulation - A comparative study," *Particuology*, vol. 7, pp. 445-450, 2009.
- [82] S. M. Iveson, J. D. Litster, K. Hapgood and B. J. Ennis, "Nucleation, growth and breakage phenomena in agitated wet granulation processes: a review," *Powder Technology*, vol. 117, pp. 3-39, 2001.
- [83] J. Litster and B. Ennis, "Chapter 8, Tumbling granulation," in *The science and engineering of granulation process*, Netherlands, Kluwer Academic Publishers, 2004, pp. 179-180.
- [84] M. Järvan, "Raskmetallisisaldus köögiviljades sõltuvalt lubiväetise liigist [in Estonian, Heavy metal content in vegetables, depending on the type of liming fertilizer]," *Agraarteadus*, vol. 3, pp. 176-187, 1998.
- [85] HSC Chemistry for Windows. Chemical reaction and equilibrium software with extensive thermochemical database. Version 4.0, Pori: Outokumpu Research, Licence for Tallinn Technical University, 2002.
- [86] H. L. Friedman, "Kinetics of thermal degradation of char-forming plastics from thermogravimetry. Application to a phenolic plastic," *Journal of Polymer Science*, vol. 6C, pp. 183-195, 1965.
- [87] "AKTS Software and SETARAM Instruments: a global solution for kinetic analysis and determination of the thermal stability of materials," Switzerland, AKTS AG, 2006, p. 88.

- [88] S. Vyazovkin, J. S. Clawson and C. A. Wight, "Thermal dissociation kinetics of solid and liquid ammonium nitrate," *Chemistry of Materials*, vol. 13, pp. 960-966, 2001.
- [89] J. Madarász, P. P. Varga and G. Pokol, "Evolved gas analyses (TG/DTAMS and TG-FTIR) on dehydration and pyrolysis of magnesium nitrate hexahydrate in air and nitrogen," *Journal of Analytical and Applied Pyrolysis*, vol. 79, pp. 475-478, 2007.
- [90] C. Ettarh and A. K. Galwey, "A kinetic and mechanistic study of the thermal decomposition of calcium nitrate," *Thermochimica Acta*, vol. 93, pp. 203-219, 1996.
- [91] M. Järvan, "Lehekaudsest väetamisest [in Estonian, About foliar fertilization]," *Infoleht nr 188/2006*, pp. 1-4, 2007.
- [92] E. Ronnen, "Micro-elements in agriculture," *Practical Hydroponics & Greenhouses*, pp. 39-48, 8 July 2007.
- [93] K. V. S. Sastry, P. Dontula and C. Hosten, "Investigation of the layering mechanism of agglomerate growth during drum pelletization," *Powder Technology*, vol. 130, no. 1-3, pp. 231-237, 2003.
- [94] N. Rahmanian, A. Najji and M. Ghadiri, "Effects of process parameters on granules properties produced in a high shear granulator," *Chemical Engineering Research and Design*, vol. 89, pp. 512-518, 2011.
- [95] T. Schæfer and C. Mathiesen, "Melt pelletization in a high shear mixer. VIII. Effects of binder viscosity," *International Journal of Pharmaceutics*, vol. 139, no. 1-2, pp. 125-243, 1996.
- [96] G. M. Walker, H. E. M. N. Moursy, C. R. Holland and M. N. Ahmad, "Effect of process parameters on the crush strength of granular fertiliser," *Powder Technology*, vol. 132, pp. 81-84, 2003.

ABSTRACT

The aims of the AN fertilizer modifications are to decrease the acidifying effect of the fertilizer on the soil, increase the thermal stability of the fertilizer and strengthen the fertilizer granules.

The current thesis reports the results of a multi-faceted study on the suitability of natural lime-containing minerals as a modifying additive for the production of secure and eco-friendly AN-based fertilizer. The AN – L/ D fertilizer granules developed do not acidify the soil, are resistant to ambient temperature fluctuations and are thermally stable. The production technology of granules in a disk granulator is quite simple. Recommendations for the choice of process parameters are proposed in this thesis.

Improvement of the thermal stability of AN fertilizer was achieved through the reduction of the nitrogen content of fertilizer by introducing the inert additive to the content of its granules. Investigations of the mechanism and kinetics of thermolysis of AN – L/ D based fertilizer showed that interactions between AN and Ca- and Mg-carbonates (contained in L/ D) with the formation of Ca- and Mg-nitrates prevent the exothermic explosive decomposition of AN. Also, micronutrients required for normal growth of plants can be added to the fertilizer granules without the risk of thermal destabilization of the fertilizer.

The covering layer made from L/ D powder strengthens the fertilizer granule and makes it resistant to ambient temperature fluctuations, which are responsible for fluctuations of density of the core of the granule (AN prill).

Thanks to the neutralizing action of L/ D on the soil, fertilization of the soil with the granules developed does not lead to soil acidification, despite the fact that the L/ D covering does not retard the dissolution of AN contained in the granule core.

The proposed technology of covering AN prills with powdered L/ D allows a wide variation of the content of nitrogen in fertilizer and allows a very high throughput capacity and convenient control of the process.

KOKKUVÕTE

Ammooniumnitraat (AN), mida iseloomustab kõrge lämmastiku sisaldus (~35%) ning suhteliselt lihtne tootmistehnoloogia, on tänapäeva põllumajanduses üks enim kasutatavaid lämmastikväetisi maailmas. Samas on tema puudusteks kasutamise kaasnep muldade mineraliseerumine ja hapestumine, tema termiline labiilsus ning väetisgraanulite nõrk mehhaaniline tugevus ja nende paatumine ladustamisel.

Käesolevas doktoritöös esitatakse AN modifitseerimisega seotud uuringute tulemused, mille raames selgitati looduslike lubjakivide ja dolomiitide sobilikkus – nii lisandina segus AN-ga kui ka AN idugraanulite katematerjalina – turvalise ja keskkonnasõbraliku AN-baasväetise saamiseks. Saadud lubimaterjalidega modifitseeritud AN graanulid on termiliselt märksa stabiilsemad, on vastupidavad – ei paatu ega purune – ümbritseva keskkonna temperatuurikõikumistele ning välistavad muldade hapendumise. Ühtlasi on käesolevas töös esitatud soovitusel granuleerimisprotsessi parameetrite osas.

AN-baasväetise termilise stabiilsuse paranemine on saavutatud väetisele lubjakivi- või dolomiidijahu lisamisega või vastava lubimaterjalist katendi tekitamisega AN-idugraanulite pinnale. Modifitseeritud AN termilise lagunemise mehhanismi ja kineetika uuringud näitasid, et reaktsioonid AN ja lubjakivis või dolomiidis sisalduvate Ca- ja Mg-karbonaatide vahel Ca- ning Mg-nitraatide tekkega ennetavad AN eksotermilist plahvatusohtlikku lagunemist. Samuti on võimalik taimedele vajalike mikrotoitainete lisamine väetisgraanulitele katendi tekitamise protsessi käigus ilma destabiliseerimise riskita. Ühtlasi tõstab lubjakivi-/dolomiidijahust katend modifitseeritud graanulite mehhaanilist tugevust ligikaudu kolm korda, tehes need vastupidavamaks ka ümbritseva keskkonna temperatuurikõikumiste suhtes.

Tänu lubjakivi-/ dolomiidijahust katendi neutraliseerivale toimele muldade väetamisel modifitseeritud graanulitega ei kaasne nende hapestumine vaatamata asjaolule, et lubjakivi-/ dolomiidijahust katend ei aeglusta graanuli tuumas sisalduva AN lagunemist-lahustumist.

Välja pakutud AN graanuli lubjakivi- või dolomiidijahuga katmistehnoloogia võimaldab reguleerida laias diapsoonis lämmastiku sisaldust väetises, garanteerib protsessi kõrge tootlikkuse ning mugava kontrolli granuleerimisprotsessi üle.

APPENDIX A: ORIGINAL PUBLICATIONS

Paper I

I. Klimova, T. Kaljuvee, L. Törn, V. Bender, A. Trikkel and R. Kuusik.

"Interactions of ammonium nitrate with different additives: thermodynamic analysis."

Reprinted with permission from:

Journal of Thermal Analysis and Calorimetry, vol. 105, no. 1, pp. 13-26, 2011.

Interactions of ammonium nitrate with different additives

Thermodynamic analysis

I. Klimova · T. Kaljuvee · L. Türn ·
V. Bender · A. Trikkel · R. Kuusik

Niinistö's Special Chapter
© Akadémiai Kiadó, Budapest, Hungary 2011

Abstract In order to elucidate the influence of Ca and Mg carbonates with or without the presence of boron, manganese and copper compounds on the thermal stability of ammonium nitrate (AN), thermodynamic analysis of different reactions between AN and additives was carried out. Temperature dependency of Gibbs free energy changes ΔG_T and equilibrium composition of reaction products were calculated for a set of reactions using the HSC software. Main solid compounds that can form in the systems of AN and carbonates, were $\text{Ca}(\text{NO}_3)_2$ and $\text{Mg}(\text{NO}_3)_2$, $\text{Ca}(\text{OH})_2$ and $\text{Mg}(\text{OH})_2$, CaO and MgO , CaO and MgO , and N-containing gaseous compounds NO, N_2O and NO_2 . As a result of H_3BO_3 , MnO_2 and CuSO_4 addition, the content of CuO, Cu_2O and MnO as solids and SO_2 , SO_3 and HBO as gaseous reaction products reached the same level. Thereby, their equilibrium concentrations did not depend on the carbonate origin of CaCO_3 , MgCO_3 or $\text{CaMg}(\text{CO}_3)_2$. Small amount of CuSO_4 , H_3BO_3 or MnO_2 additive (0.01–0.05 mol) in the system, practically, did not influence the temperature dependencies of ΔG_T of the reactions between AN and CaCO_3 or $\text{CaMg}(\text{CO}_3)_2$. The influence of additives taken in the larger amount (0.5 mol) was evident and, depending on the additive and reaction, shifted their proceeding temperatures in either direction by more than 300–400 K.

Keywords Thermodynamic analysis · Thermodynamic equilibrium · Ammonium nitrate · Calcium carbonate · Magnesium carbonate

Introduction

Ammonium nitrate is the main nitrogen fertilizer used in agriculture because of its high nitrogen content (35%), full solubility in water and relatively simple manufacturing technology [1, 2]. However, the thermal instability of AN requires definite precautions in its storing, transportation and handling [3, 4]. Exothermic decomposition of AN can be expressed by the following generalized reaction equation (i) [4]:



Using combined TG-DTA-FTIR techniques, it was previously found that limestone and dolomite additives stabilize AN because of the interactions between AN and Ca, Mg carbonates with the formation of Ca, Mg nitrates excluding exothermic explosive decomposition of AN [5, 6]. In order to increase the nutritional value of fertilizers, it is possible to mix them with microelements needed for plants. Boron, manganese and copper deficiency is widely met in Estonian soils [7]. So, in this article, the influence of H_3BO_3 , MnO_2 and CuSO_4 additives on the thermal behaviour of AN mixed with limestone and/or dolomite has been estimated using thermodynamic calculations as a tool before TA-FTIR measurements.

I. Klimova · T. Kaljuvee (✉) · L. Türn · V. Bender ·
A. Trikkel · R. Kuusik
Laboratory of Inorganic Materials, Faculty of Chemical and
Materials Technology, Tallinn University of Technology,
Tallinn, Estonia
e-mail: tiidu@staff.ttu.ee

Thermodynamic calculations

Thermodynamic analysis of interactions between substances provides composition of the equilibrium system at different

temperatures and different concentrations of the initial compounds, which is required in establishing reactions responsible for the interaction. In isolated reversible systems at constant pressure and temperature, the equilibrium criterion is expressed by the minimum of Gibbs energy. Using the HSC software [8], chemical processes in complex systems can be predicted, based on thermodynamic analysis of equilibrium compositions. The HSC built-in database [8] containing thermodynamic data of more than 15000 species collected from different articles and databases was used as the source for thermodynamic properties of the substances involved in the equilibrium systems studied.

The thermodynamic analysis results can differ from experimental data because this analysis does not count the time required to establish the equilibrium state. However, these results allow to predict thermodynamic probability of the chemical reactions of interest under certain conditions.

Here, thermodynamic analysis of different reactions between AN and additives was carried out to elucidate the influence of Ca, Mg carbonates with or without the presence of boron, manganese and copper compounds on the thermal behaviour of AN. The temperature dependency of Gibbs free energy changes ΔG_T and equilibrium composition of reaction products were calculated for a set of reactions (Table 1). Calculations were based on the AN/carbonates/copper, boron or manganese additive stoichiometry 2/1/0.01, 2/1/0.05 or 2/1/0.5. The amount of carbonates was varied from 0.2 to 2.1 mol with a step of 0.1. The values of ΔG_T were calculated in the temperature range of 273–2073 K.

Results and discussion

Equilibrium in the multi-component system based on AN–CaCO₃/MgCO₃/CaMg(CO₃)₂

Calculations were based on the initial amounts of 2 mol of AN and 1 mol of CaCO₃(s) or MgCO₃(s) or 0.5 mol CaMg(CO₃)₂(s).

The list of the main compounds and their concentrations in equilibrium (Fig. 1) as well as their variations depending on the temperature do not depend much on the origin of carbonate—CaCO₃(s), MgCO₃(s) or CaMg(CO₃)₂(s) being quite similar in the case of each. One can see that a rapid decrease in the content of Mg(NO₃)₂(s) and Ca(NO₃)₂(s), with the simultaneous increase in the amount of different N-containing gaseous compounds in the system occurs at temperatures up to 673–773 K. The equilibrium content of most of these gaseous compounds continues to increase with the temperature growth up to 2073 K, but the equilibrium amount of many of them e.g. NH(g), NH₂(g), NH₃(g) is small and hardly exceeds the 10^{−10} mol level at

temperatures higher than 1573–1773 K. The content of N₂O(g) and HNO₂(g) reach to 10^{−7} mol level at 1273–1373 K, HNO(g) at 1975 K; NO₂(g) reach to 10^{−5} mol at 773–873 K and NO(g) at 673–773 K gaining the 10^{−2}–10^{−1} mol level at 2073 K.

The same changes can be followed after the increase in the content of Mg(OH)₂(s) and Ca(OH)₂(s) at temperatures up to 500–600 K and 800–1000 K, respectively. Here, the content of Ca, Mg-carbonates and -hydroxides starts to decrease with temperature resulting in the formation and increase in the content of solid CaO₂, MgO₂, CaO and MgO and gaseous CO, CO₂, HO, H₂. The content of gaseous compounds like O₂, N₂ and H₂O does not change in the temperature interval from 273 K to 2073 K.

It can be seen in the equilibrium diagrams of AN with Ca, Mg-carbonates as well as of AN with CaO(s) or MgO(s) that the content of NO₂(g) and N₂O(g) in equilibrium differed slightly (6–7%) as compared to their content in the case of pure ammonium nitrate, thereby, the NO(g) content does not differ at all (Table 2).

At constant temperature and while keeping the amount of AN constant on the level of 2 mol, the equilibrium amount of gaseous compounds does not depend on the content of carbonates varied between 0.2 and 2.1 mol.

Equilibrium in the multi-component system based on AN–CaCO₃/CaMg(CO₃)₂–Cu, B, Mn additives at the mole ratio of 2:1/0.5:0.01 and 2:1/0.5:0.05

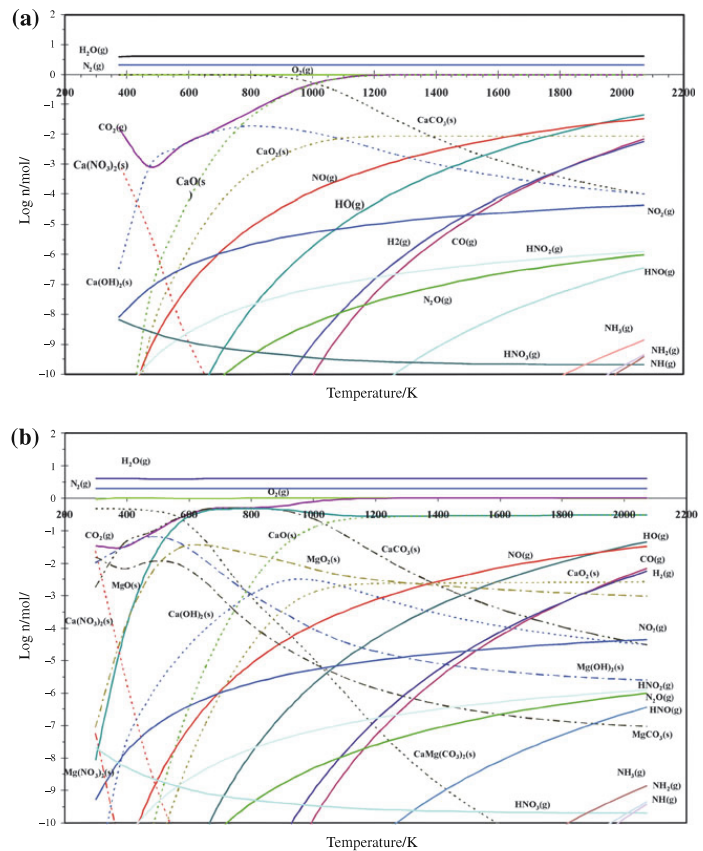
CuSO₄

In the systems with CuSO₄(s) additive it can be seen that in addition to nitrogen-containing gases also sulphur-containing gaseous compounds like H₂S, HS, SO, SO₂ and SO₃ are present in the equilibrium mixture (Fig. 2, Table 3). The content of nitrogen-containing gases does not depend on the content of CuSO₄(s) (whether 0.01 or 0.05 mol) in the system. The content of sulphur-containing gases is proportionally higher at higher content of CuSO₄(s) (Table 3).

Comparing the systems with CuSO₄(s) additive based on AN with and without carbonates, there are no differences in the content of NO(g) in gaseous phase in the temperature interval from 373 to 2073 K. The content of NO₂(g) and N₂O(g) is on the same level at lower temperatures, but in the systems with carbonates, the increase in temperature is accompanied by the decrease in the content of both gases of about 7–8% (Table 3).

At lower temperatures up to 773–873 K the amount of SO₂(g) and SO₃(g) in equilibrium is 10^{−15}–10^{−19} mol in the system of AN with carbonates, and 10^{−3}–10^{−5} mol without carbonates. The content of SO(g) is 10^{−34}–10^{−35} mol and 10^{−21} mol, respectively, in the system with or without carbonates. At intermediate temperatures between

Fig. 1 Temperature dependencies of equilibrium amounts of compounds (log n, mol) in the system $2\text{NH}_4\text{NO}_3\text{--CaCO}_3$ (a) and $2\text{NH}_4\text{NO}_3\text{--}0.5\text{CaMg}(\text{CO}_3)_2$ (b)



873 and 1473 K the $\text{SO}_2(\text{g})$ and $\text{SO}_3(\text{g})$ content is 10^{-6} – 10^{-9} mol and the content is $\text{SO}(\text{g})$ 10^{-15} – 10^{-16} mol with carbonates. Without carbonates these amounts are 10^{-2} – 10^{-4} mol and 10^{-10} mol, respectively. At temperatures above 1473 K the content of $\text{SO}_2(\text{g})$ and $\text{SO}_3(\text{g})$ is 10^{-2} – 10^{-5} mol and of $\text{SO}(\text{g})$ 10^{-6} – 10^{-7} mol in both systems—with and without carbonates (Table 3, Fig. 2).

It can be seen that in the system of AN with $\text{CuSO}_4(\text{s})$, at the mole ratio of AN/CuSO_4 , 1/0.01 or 1/0.05 the content of $\text{CuSO}_4(\text{s})$ began to decrease at 700–800 K being at 1273 K on the levels of 1.26×10^{-7} and 3.16×10^{-6} , and at 1773 K 6.76×10^{-12} and 1.70×10^{-10} mol, respectively. One intermediate Cu-containing compound is $\text{Cu}(\text{OH})_2(\text{s})$, but its maximum content at 873–973 K does not exceed 10^{-6} mol. The content of $\text{CuO}(\text{s})$ at 973–1073 K reaches 10^{-2} mol and the same level of $\text{Cu}_2\text{O}(\text{s})$ can be seen at 1273–1373 K (Fig. 2a).

In the system of AN and carbonates with $\text{CuSO}_4(\text{s})$, the $\text{Cu}(\text{OH})_2(\text{s})$ content decreases from 10^{-3} mol at 473 K to

10^{-7} mol at temperatures higher than 1073–1373 K. The content of $\text{CuO}(\text{s})$ is 10^{-3} – 10^{-2} mol in the broad temperature interval studied—from 373 K up to 2073 K. The content of $\text{Cu}_2\text{O}(\text{s})$ reaches 10^{-5} mol at 873–1073 K and 10^{-3} – 10^{-2} mol at 1573 K. The content of $\text{CaSO}_4(\text{s})$ is constant— 10^{-2} mol up to 1400–1500 K and decreases to 10^{-4} mol at 2073 K. The amount of $\text{MgSO}_4(\text{s})$ varies in between 10^{-3} – 10^{-2} mol along the temperature range from 373 to 2073 K. The $\text{CaSO}_3(\text{s})$ and $\text{MgSO}_3(\text{s})$ content reaches the maximum of 10^{-5} and 10^{-12} mol, respectively, at 1773 K and 1573 K. (Fig. 2b, c).

H_3BO_3

Comparing the systems with $\text{H}_3\text{BO}_3(\text{s})$ additive based on AN with carbonates or without carbonates, the content of $\text{NO}(\text{g})$ remains practically on the same level at any temperature in all the systems studied. The $\text{NO}_2(\text{g})$ and $\text{N}_2\text{O}(\text{g})$ content at lower temperatures is also on the same

Table 2 Equilibrium concentrations of NO, NO₂ and N₂O at different temperatures

System	Amount of compound/mol		
	NO	NO ₂	N ₂ O
Temperature/K			
NH₄NO₃ (AN)			
773	5.01×10^{-6}	1.75×10^{-6}	2.70×10^{-10}
1273	1.26×10^{-3}	1.31×10^{-5}	4.43×10^{-8}
1773	1.38×10^{-2}	3.32×10^{-5}	4.39×10^{-7}
2AN + CaCO₃			
773	5.01×10^{-6}	1.74×10^{-6}	2.70×10^{-10}
1273	1.24×10^{-3}	1.22×10^{-5}	4.16×10^{-8}
1773	1.38×10^{-2}	3.14×10^{-5}	4.09×10^{-7}
2AN + MgCO₃			
773	4.94×10^{-6}	1.60×10^{-6}	2.51×10^{-10}
1273	1.24×10^{-3}	1.22×10^{-5}	4.14×10^{-8}
1773	1.38×10^{-2}	3.12×10^{-5}	4.10×10^{-7}
2AN + 0.5CaMg(CO₃)₂			
773	4.97×10^{-6}	1.67×10^{-6}	2.61×10^{-10}
1273	1.24×10^{-3}	1.22×10^{-5}	4.16×10^{-8}
1773	1.38×10^{-2}	3.14×10^{-5}	4.10×10^{-7}
2AN + CaO			
773	5.01×10^{-6}	1.80×10^{-6}	2.79×10^{-10}
1273	1.24×10^{-3}	1.30×10^{-5}	4.42×10^{-8}
1773	1.38×10^{-2}	3.31×10^{-5}	4.37×10^{-7}
2AN + MgO			
773	4.93×10^{-6}	1.70×10^{-6}	2.70×10^{-10}
1273	1.24×10^{-3}	1.30×10^{-5}	4.43×10^{-8}
1773	1.38×10^{-2}	3.32×10^{-5}	4.39×10^{-7}

level, but when increasing the temperature, the increase in the content of both gases is about 7–8%, like it is in the case of CuSO₄(s) additive (Table 3).

The most probable gaseous compound of boron formed in these systems is HBO(g) whose content seems to be on the level of the added amount of H₃BO₃(s) -1×10^{-2} or 5×10^{-2} mol. The content of the other gaseous boron compounds, like H₃BO₂, HBO₂, BO₂, BO is 10^{-35} – 10^{-11} mol and their content is increasing with temperature (Table 3).

MnO₂

No differences in the content of N-containing gaseous compounds were found, when comparing AN–carbonates systems with and without MnO₂(s) additive, as well as when comparing with these based on pure AN with MnO₂(s) (Tables 2 and 3).

The content of MnO₂(s), MnO(s) and Mn(OH)₂(s) was 3–15 times higher (Table 3) and that of Mn₃O₄(s) and Mn₂O₃(s) 10^3 – 10^1 times lower in the systems with carbonates as compared to the systems without carbonates.

Probable reactions

Considering the data from equilibrium calculations and that thermodynamically the most probable (present in the highest amounts) Ca, Mg-containing compounds were CaO(s), MgO(s), CaO₂(s), MgO₂(s), Ca(OH)₂(s), Mg(OH)₂(s), Ca(NO₃)₂(s) and Mg(NO₃)₂(s) and N-containing compounds NO(g), NO₂(g) and N₂O(g), the temperature dependencies of Gibbs free energy changes ΔG_T were calculated for reactions (R) 1–116 in the temperature range of 273–2073 K to estimate the most probable reactions in the systems studied (Table 1). The calculations were based on the initial amount of two moles of AN.

System 2AN–CaCO₃/0.5CaMg(CO₃)₂

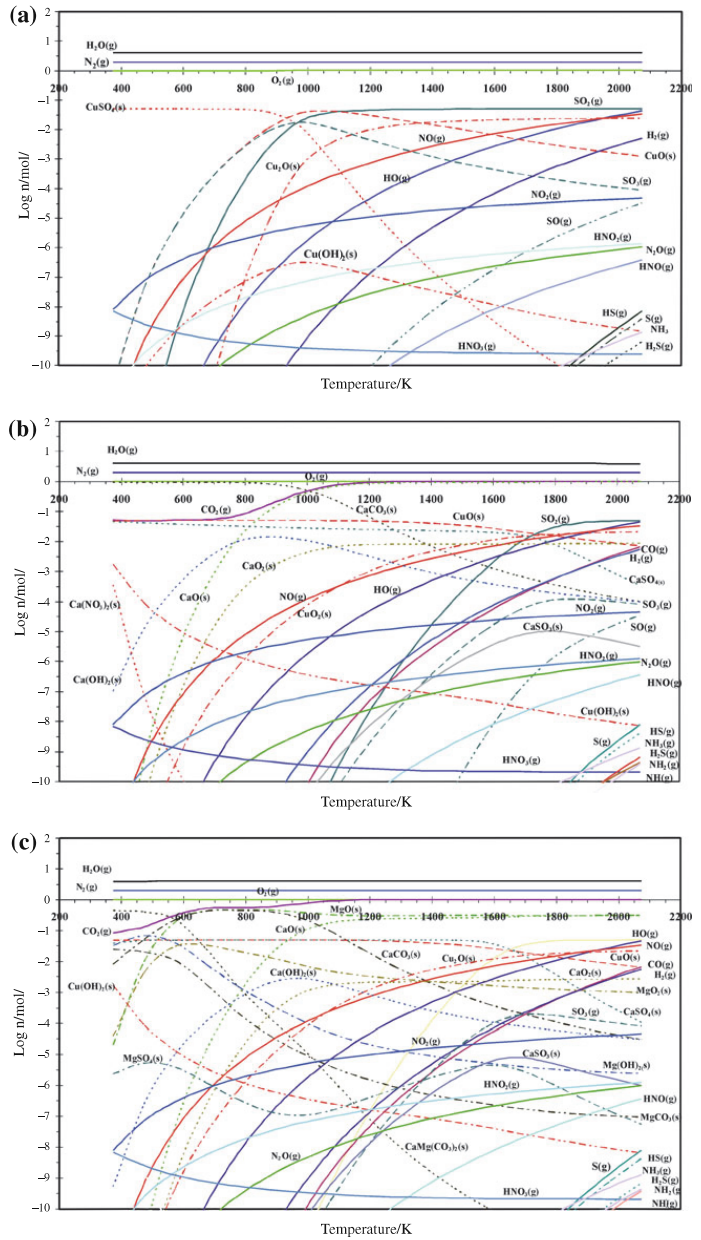
Reactions in the 2AN–CaCO₃ system with the simultaneous formation of NO(g) and N₂(g) are more probable than those where only NO(g) is formed. The NO₂(g) or N₂O(g) formation becomes more probable at a higher content of the simultaneously formed N₂(g) in the system. Most of these reactions are already probable at room temperature or over 373–473 K (Fig. 3). For example, if simultaneous formation of NO(g) and N₂(g) is assumed (R 5, 7, 9), the formation of Ca(OH)₂(s), CaO(s) and CaO₂(s) is already probable at room temperature, but if only the formation of NO(g) is assumed (R 4, 6, 8), the Ca(OH)₂(s) and CaO(s) formation becomes probable at temperatures over 600–620 K and CaO₂(s) over 850 K. The formation of Ca(NO₃)₂(s) together with NO(g) and N₂(g) (R 3) is probable at temperatures over 1000 K, but with N₂(g) alone (R 2), over 473 K (Fig. 3a).

The formation of 2 mol of NO₂(g) with 1 mol of N₂(g) (R 13, 15, 17) instead of 2.5 or 3 mol of NO₂(g) with 0.75 or 1 mol of N₂(g) (R 12, 14, 16) shifts the temperature of possible formation of Ca(OH)₂(s) and CaO(s) from 370–420 K to 680 and 980 K, respectively, and of CaO₂(s) formation from 680 to 980 K. The formation of Ca(NO₃)₂(s) with NO(g) and N₂(g) as reaction products becomes probable at $T > 973$ K, and with N₂(g) alone, at $T > 473$ K (Fig. 3b).

The formation of N₂O(g) (with or without N₂(g)) and solid phases like Ca(OH)₂, CaO and CaO₂ is already probable at room temperature and is definitely more probable than the explosive decomposition of AN. The formation of Ca(NO₃)₂(s) with N₂O(g) becomes probable at $T > 1170$ K and with N₂(g) over 470 K (Fig. 3c).

In the system 2AN–0.5CaMg(CO₃)₂ with NO(g) as the gaseous product, the formation of Ca(OH)₂(s) and Mg(OH)₂(s) (R 64) becomes probable at $T > 590$ K; CaO(s) and MgO(s) (R 66) at $T > 600$ K, and CaO₂(s) and MgO₂(s) (R 65) at $T > 810$ K i.e. at 20–40 K lower temperatures than in the case of the respective reactions in the

Fig. 2 Temperature dependencies of equilibrium amounts of compounds (log n, mol) in the system $2\text{NH}_4\text{NO}_3-0.05\text{CuSO}_4$ (a), $2\text{NH}_4\text{NO}_3-\text{CaCO}_3-0.05\text{CuSO}_4$ (b) and $2\text{NH}_4\text{NO}_3-0.5\text{CaMg}(\text{CO}_3)_2-0.05\text{CuSO}_4$ (c)



system $2\text{AN}-\text{CaCO}_3$. Thereby, the formation of $\text{Ca}(\text{NO}_3)_2(\text{s})$, $\text{Mg}(\text{NO}_3)_2(\text{s})$ and $\text{NO}(\text{g})$ with the simultaneous formation of $\text{N}_2(\text{g})$ (R63) becomes probable at $T > 1050$ K or if only $\text{N}_2(\text{g})$ (and no $\text{NO}(\text{g})$) is formed (R 64), at $T > 530$ K, i.e. at 50–60 K higher temperatures than in the case of the system $2\text{AN}-\text{CaCO}_3$ (Fig. 4).

The formation of $\text{NO}_2(\text{g})$ and $\text{N}_2(\text{g})$ as N-containing gaseous compounds with $\text{Ca}(\text{OH})_2(\text{s})$ and $\text{Mg}(\text{OH})_2(\text{s})$ (R 82) is probable at temperatures over 373 K, with $\text{CaO}_2(\text{s})$ and $\text{MgO}_2(\text{s})$ (R 83) over 640 K, and with $\text{CaO}(\text{s})$ and $\text{MgO}(\text{s})$ (R 84) over 400 K i.e. at 20–50 K lower temperatures than in the system $2\text{AN}-\text{CaCO}_3$. Reactions with $\text{Ca}(\text{NO}_3)_2(\text{s})$,

Table 3 Equilibrium concentrations of different compounds at different temperatures

System	Amount of compound/mol					
	NO	NO ₂	N ₂ O	SO	SO ₂	SO ₃
2AN + 0.01CuSO₄						
773	5.01×10^{-6}	1.75×10^{-6}	2.70×10^{-10}	3.16×10^{-21}	3.24×10^{-5}	7.08×10^{-4}
1273	1.26×10^{-3}	1.31×10^{-5}	4.43×10^{-8}	1.02×10^{-10}	9.55×10^{-3}	5.24×10^{-4}
1773	1.38×10^{-2}	3.32×10^{-5}	4.39×10^{-7}	3.39×10^{-7}	1.10×10^{-3}	4.37×10^{-5}
2AN + 0.05CuSO₄						
773	5.01×10^{-6}	1.75×10^{-6}	2.70×10^{-10}	7.24×10^{-21}	7.40×10^{-5}	1.62×10^{-3}
1273	1.26×10^{-3}	1.31×10^{-5}	4.43×10^{-8}	5.13×10^{-10}	4.79×10^{-2}	2.69×10^{-3}
1773	1.38×10^{-2}	3.32×10^{-5}	4.39×10^{-7}	1.70×10^{-6}	5.01×10^{-2}	2.19×10^{-4}
2AN + CaCO₃ + 0.01CuSO₄						
773	5.01×10^{-6}	1.75×10^{-6}	2.70×10^{-10}	3.23×10^{-35}	3.31×10^{-19}	7.08×10^{-18}
1273	1.26×10^{-3}	1.22×10^{-5}	4.17×10^{-8}	6.76×10^{-16}	5.82×10^{-8}	3.09×10^{-9}
1773	1.38×10^{-2}	3.16×10^{-5}	4.10×10^{-7}	1.86×10^{-7}	5.01×10^{-3}	2.04×10^{-5}
2AN + CaCO₃ + 0.05CuSO₄						
773	5.01×10^{-6}	1.75×10^{-6}	2.70×10^{-10}	2.63×10^{-34}	2.69×10^{-18}	5.89×10^{-17}
1273	1.26×10^{-3}	1.23×10^{-5}	4.17×10^{-8}	3.55×10^{-15}	3.09×10^{-7}	1.58×10^{-8}
1773	1.38×10^{-2}	3.16×10^{-5}	4.12×10^{-7}	9.20×10^{-7}	2.51×10^{-2}	1.04×10^{-4}
2AN + 0.5CaMg(CO₃)₂ + 0.01CuSO₄						
773	5.01×10^{-6}	1.66×10^{-6}	2.70×10^{-10}	3.23×10^{-35}	6.92×10^{-17}	1.45×10^{-15}
1273	1.26×10^{-3}	1.22×10^{-5}	4.17×10^{-8}	6.76×10^{-16}	2.34×10^{-6}	1.20×10^{-7}
1773	1.38×10^{-2}	3.16×10^{-5}	4.10×10^{-7}	1.86×10^{-7}	4.47×10^{-2}	1.86×10^{-4}
2AN + 0.5CaMg(CO₃)₂ + 0.05CuSO₄						
773	5.01×10^{-6}	1.70×10^{-6}	2.70×10^{-10}	2.63×10^{-34}	6.93×10^{-17}	1.44×10^{-15}
1273	1.26×10^{-3}	1.23×10^{-5}	4.17×10^{-8}	3.55×10^{-15}	2.32×10^{-6}	1.20×10^{-7}
1773	1.38×10^{-2}	3.16×10^{-5}	4.12×10^{-7}	9.20×10^{-7}	4.47×10^{-2}	1.86×10^{-4}
Temperature/K	NO	NO ₂	N ₂ O	HBO	HBO ₂	BO ₂
2AN + 0.01H₃BO₃						
773	5.01×10^{-6}	1.73×10^{-6}	2.69×10^{-10}	1×10^{-2}	7.41×10^{-25}	7.50×10^{-31}
1273	1.26×10^{-3}	1.32×10^{-5}	4.47×10^{-8}	1×10^{-2}	8.51×10^{-18}	1.32×10^{-20}
1773	1.38×10^{-2}	3.32×10^{-5}	4.37×10^{-7}	1×10^{-2}	9.77×10^{-15}	3.98×10^{-16}
2AN + 0.05 H₃BO₃						
773	5.01×10^{-6}	1.73×10^{-6}	2.69×10^{-10}	5×10^{-2}	3.72×10^{-24}	3.80×10^{-30}
1273	1.26×10^{-3}	1.32×10^{-5}	4.47×10^{-8}	5×10^{-2}	3.98×10^{-17}	6.61×10^{-20}
1773	1.38×10^{-2}	3.32×10^{-5}	4.37×10^{-7}	5×10^{-2}	5.01×10^{-14}	2.00×10^{-15}
2AN + CaCO₃ + 0.01 H₃BO₃						
773	5.01×10^{-6}	1.74×10^{-6}	2.69×10^{-10}	1×10^{-2}	7.41×10^{-25}	7.58×10^{-31}
1273	1.25×10^{-3}	1.22×10^{-5}	4.16×10^{-8}	1×10^{-2}	7.94×10^{-18}	1.28×10^{-20}
1773	1.38×10^{-2}	3.16×10^{-5}	4.09×10^{-7}	1×10^{-2}	9.33×10^{-15}	3.89×10^{-16}
2AN + CaCO₃ + 0.05 H₃BO₃						
773	5.01×10^{-6}	1.73×10^{-6}	2.69×10^{-10}	5×10^{-2}	3.71×10^{-24}	3.80×10^{-30}
1273	1.26×10^{-3}	1.26×10^{-5}	4.17×10^{-8}	5×10^{-2}	3.98×10^{-17}	6.46×10^{-20}
1773	1.38×10^{-2}	3.16×10^{-5}	4.11×10^{-7}	5×10^{-2}	4.68×10^{-14}	1.90×10^{-15}
2AN + 0.5CaMg(CO₃)₂ + 0.01 H₃BO₃						
773	5.01×10^{-6}	1.72×10^{-6}	2.65×10^{-10}	1×10^{-2}	7.24×10^{-25}	7.31×10^{-31}
1273	1.26×10^{-3}	1.23×10^{-5}	4.16×10^{-8}	1×10^{-2}	7.94×10^{-18}	1.29×10^{-20}
1773	1.38×10^{-2}	3.16×10^{-5}	4.10×10^{-7}	1×10^{-2}	9.24×10^{-15}	3.80×10^{-16}

Table 3 continued

Temperature/K	NO	NO ₂	N ₂ O	HBO	HBO ₂	BO ₂
2AN + 0.5CaMg(CO ₃) ₂ + 0.05 H ₃ BO ₃						
773	5.01 × 10 ⁻⁶	1.71 × 10 ⁻⁶	2.63 × 10 ⁻¹⁰	5 × 10 ⁻²	3.63 × 10 ⁻²⁴	3.71 × 10 ⁻³⁰
1273	1.26 × 10 ⁻³	1.24 × 10 ⁻⁵	4.17 × 10 ⁻⁸	5 × 10 ⁻²	3.98 × 10 ⁻¹⁷	6.46 × 10 ⁻²⁰
1773	1.38 × 10 ⁻²	3.16 × 10 ⁻⁵	4.12 × 10 ⁻⁷	5 × 10 ⁻²	4.67 × 10 ⁻¹⁴	1.92 × 10 ⁻¹⁵
Temperature/K	NO	NO ₂	N ₂ O	MnO	MnO ₂	Mn(OH) ₂
2AN + 0.01MnO ₂						
773	5.01 × 10 ⁻⁶	1.73 × 10 ⁻⁶	2.69 × 10 ⁻¹⁰	3.00 × 10 ⁻⁶	2.92 × 10 ⁻³	3.63 × 10 ⁻¹¹
1273	1.26 × 10 ⁻³	1.32 × 10 ⁻⁵	4.45 × 10 ⁻⁸	4.75 × 10 ⁻⁴	1.41 × 10 ⁻⁴	2.32 × 10 ⁻¹²
1773	1.38 × 10 ⁻²	3.32 × 10 ⁻⁵	4.37 × 10 ⁻⁷	3.60 × 10 ⁻³	3.36 × 10 ⁻⁵	1.47 × 10 ⁻¹³
2AN + 0.05 MnO ₂						
773	5.01 × 10 ⁻⁶	1.73 × 10 ⁻⁶	2.69 × 10 ⁻¹⁰	1.50 × 10 ⁻⁵	1.47 × 10 ⁻²	1.81 × 10 ⁻¹⁰
1273	1.26 × 10 ⁻³	1.31 × 10 ⁻⁵	4.47 × 10 ⁻⁸	2.40 × 10 ⁻³	7.07 × 10 ⁻⁴	1.15 × 10 ⁻¹¹
1773	1.38 × 10 ⁻²	3.32 × 10 ⁻⁵	4.45 × 10 ⁻⁷	1.80 × 10 ⁻²	1.69 × 10 ⁻⁴	7.31 × 10 ⁻¹³
2AN + CaCO ₃ + 0.01 MnO ₂						
773	5.01 × 10 ⁻⁶	1.73 × 10 ⁻⁶	2.69 × 10 ⁻¹⁰	9.86 × 10 ⁻⁶	9.57 × 10 ⁻³	1.18 × 10 ⁻¹⁰
1273	1.25 × 10 ⁻³	1.25 × 10 ⁻⁵	4.17 × 10 ⁻⁸	6.08 × 10 ⁻³	1.69 × 10 ⁻³	2.60 × 10 ⁻¹¹
1773	1.38 × 10 ⁻²	3.16 × 10 ⁻⁵	4.07 × 10 ⁻⁷	9.86 × 10 ⁻³	8.59 × 10 ⁻⁵	3.52 × 10 ⁻¹³
2AN + CaCO ₃ + 0.05 MnO ₂						
773	5.01 × 10 ⁻⁶	1.73 × 10 ⁻⁶	2.69 × 10 ⁻¹⁰	4.33 × 10 ⁻⁵	4.21 × 10 ⁻²	5.18 × 10 ⁻¹⁰
1273	1.24 × 10 ⁻³	1.26 × 10 ⁻⁵	4.16 × 10 ⁻⁸	1.90 × 10 ⁻²	5.30 × 10 ⁻³	8.12 × 10 ⁻¹¹
1773	1.38 × 10 ⁻²	3.16 × 10 ⁻⁵	4.16 × 10 ⁻⁷	4.81 × 10 ⁻²	4.22 × 10 ⁻⁴	1.71 × 10 ⁻¹²
2AN + 0.5CaMg(CO ₃) ₂ + 0.01 MnO ₂						
773	5.01 × 10 ⁻⁶	1.66 × 10 ⁻⁶	2.63 × 10 ⁻¹⁰	1.07 × 10 ⁻⁵	9.99 × 10 ⁻³	1.20 × 10 ⁻¹⁰
1273	1.26 × 10 ⁻³	1.22 × 10 ⁻⁵	4.17 × 10 ⁻⁸	7.34 × 10 ⁻³	2.03 × 10 ⁻³	3.13 × 10 ⁻¹¹
1773	1.38 × 10 ⁻²	3.16 × 10 ⁻⁵	4.07 × 10 ⁻⁷	9.91 × 10 ⁻³	8.64 × 10 ⁻⁵	3.54 × 10 ⁻¹³
2AN + 0.5CaMg(CO ₃) ₂ + 0.05 MnO ₂						
773	5.01 × 10 ⁻⁶	1.66 × 10 ⁻⁶	2.57 × 10 ⁻¹⁰	5.32 × 10 ⁻⁵	4.98 × 10 ⁻²	6.00 × 10 ⁻¹⁰
1273	1.26 × 10 ⁻³	1.24 × 10 ⁻⁵	4.16 × 10 ⁻⁸	2.37 × 10 ⁻²	6.61 × 10 ⁻³	1.01 × 10 ⁻¹⁰
1773	1.38 × 10 ⁻²	3.16 × 10 ⁻⁵	4.16 × 10 ⁻⁷	4.94 × 10 ⁻²	2.73 × 10 ⁻⁴	8.09 × 10 ⁻¹³

Mg(NO₃)₂(s) and NO₂(g) + N₂(g) formation (R 80) are probable at $T > 1000$ K, and with only N₂(g) formation (R 81) at $T > 540$ K or at 50 K higher temperature than in the system 2AN–CaCO₃.

The formation of N₂O(g) (with or without N₂(g)) along with Ca(OH)₂(s) and Mg(OH)₂(s), CaO(s) and MgO(s) or CaO₂(s) and MgO₂(s) (R 99–104) is also probable at room temperature like in the system 2AN–CaCO₃. Ca(NO₃)₂(s) and Mg(NO₃)₂(s) formation with N₂O(g) (R98) is probable at temperatures over 1200 K and with N₂(g) (R 97) over 550 K which is by 30 K (R 98) and 80 K (R 97) higher than in 2AN–CaCO₃ system.

System 2AN–CaCO₃/0.5CaMg(CO₃)₂–CuSO₄, H₃BO₃ or MnO₂

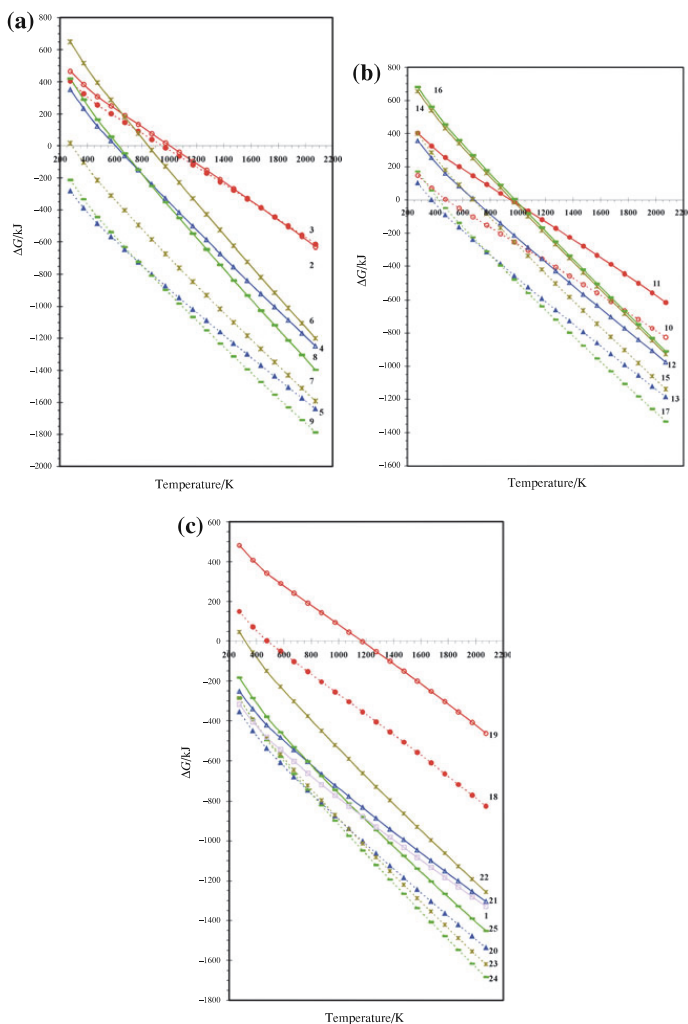
The influence of CuSO₄(s), H₃BO₃(s) and MnO₂(s) additive (initial amount 0.05 mol) in the systems 2AN–CaCO₃

and 2AN–0.5CaMg(CO₃)₂ on the temperature dependencies of ΔG_T for the reactions between AN(s) and CaCO₃(s) or AN(s) and CaMg(CO₃)₂(s) with the NO(g), NO₂(g) or N₂O(g) formation as gaseous N-containing compounds and CaO(s), MgO(s); CaO₂(s), MgO₂(s); Ca(OH)₂(s), Mg(OH)₂(s) and Ca(NO₃)₂(s), Mg(NO₃)₂(s) as solids was minor (shift by 5–10 K) or was absent at all.

CuSO₄(s) additive (0.5 mol) shifted the probability of the formation of NO(g), Ca(NO₃)₂(s) and Mg(NO₃)₂(s) (R 26, 68) 70–80 K towards higher temperatures as compared to that without the additive (R 3, 63) and the formation of Ca(OH)₂(s) and Mg(OH)₂(s), CaO₂(s) and MgO₂(s), CaO(s) and MgO(s) as solids and NO(g) (R 27–29, R 69–71) 20–50 K towards lower temperatures (Table 4, Figs. 3a, 4).

The temperature of probable NO₂(g) formation is increased, depending on the solid compound formed, 40–100 K towards higher temperatures (R 30–33, R 85–88) (Table 4, Fig. 3b).

Fig. 3 Temperature dependencies of Gibbs free energy changes ΔG_T in the system $2\text{NH}_4\text{NO}_3\text{-CaCO}_3$ with formation of NO (a) (reactions 2–9), NO_2 (b) (reactions 10–17) and N_2O (c) (reactions 1, 18–25)

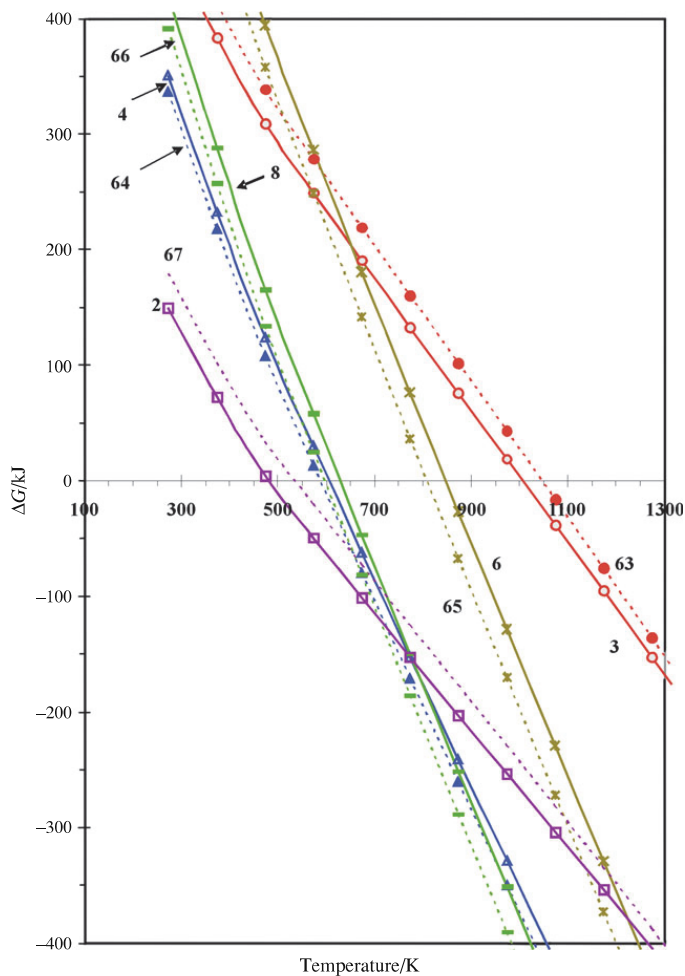


The $\text{N}_2\text{O}(\text{g})$ formation together with $\text{Ca}(\text{OH})_2(\text{s})$ and $\text{Mg}(\text{OH})_2(\text{s})$ $\text{CaO}_2(\text{s})$ and $\text{MgO}_2(\text{s})$ $\text{CaO}(\text{s})$ and $\text{MgO}(\text{s})$ (R 35–37; R 106–108) is probable at room temperature, however, these reactions are less probable (ΔG_T values are higher) as compared to those in the system without the CuSO_4 additive (R 21, 22, 25; R 99, 101, 104). The temperature at which the reactions with the formation of Ca, Mg-nitrates in the additive-containing system becomes probable is moved in the system $2\text{AN-0.5CaMg}(\text{CO}_3)_2$ 130 K (R 98, 105) and in the system 2AN-CaCO_3 170 K (R 19, 34) towards lower temperatures—respectively, to 1050 K and 1000 K (Table 4, Fig. 3c).

$\text{H}_3\text{BO}_3(\text{s})$ additive (0.5 mol) in the system 2AN-CaCO_3 and $2\text{AN-0.5CaMg}(\text{CO}_3)_2$, practically, does not influence the temperature dependencies of ΔG_T of the reactions between AN and $\text{CaCO}_3(\text{s})$ or $\text{CaMg}(\text{CO}_3)_2(\text{s})$ with the formation of solid Ca, Mg-nitrates and $\text{NO}(\text{g})$ (R 38, 3; R 72, 63), but in the case of formation of $\text{Ca}(\text{OH})_2(\text{s})$ and $\text{Mg}(\text{OH})_2(\text{s})$ $\text{CaO}_2(\text{s})$ and $\text{MgO}_2(\text{s})$ $\text{CaO}(\text{s})$ and $\text{MgO}(\text{s})$ (R 40–42, 4, 6, 8; R 73–75, R 64–66), the temperatures at which these reactions become probable are decreased by 170–260 K (Table 4, Figs. 3a, 4).

The formation temperatures of $\text{NO}_2(\text{g})$ are decreased by 30 K (R 43, 45–46, 11, 14, 16; R 85, 87–88, 80, 83–84)

Fig. 4 Temperature dependencies of Gibbs free energy changes ΔG_T in the systems $2\text{NH}_4\text{NO}_3\text{--CaCO}_3$ and $2\text{NH}_4\text{NO}_3\text{--}0.5\text{CaMg}(\text{CO}_3)_2$ with formation of NO (reactions 2–4, 6, 8, 63–67)



except for the reactions with Ca,Mg-hydroxides formation (R 40, 12; R 90, 82) in the case of which these are shifted 20–30 K towards higher temperatures (Table 4, Fig. 3b).

The $\text{N}_2\text{O}(\text{g})$, and $\text{Ca}(\text{NO}_3)_2(\text{s})$, and $\text{Mg}(\text{NO}_3)_2(\text{s})$ formation in the presence of $\text{H}_3\text{BO}_3(\text{s})$ can take place at 700 K (R 47) instead of 1170 K (R 19) as in the system 2AN--CaCO_3 and at 750 K (R 109) instead of 1210 K (R 98) as in the system $2\text{AN--}0.5\text{CaMg}(\text{CO}_3)_2$ (Table 4, Fig. 3c). The formation of the other solid phases studied can occur at room temperature (R48–50; R 110–112), however, these reactions are less probable as compared to these in the system without the boron additive (R 21–22, 25; R 99, 101, 104).

$\text{MnO}_2(\text{s})$ additive (0.5 mol) in the system 2AN--CaCO_3 and $2\text{AN--}0.5\text{CaMg}(\text{CO}_3)_2$ moves the temperatures of $\text{NO}(\text{g})$ formation together with $\text{Ca}(\text{NO}_3)_2(\text{s})$ and $\text{Mg}(\text{NO}_3)_2(\text{s})$ 70–80 K in the direction of higher temperatures

(R 51, 3; R 76, 63) and with $\text{Ca}(\text{OH})_2(\text{s})$ and $\text{Mg}(\text{OH})_2(\text{s})$; $\text{CaO}_2(\text{s})$ and $\text{MgO}_2(\text{s})$; $\text{CaO}(\text{s})$ and $\text{MgO}(\text{s})$ 60–70 K towards lower temperatures (R 52–54; R 77–79) as compared to the temperatures without manganese dioxide additive in the system (R 4, 6, 8; R 64–66) (Table 4, Figs. 3a, 4).

The temperature of probable $\text{NO}_2(\text{g})$ formation with $\text{Ca}(\text{NO}_3)_2(\text{s})$ as the solid product in AN--CaCO_3 system is increased up to 320 K (R 55, 11) and of the formation of the other solid phases under consideration by 40–70 K towards higher temperatures (R 56–58, 12, 14, 16; R 93–96, 80, 82–84) (Table 4, Fig. 3b).

In the presence of the additive, the temperature of the probable formation of $\text{N}_2\text{O}(\text{g})$ and Ca, Mg-nitrates(s) is shifted by 160 K in $2\text{AN--}0.5\text{CaMg}(\text{CO}_3)_2$ system (R 113, 98) and by 200 K in 2AN--CaCO_3 system (R 59, 19) in the

Table 4 The influence of CuSO_4 , H_3BO_3 and MnO_2 additive on the change in temperature/ $\pm \Delta T/\text{K}$ at which reactions in the system $2\text{AN}-\text{CaCO}_3$ and $2\text{AN}-0.5\text{CaMg}(\text{CO}_3)_2$ become thermodynamically probable

System Solid compound	N-containing gaseous compound		
	NO	NO_2	N_2O
$2\text{AN} + \text{CaCO}_3 + 0.5\text{CuSO}_4$			
$\text{Ca}(\text{NO}_3)_2$	+80	+80	-170
$\text{Ca}(\text{OH})_2$	-30	+90	At room temperature,
CaO_2	-50	+50	But less probable
CaO	-30	+50	Than without additive
$2\text{AN} + 0.5\text{CaMg}(\text{CO}_3)_2 + 0.5\text{CuSO}_4$			
$\text{Ca}(\text{NO}_3)_2, \text{Mg}(\text{NO}_3)_2$	+70	+90	-130
$\text{Ca}(\text{OH})_2, \text{Mg}(\text{OH})_2$	-20	+100	At room temperature,
$\text{CaO}_2, \text{MgO}_2$	-40	+70	But less probable
CaO, MgO	-30	+40	Than without additive
$2\text{AN} + \text{CaCO}_3 + 0.5\text{H}_3\text{BO}_3$			
$\text{Ca}(\text{NO}_3)_2$	+10	-30	-470
$\text{Ca}(\text{OH})_2$	-190	+30	At room temperature,
CaO_2	-260	-20	But less probable
CaO	-180	-20	Than without additive
$2\text{AN} + 0.5\text{CaMg}(\text{CO}_3)_2 + 0.5\text{H}_3\text{BO}_3$			
$\text{Ca}(\text{NO}_3)_2, \text{Mg}(\text{NO}_3)_2$	~ 0	-30	-460
$\text{Ca}(\text{OH})_2, \text{Mg}(\text{OH})_2$	-180	+20	At room temperature,
$\text{CaO}_2, \text{MgO}_2$	-210	~ 0	But less probable
CaO, MgO	-170	-20	Than without additive
$2\text{AN} + \text{CaCO}_3 + 0.5\text{MnO}_2$			
$\text{Ca}(\text{NO}_3)_2$	+80	+320	-200
$\text{Ca}(\text{OH})_2$	-70	+70	At room temperature,
CaO_2	-70	+50	But less probable
CaO	-60	+40	Than without additive
$2\text{AN} + 0.5\text{CaMg}(\text{CO}_3)_2 + 0.5\text{MnO}_2$			
$\text{Ca}(\text{NO}_3)_2, \text{Mg}(\text{NO}_3)_2$	+70	+70	-160
$\text{Ca}(\text{OH})_2, \text{Mg}(\text{OH})_2$	-70	+40	At room temperature,
$\text{CaO}_2, \text{MgO}_2$	-60	+60	But less probable
CaO, MgO	-70	+50	Than without additive

direction of lower temperatures—from 1170 to 970 K and from 1210 to 1050 K, respectively (Table 4, Fig. 3c). The solid phases like $\text{Ca}(\text{OH})_2(\text{s})$ and $\text{Mg}(\text{OH})_2(\text{s})$; $\text{CaO}_2(\text{s})$ and $\text{MgO}_2(\text{s})$; $\text{CaO}(\text{s})$ and $\text{MgO}(\text{s})$ can form at room temperature (R 60–62; R 114–116), but these reactions are also less probable as compared to those in the system without MnO_2 additive (R21–22, 25; R 99, 101, 104).

Conclusions

Thermodynamic analysis of the systems of AN with and without Ca and Mg carbonates with and without the presence of CuSO_4 , H_3BO_3 or MnO_2 additive was carried out

using the HSC software and getting the basics for future TA-measurements.

The list of the main compounds and their content in the equilibrium mixtures do not depend notably on the origin of Ca,Mg-carbonates. The main solid compounds that can form in the systems of AN and Ca,Mg-carbonates are $\text{Ca}(\text{NO}_3)_2(\text{s})$ and $\text{Mg}(\text{NO}_3)_2(\text{s})$; $\text{Ca}(\text{OH})_2(\text{s})$ and $\text{Mg}(\text{OH})_2(\text{s})$; $\text{CaO}_2(\text{s})$ and $\text{MgO}_2(\text{s})$; $\text{CaO}(\text{s})$ and $\text{MgO}(\text{s})$ and N-containing gaseous compounds $\text{NO}(\text{g})$, $\text{N}_2\text{O}(\text{g})$ and $\text{NO}_2(\text{g})$, the yield of which reaches 10^{-7} – 10^{-5} mol. In the case of addition of $\text{H}_3\text{BO}_3(\text{s})$, $\text{MnO}_2(\text{s})$ or $\text{CuSO}_4(\text{s})$ into the system, the content of $\text{CuO}(\text{s})$, $\text{Cu}_2\text{O}(\text{s})$ or $\text{MnO}(\text{s})$ and $\text{SO}_2(\text{g})$, $\text{SO}_3(\text{g})$ or $\text{HBO}(\text{g})$ reaches the same level. Thereby, their equilibrium concentrations do not depend on the origin of the carbonate— $\text{CaCO}_3(\text{s})$, $\text{MgCO}_3(\text{s})$ or $\text{CaMg}(\text{CO}_3)_2(\text{s})$.

At constant temperature, the equilibrium amount of gaseous compounds does not depend on the content of carbonates (from 0.2 to 2.1 mol in the system) at the constant amount of AN (2 mol).

The reactions of AN and $\text{CaCO}_3(\text{s})$ or $\text{CaMg}(\text{CO}_3)_2(\text{s})$ with the formation of $\text{NO}(\text{g})$, $\text{NO}_2(\text{g})$ or $\text{N}_2\text{O}(\text{g})$ with the simultaneous formation of $\text{N}_2(\text{g})$ are more probable than those without $\text{N}_2(\text{g})$ formation and most of these reactions are probable at room temperature or at temperatures over 373–473 K. In the system of AN and $\text{CaMg}(\text{CO}_3)_2(\text{s})$, the temperatures at which these reactions become probable are shifted 20–50 K towards lower temperatures, except for the reactions with the formation of solid Ca, Mg-nitrates which become probable at 30–80 K higher temperatures as compared to the AN– CaCO_3 system.

Practically, the amount of 0.01 or 0.05 mol of $\text{CuSO}_4(\text{s})$, $\text{H}_3\text{BO}_3(\text{s})$ or $\text{MnO}_2(\text{s})$ additive in the system does not influence the temperature dependencies of ΔG_T of the reactions between AN and $\text{CaCO}_3(\text{s})$ or $\text{CaMg}(\text{CO}_3)_2(\text{s})$. The influence of additives taken in the amount of 0.5 mol was evident and, depending on the additive and the reaction, shifted their proceeding temperatures in the lower or higher direction even more than 300–400 K.

So, the information revealed can be used as fundamental data for applied aims—for the selection of suitable additives and their optimum amounts to obtain a stable non-explosive final product.

Acknowledgements This work was supported by the Estonian Ministry of Education and Research (SF0140082s08), the Estonian Science Foundation (G7548).

References

1. International fertilizer industry association's public statistics. Fertilizer supply statistics. 2009. Available at <http://www.fertilizer.org/ifa/statistics.asp>. Accessed on 28 March 2011.

2. van Weerden TJ, Jarvis SC. Ammonia emission factors for N fertilizers applied to two contrasting grassland soils. *Environ Pollut.* 1997;95:205–11.
3. Dechy N, Bourdeaux T, Ayrault N, Kordek MA, Le Coze JC. First lessons of the Toulouse ammonium nitrate disaster, 21st September, AZF plant, France. *J Hazard Mater.* 2004;111:131–8.
4. Oxley JC, Smith JL, Rogers E. Ammonium nitrate: thermal stability and explosivity modifiers. *Thermochim Acta.* 2002;384: 23–45.
5. Kaljuvee T, Rudjak I, Edro E, Trikkel A. Heating rate effect on thermal behavior of ammonium nitrate and its blends with limestone and dolomite. *J Therm Anal Calorim.* 2009;97:215–21.
6. Rudjak I, Kaljuvee T, Trikkel A, Mikli V. Thermal behavior of ammonium nitrate prills coated with limestone and dolomite powder. *J Therm Anal Calorim.* 2010;99:749–54.
7. Sinclair AH, Edwards AC. Micronutrient deficiencies in global crop production. In: Alloway BJ, editor. *Micronutrient deficiency problems in agricultural crops in Europe.* Netherlands: Springer; 2008. p. 225–44.
8. HSC Chemistry[®] for Windows. Chemical reaction and equilibrium software with extensive thermochemical database. Version 4.0 Pori: Outokumpu Research, Licence for Tallinn Technical University; 2002.

Paper II

T. Kaljuvee, **I. Rudjak**, E. Edro and A. Trikkel.

"Heating rate effect on the thermal behavior of ammonium nitrate and its blends with limestone and dolomite."

Reprinted with permission from:

Journal of Thermal Analysis and Calorimetry, vol. 97, no. 1, pp. 215-221, 2009.

Heating rate effect on the thermal behavior of ammonium nitrate and its blends with limestone and dolomite

T. Kaljuvee · I. Rudjak · E. Edro · A. Trikkel

ICTAC2008 Conference
© Akadémiai Kiadó, Budapest, Hungary 2009

Abstract The effect of heating rate on the thermal behavior of ammonium nitrate (AN) and on the kinetic parameters of decomposition of AN and its blends with limestone and dolomite was studied on the basis of commercial fertilizer-grade AN and several Estonian limestone and dolomite samples. Experiments were carried out under dynamic heating conditions up to 900 °C at heating rates of 2, 5, 10 and 20 °C min⁻¹ in a stream of dry air using Setaram Labsys 2000 equipment. For calculation of kinetic parameters, the TG data were processed by differential isoconversional method of Friedman. The variation of the value of activation energy E along the reaction progress α showed a complex character of decomposition of AN—interaction of AN with limestone and dolomite additives with the formation of nitrates as well as decomposition of these nitrates at higher temperatures.

Keywords Ammonium nitrate · Dolomite · Kinetics · Limestone · TG–DTA · Thermal stability

Introduction

The kinetics of decomposition (gasification) of AN in solid [1–5] and liquid phase [1, 6–8] as well as of phase stabilized AN (PSAN) [9, 10] has been studied by several authors, but there is no data about AN blends with dolomite and limestone as additives.

Earlier, the influence of different lime-containing materials on the thermal behavior of ammonium nitrate

(AN) was studied using combined TG–DTA–EGA (FTIR) equipment varying the amount of additives in a wide range from 5 mass% to mole ratio of AN/(CaO + MgO) = 2:1 [11].

The aim of this research was to study the effect of heating rate (non-isothermal conditions) on the thermal behavior of AN and on the kinetic parameters of decomposition of AN and its blends with limestone and dolomite.

Experimental

Materials

Commercial fertilizer-grade AN (34.4% N) (Tserepovetski Azot Ltd, Russia) was under investigation. Three Estonian limestone (from Võhmuta, Vasalemma, and Karinu deposits) and three dolomite (Kurevere, Anelema and Anelema wastes) previously ground (<45 μm) samples were used as additives to AN. Anelema wastes were obtained as a fine fraction from rubble manufacturing. The chemical composition and specific surface area (SSA) of the limestone and dolomite samples are presented in Table 1. The content of total CaO in limestone was 52.9–54.2 mass% and of total MgO 1.1–2.8 mass%. In dolomite samples, the content of total CaO was in between 26.0 and 29.0 mass% and of total MgO 24.3–26.6 mass%. The content of insoluble residue in limestone samples was 0.8–1.3 mass%, in Kurevere and Anelema dolomite samples 3.2 and 5.8 mass%, respectively, and in Anelema wastes 12.4 mass%. The SSA of the samples studied was relatively small (from 0.74 to 2.44 m² g⁻¹), being somewhat bigger for dolomite samples.

More precise characterization of limestone and dolomite samples used has been presented in [11] showing that all

T. Kaljuvee (✉) · I. Rudjak · E. Edro · A. Trikkel
Laboratory of Inorganic Materials, Tallinn University
of Technology, Ehitajate tee 5, 19086 Tallinn, Estonia
e-mail: tiidu@staff.tu.ee

Table 1 Chemical composition and specific surface area (SSA) of limestone and dolomite samples

Sample	Chemical composition (mass %) ^a							BET SSA (m ² g ⁻¹)
	CaO	MgO	CO ₂	I.R. ^b	Al ₂ O ₃	Fe ₂ O ₃	S _{sulphate}	
Karinu	52.92	2.76	38.98	0.80	1.72	0.08	0.04	0.74
Võhmuta	53.17	1.50	39.87	1.33	1.81	0.04	0.06	1.56
Vasalemma	54.22	1.14	40.45	0.75	1.50	0.09	0.09	0.89
Kurevere	29.04	24.40	41.87	3.17	0.64	0.21	0.09	1.70
Anelema	28.85	26.63	40.81	5.83	0.84	0.14	0.10	2.44
Anelema wastes	25.95	24.29	35.58	12.41	1.41	0.37	0.10	5.79

^a Per dry mass

^b Insoluble residue in aqua regia

samples except Anelema wastes were relatively pure limestone and dolomite.

mass of AN (6 ± 0.2 mg), the content of additives in the blends was 20 mass%.

Methods

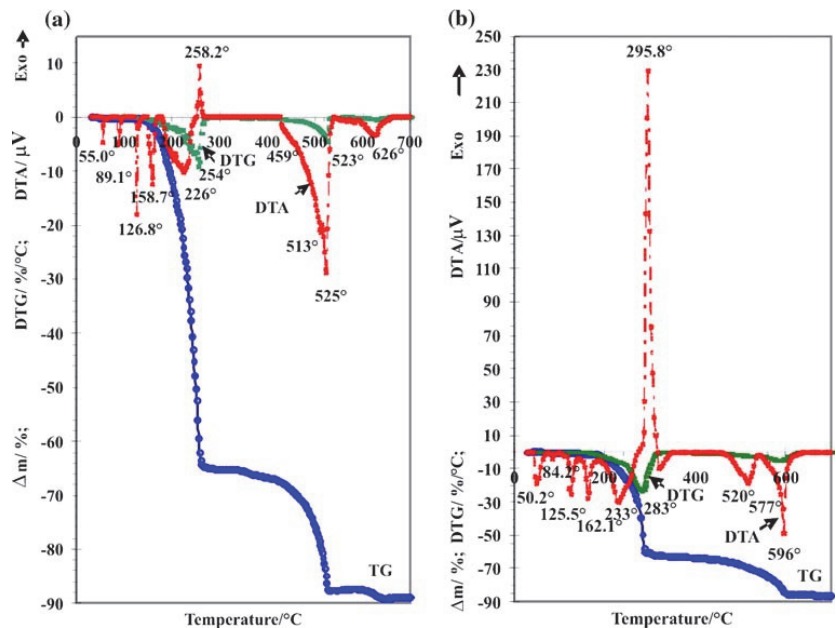
To study the effect of heating rate on thermal stability of AN, thermogravimetric equipment (Setaram Labsys 2000) capable of simultaneous recording of mass loss (TG), differential mass loss (DTG) and differential thermal analyses curve (DTA) was used. The experiments were carried out under dynamic heating conditions from 30 to 900 °C, or in the case of neat AN to 400 °C, at heating rates of 2, 5, 10 and 20 °C min⁻¹ in a stream of dry air (flow rate 120 mL min⁻¹). Standard 100 µL alumina crucibles were used. Sample mass was calculated on the basis of constant

Results and discussion

Thermal analysis

No systematic dependence of the temperatures of endoeffect minimums on DTA curves corresponding to the principal transitions of AN_{IV} ↔ AN_{III} ↔ AN_{II} ↔ AN_I on the heating rate were fixed. The most evident phenomenon was that at lower heating rates these endoeffects occurred at higher temperatures, but the transition of AN_I ↔ AN_{melt} was always shifted towards higher temperatures at higher heating rates.

Fig. 1 Thermal analysis curves of AN blend with Vasalemma limestone at a heating rate of 2 °C min⁻¹ (a) and 20 °C min⁻¹ (b)



For example, for neat AN at the heating rates of 2 and 20 °C min⁻¹ the peaks of phase transitions of AN_{IV} ↔ AN_{III} ↔ AN_{II} ↔ AN_I on the DTA curves were fixed, respectively, at 53.7 and 52.2 °C, 90.4 and 86.4 °C, 126.1 and 127.1 °C, but of AN_I ↔ AN_{melt} at 165.2 and 167.2 °C. For the blend of AN with 20% Vasalemma limestone these transitions at the heating rates of 2 °C min⁻¹ (Fig. 1a) and 20 °C min⁻¹ (Fig. 1b) occurred at 55.0 and 50.2 °C, 89.1 and 84.2 °C, 126.8 and 125.5 °C, respectively, and of AN_I ↔ AN_{melt} at 158.7 and 162.1 °C.

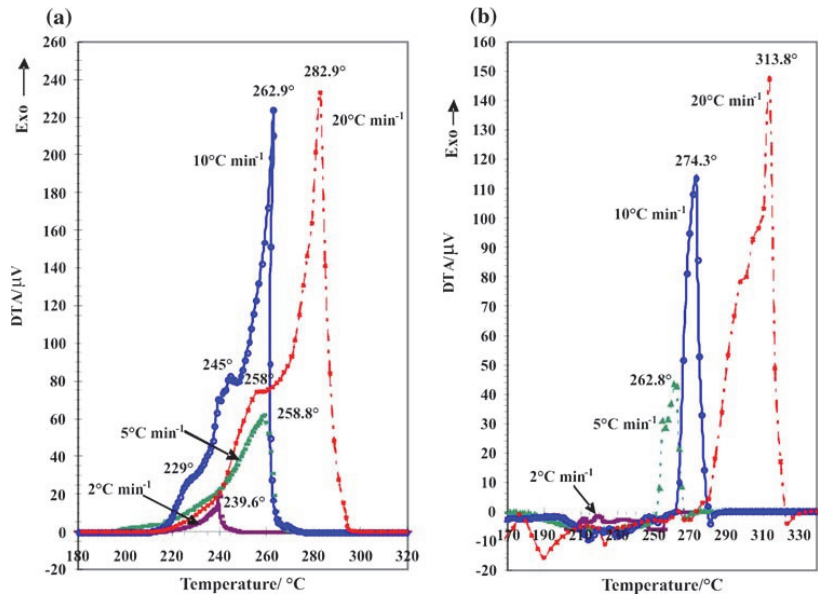
At higher temperatures and in the case of neat AN these phase transitions were followed at the heating rates of 2, 5, 10 and 20 °C min⁻¹ by the decomposition exotherm of AN with maximums on the DTA curve respectively at 239.6, 258.8, 262.9 °C (shoulders at 229 and 245 °C) and 282.9 °C (shoulder at 258 °C), thereby, the higher the heating rate the more intensive the exotherm was (Fig. 2a).

At thermal treatment of AN blends with limestone or dolomite additives a multi-peaked endotherm was fixed on the DTA curves in the temperature interval of 180–280 °C, characterizing interaction of AN with CaCO₃ and MgCO₃·CaCO₃ from natural limestone and dolomite leading to the formation of calcium and magnesium nitrates [11]. This endoeffect was followed, as a rule, by a more or less intensive exoeffect, characterizing the decomposition of residual AN. The decomposition exotherm of AN was shifted towards higher temperatures and the intensities of exotherms at that were much smaller as compared to neat AN. At the heating rate of 2 °C min⁻¹, it was especially miserable or missing at all.

For example, at the heating rate of 2 °C min⁻¹ for AN with Vasalemma limestone additive an endotherm with minimum at 226 °C was fixed on the DTA curve, which was followed by a weak exoeffect with maximum at 258.2 °C (Fig. 1a). The total mass loss at heating up to 315 °C was 65.1%. At the heating rate of 20 °C min⁻¹ the endo- and exoeffect (the last one very intensive), were fixed with minimum at 233 °C and maximum at 295.8 °C, respectively, and the total mass loss at heating up to 320 °C was 62.0% (Fig. 1b). For the AN blend with Vöhmata limestone, the decomposition exotherm of AN at the heating rate of 2 °C min⁻¹ was missing and the maximum of the exotherm on the DTA curve at heating rates of 5, 10 and 20 °C min⁻¹ was shifted, respectively, 4.0, 11.4 and 30.9 °C towards higher temperatures as compared to neat AN (Fig. 2a, b).

With the following increase in temperature the endotherms in between 350 and 600 °C characterized the decomposition of previously formed Mg(NO₃)₂ and Ca(NO₃)₂ and in between 600 and 700 °C the decomposition of residual carbonates. On the DTA curve of AN with Vasalemma limestone additive at the heating rate of 2 °C min⁻¹, an endotherm with minimums at 513 and 525 °C, and with a shoulder at 459 °C, and another with minimum at 626 °C were fixed (Fig. 1a). The total mass loss at heating up to 535 and 700 °C was 87.5 and 89.0%, respectively. At the heating rate of 20 °C min⁻¹ two endoeffects with minimums at 520 and 596 °C (and a shoulder at 577 °C) and no endotherms at higher temperatures were fixed on the DTA curve. The total mass loss at

Fig. 2 DTA curves of neat AN (a) and AN blends with Vöhmata limestone (b) at different heating rates



heating up to 610 and 700 °C was 85.4 and 86.2% (Fig. 1b), respectively, which means that there was only a small amount of unreacted carbonates left.

Determination of kinetic parameters

The decomposition of AN and the interaction of AN with limestone or dolomite additives with formation of nitrates as well as the following decomposition of the nitrates at higher temperatures have a complicated multi-step mechanism (Figs. 1, 2). In such situation, the reaction rate can be described only by complex equations, where the activation energy E is no more constant but is dependent on the reaction progress α ($E = E(\alpha)$). The kinetic parameters are evaluated by isoconversional method which involves determination of temperatures corresponding to certain, arbitrarily chosen values of α recorded in the experiments carried out at different heating rates β [12–15].

The differential isoconversional method of Friedman [12] was used to calculate kinetic parameters from non-isothermal experiments. After baseline correction and normalization, the TG data obtained at different heating rates were processed with the AKTS Advanced Thermokinetics software [16].

From the generally accepted equation of the non-isothermal kinetics:

$$\beta \frac{d\alpha}{dT} = f(\alpha) A(\alpha) \exp\left(-\frac{E(\alpha)}{RT}\right) \tag{1}$$

where α is the degree of conversion, $f(\alpha)$ is the function dependent on the reaction mechanism, β is the heating rate,

T is the temperature in K, A pre-exponent factor in s^{-1} and R is the gas constant, an equation corresponding to the Friedman’s differential isoconversional method can be obtained as follows:

$$\ln\left(\beta \frac{d\alpha}{dT}\right) = \ln[A(\alpha)f(\alpha)] - \frac{E(\alpha)}{RT} \tag{2}$$

Replacing $\beta(d\alpha/dT)$ with $d\alpha/dt$ in the Eq. 2, the Friedman analysis, based on the Arrhenius equation, applies the logarithm of the conversion rate $d\alpha/dt$ as a function of the reciprocal temperature at different degrees of conversion:

$$\ln \frac{d\alpha}{dt} \Big|_{\alpha_i} = \ln[A_i f(\alpha_{i,j})] - \frac{E_i}{RT_{ij}} \tag{3}$$

As the function dependent on the reaction model $f(\alpha)$ is assumed to be a constant at each conversion degree $\alpha_{i,j}$ (i —index of conversion; j —index of heating rate), the dependence of the logarithm of the reaction rate over $1/T$ is linear with the slope of E_j/R .

The reaction rates for the decomposition of neat AN and its blend with Vasalemma limestone with formation of nitrates at lower temperatures (step I) are presented in Fig. 3. The conversion rates ($d\alpha/dt$), measured at different temperatures for different heating rates allowed to determine the kinetic parameters A and E presented in Fig. 4 for the overall process as a function of reaction progress. The data for step II, decomposition of the nitrates formed at lower temperatures during step I, are presented in Fig. 5.

Fig. 3 Reaction rate $d\alpha/dt$ (DTG, normalized signals) for the decomposition of neat AN (a) and for the step I of AN blend with Vasalemma limestone (b) as a function of temperature for different heating rates. (The values of the heating rate in $(^\circ\text{C min}^{-1})$ are marked on the curves)

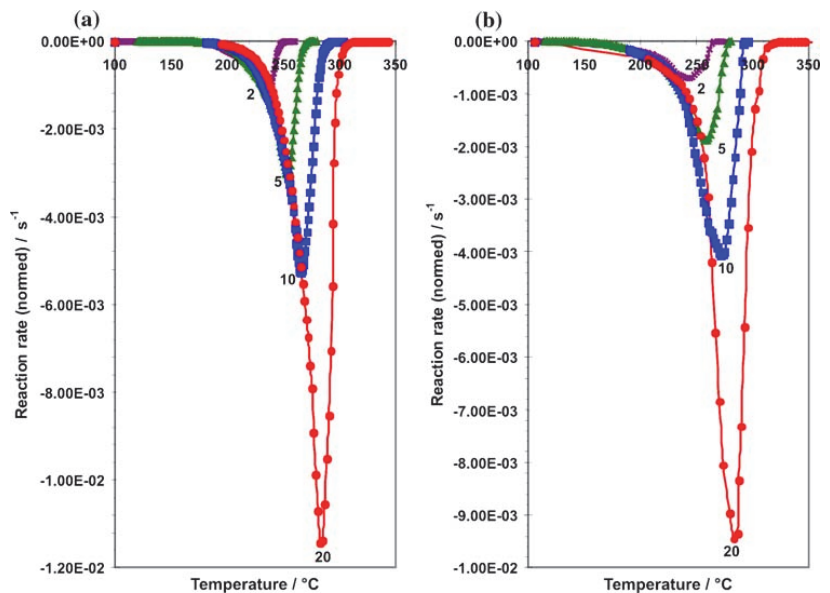


Fig. 4 Activation energy E and pre-exponential factor A determined by Friedman analysis as a function of the reaction progress for the decomposition of neat AN (a) and for the step I of AN blend with Vasalemma limestone (b)

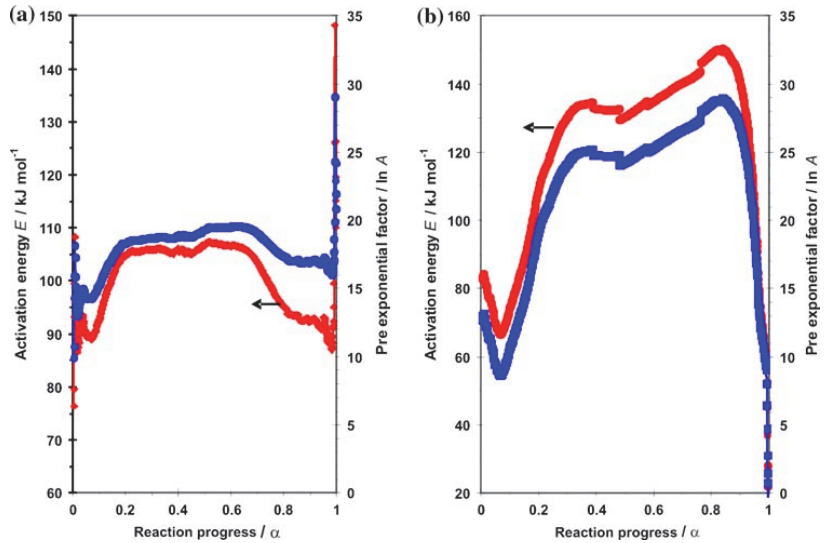
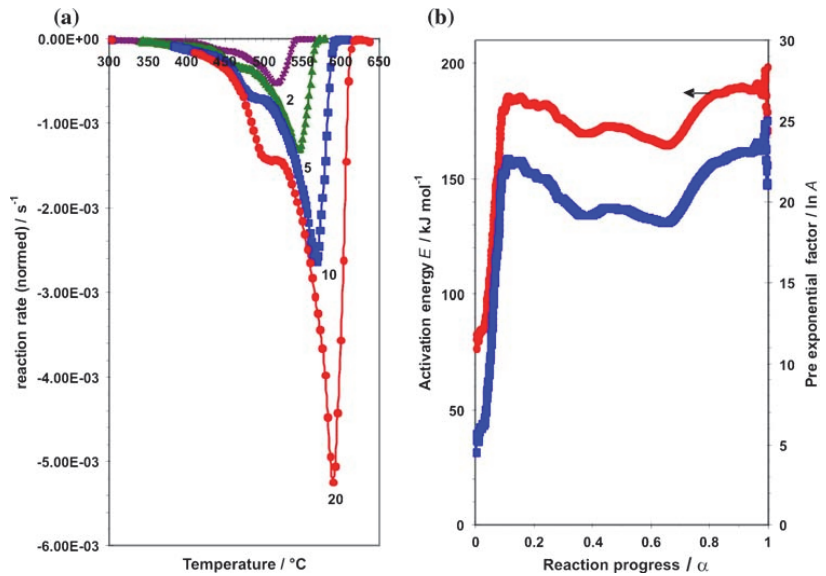


Fig. 5 Reaction rate dz/dt (a), activation energy E and pre-exponential factor A (b) for the step II of AN blend with Vasalemma limestone



The values of the activation energy for all the blends studied are presented in Table 2.

The results presented in Table 2, and in Fig. 4 and 5b express the complex character of the decomposition of AN and its interactions with limestone or dolomite additives as well as prove the formation (step I) and decomposition of nitrates (step II), whereas the values of activation energy and pre-exponential factor are visibly dependent on the reaction extent.

For neat AN, the activation energy in the range of conversion (decomposition) degree of $0.1 < \alpha < 0.9$ varies

in between 92.4 and 106.8 kJ mole^{-1} (pre-exponential factor A from $4.41 \cdot 10^6$ to $2.94 \cdot 10^8 \text{ s}^{-1}$) (Fig. 4a) being at that 0.9–12.9 kJ mole^{-1} higher than this calculated in [1] by DSC signals ($E = 92.7 \pm 1.2 \text{ kJ mole}^{-1}$, sample mass $\sim 1 \text{ mg}$) using isoconversional method for non-isothermal gasification of AN.

For AN blends with limestone and dolomite the value of activation energy in the same range of α (decomposition and interactions of AN with limestone and dolomite additives—step I) varied much more than for neat AN. For example, for AN blend with Vöhmata limestone

Table 2 The activation energy E (kJ mole⁻¹) and pre-exponent factor $\ln A$ versus reaction progress α

Sample	α																	
	0.1	0.2	0.3	0.4	0.5	0.6	0.7	0.8	0.9	$\ln A$	E	$\ln A$	E					
<i>Step I</i>																		
Neat AN	92.7	15.3	104.8	18.3	106.0	18.7	106.0	18.9	106.8	19.3	106.6	19.5	103.5	19.1	95.1	17.4	92.4	17.0
AN + 20% Vöhmuta	58.5	7.2	76.1	11.4	83.5	13.0	92.7	15.5	88.5	14.8	82.0	13.5	78.6	12.9	76.7	12.7	73.8	12.1
AN + 20% Karinu	119.7	22.8	113.8	20.6	98.3	16.5	100.0	16.9	119.3	21.7	109.6	19.7	107.4	19.3	106.5	19.2	102.8	18.6
AN + 20% Vasalemma	74.6	10.7	109.3	19.2	130.2	24.2	132.8	24.8	130.4	24.3	135.0	25.3	140.4	26.6	148.8	28.6	140.7	26.8
AN + 20% Kurevere	106.3	18.1	108.5	18.9	125.5	23.0	123.8	22.6	116.6	21.1	108.3	19.2	97.9	16.9	30.2	1.7	57.9	8.2
AN + 20% Anelema	172.4	34.6	154.4	30.6	141.3	27.6	131.9	25.4	126.6	24.3	124.4	23.8	125.4	24.1	126.0	24.3	125.3	24.1
AN + 20% Anelema wastes	86.2	13.8	85.7	14.1	90.8	15.5	95.7	16.8	98.8	17.6	100.5	18.1	102.4	18.6	105.6	19.4	105.2	19.3
<i>Step II</i>																		
AN + 20% Vöhmuta	292.9	40.8	178.8	21.4	156.3	17.4	174.2	19.3	171.9	19.5	201.9	23.9	264.0	33.2	212.7	26.1	210.5	26.0
AN + 20% Karinu	195.6	24.3	178.8	21.0	144.1	14.7	164.3	17.8	181.1	20.3	202.4	23.6	207.0	24.6	179.4	20.9	174.2	20.4
AN + 20% Vasalemma	180.1	21.8	182.9	21.8	175.8	20.2	170.2	19.2	172.2	19.6	167.2	19.0	169.2	19.5	185.5	22.2	189.6	23.0
AN + 20% Kurevere	106.2	12.4	67.7	4.9	59.7	3.1	70.9	5.2	86.5	7.9	105.2	10.9	104.5	10.9	85.2	8.0	63.9	4.9
AN + 20% Anelema	66.2	4.7	73.8	6.0	87.8	8.4	114.0	12.8	159.3	20.4	174.4	22.9	152.9	19.6	143.9	18.3	143.0	18.2
AN + 20% Anelema wastes	100.0	10.9	109.8	12.1	108.9	11.9	112.2	12.3	121.1	13.8	130.2	15.4	126.8	15.0	127.9	15.3	141.2	17.5

from 58.5 to 92.7 kJ mole⁻¹ (pre-exponential factor A in between $1.3 \cdot 10^3$ and $5.4 \cdot 10^6$ s⁻¹), with Kurevere dolomite from 30.2 to 125.5 kJ mole⁻¹ (A in between 5.5 and $9.7 \cdot 10^9$ s⁻¹). For step II (decomposition of Mg and Ca nitrates), the value of activation energy also varied in a great extent: for the AN blend with Vöhmata limestone from 156.3 to 292.9 kJ mole⁻¹ (A in between $3.6 \cdot 10^7$ and $5.2 \cdot 10^{17}$ s⁻¹) and with Anelema dolomite from 66.2 to 174.4 kJ mole⁻¹ (A in between $1.1 \cdot 10^2$ and $8.8 \cdot 10^9$ s⁻¹) (Table 2). These results indicate that neither the decomposition of AN nor the interactions in the AN blends with limestone or dolomite additives follow a simple, but a complex reaction mechanism including stages with both lower and higher activation energies as compared to decomposition of neat AN.

Conclusions

No systematic dependence of the temperatures of endo-effect minimums on DTA curves corresponding to the principal transitions of AN_{IV} ↔ AN_{III} ↔ AN_{II} ↔ AN_I on the heating rate were fixed, but the transition of AN_I ↔ AN_{melt} was always shifted towards higher temperatures at higher heating rates.

These phase transitions at thermal treatment of neat AN were followed by the decomposition exotherm of AN in the temperature interval from 200 to 310 °C, thereby, the higher the heating rate, the more intensive the exotherm was.

At thermal treatment of AN blends with limestone or dolomite a multi-peaked endotherm was fixed on the DTA curves in the range of 180–280 °C, characterizing the interaction of AN with CaCO₃ and MgCO₃·CaCO₃ contained in natural limestone and dolomite. This endoeffect was followed, as a rule, by a more or less intensive exoeffect characterizing the decomposition of residual AN. The decomposition exotherm of AN was shifted towards higher temperatures and the intensities of these exotherms were much smaller as compared to neat AN, missing for some blends at the heating rate of 2 °C min⁻¹ at all.

The endotherms in between 350 and 600 °C characterized the decomposition of previously formed Mg(NO₃)₂ and Ca(NO₃)₂.

The variation of the value of activation energy E along the reaction progress α shows the complex character of decomposition of AN, the interaction of AN with limestone and dolomite additives with formation of nitrates as well as the decomposition of the nitrates formed at previous stages.

For neat AN, the activation energy in the range of conversion (decomposition) degree of $0.1 < \alpha < 0.9$ ranges from 92.4 to 106.8 kJ mole⁻¹. For the blends of AN with limestone and dolomite, the value of activation energy in the same range of α varied in a greater extent than for neat

AN—depending on the limestone or dolomite added for step I (decomposition and interactions of AN with limestone and dolomite additives) from 30.2 to 172.4 kJ mole⁻¹, for step II (decomposition of Mg and Ca nitrates) from 59.7 to 292.9 kJ mole⁻¹.

Acknowledgements This work was partly supported by Estonian Science Foundation (G7548).

References

1. Vyazovkin S, Clawson JS, Wight CA. Thermal dissociation kinetics of solid and liquid ammonium nitrate. *Chem Mater*. 2001; 13:960–6.
2. Oxley JC, Kauchik SM, Gilson NS. Thermal decomposition of ammonium nitrate-based composites. *Thermochim Acta*. 1989;153: 269–86.
3. Olszak-Humienik M. On the thermal stability of some ammonium salts. *Thermochim Acta*. 2001;378:107–12.
4. Oxley JC, Smith JL, Rogers E, Yu Ming. Ammonium nitrate: thermal stability and explosivity modifiers. *Thermochim Acta*. 2002;384:23–45.
5. Zeman S, Kohlčiček P, Maranda A. A study of chemical micro-mechanism governing detonation initiation of condensed explosive mixtures by means of differential thermal analysis. *Thermochim Acta*. 2003;398:185–94.
6. Brower KR, Oxley JC, Tewari M. Evidence for homolytic decomposition of ammonium nitrate at high temperature. *J Phys Chem*. 1989;93:1029–33.
7. Koga N, Tanaka H. Effect of sample mass on the kinetics of thermal decomposition of a solid. Part 1. Isothermal mass-loss process of molten NH₄NO₃. *Thermochim Acta*. 1992;209: 127–34.
8. Koga N, Tanaka H. Effect of sample mass on the kinetics of thermal decomposition of a solid. Part 3. Non-isothermal mass-loss process of molten NH₄NO₃. *Thermochim Acta*. 1994;240:141–51.
9. Carvalheira P, Gadiot GMHJL, de Klerk WPC. Thermal decomposition of phase-stabilised ammonium nitrate (PSAN), hydroxyl-terminated polybutadiene (HTPB) based propellants. The effect of iron(III)oxide burning-rate catalyst. *Thermochim Acta*. 1995;269/270:273–93.
10. Simões PN, Pedroso LM, Portugal AA, Campos JL. Study of the decomposition of phase stabilized ammonium nitrate (PSAN) by simultaneous thermal analysis: determination of kinetic parameters. *Thermochim Acta*. 1998;319:55–65.
11. Kaljuvee T, Edro E, Kuusik R. Influence of lime-containing additives on the thermal behaviour of ammonium nitrate. *J Therm Anal Cal*. 2008;92:215–21.
12. Friedman HL. Kinetics of thermal degradation of char-forming plastics from thermogravimetry. Application to a phenolic plastic. *J Polym Sci*. 1965;6C:183–95.
13. Flynn IH, Wall LA. A quick, direct method for the determination of activation energy from thermogravimetric data. *Polym Lett*. 1966;4:323–8.
14. Ozawa T. Kinetic analysis of derivative curves in thermal analysis. *Therm J. Anal Cal*. 1970;2:301–24.
15. Vyazovkin S. Model-free kinetics. Staying free of multiplying entities without necessity. *J Therm Anal Cal*. 2006;83:45–51.
16. AKTS AG. AKTS Software and SETARAM Instruments: a global solution for kinetic analysis and determination of the thermal stability of materials. Siders: AKTS AG; 2006. 88 pp.

Paper III

I. Rudjak, T. Kaljuvee, A. Trikkel and V. Mikli.

"Thermal behaviour of ammonium nitrate prills coated with limestone and dolomite powder."

Reprinted with permission from:

Journal of Thermal Analysis and Calorimetry, vol. 99, no. 3, pp. 749-754, 2010.

Thermal behaviour of ammonium nitrate prills coated with limestone and dolomite powder

I. Rudjak · T. Kaljuvee · A. Trikkel · V. Mikli

MEDICTA2009 Conference
© Akadémiai Kiadó, Budapest, Hungary 2009

Abstract The thermal behaviour of ammonium nitrate (AN) and its prills coated with limestone and dolomite powder was studied on the basis of commercial fertilizer-grade AN and six Estonian limestone and dolomite samples. Coating of AN prills was carried out on a plate granulator and a saturated solution of AN was used as a binding agent. The mass of AN prills and coating material was calculated based on the mole ratio of AN/(CaO + MgO) = 2:1. Thermal behaviour of AN and its coated prills was studied using combined TG-DTA-FTIR equipment. The experiments were carried out under dynamic heating conditions up to 900 °C at the heating rate of 10 °C min⁻¹ and for calculation of kinetic parameters, additionally, at 2, 5 and 20 °C min⁻¹ in a stream of dry air. A model-free kinetic analysis approach based on the differential isoconversional method of Friedman was used to calculate the kinetic parameters. The results of TG-DTA-FTIR analyses and the variation of the value of activation energy E along the reaction progress α indicate the complex character of the decomposition of neat AN as well as of the interactions occurring at thermal treatment of AN prills coated with limestone and dolomite powder.

Keywords Coated ammonium nitrate · Dolomite · Kinetics · Limestone · TG-DTA · Thermal stability

Introduction

Ammonium nitrate (AN) is one of the most widespread nitrogen mineral fertilizers used in the agriculture [1]. Unfortunately, thermal instability of AN, especially, if contaminated with impurities even on the low level, makes its handling and storage unpredictable which has led to several catastrophic explosions [2–4].

The thermal behaviour and the possibilities of increasing the thermal stability of AN have been studied by several authors [4–11]. Normally, solid AN follows four polymorphic phase transitions at ambient pressure—the transition AN_{IV} ↔ AN_{III} occurs at 32 °C and AN_{III} ↔ AN_{II} at 84 °C. In addition, a metastable transition AN_{IV} ↔ AN_{II} is possible at 50 °C [10–12]. The phase transition AN_{IV} ↔ AN_{III} causes drastic changes in the physical and thermodynamic properties of AN (note that AN_{IV} ↔ AN_{II} does not) [12] with the following decrease in the thermal stability of AN. Therefore, avoiding the AN_{IV} ↔ AN_{III} transition at manufacturing, storing and handling of AN has a great importance considering practical applications.

Another possibility to reduce the explosive potentiality of AN is to use additives which retard the decomposition of AN by increasing the reaction zone or stabilize thermal properties of AN [4, 7, 11, 13]. In [4] the influence of different reactive-grade sulphate, phosphate, and carbonate additives on the thermal stability of AN were studied. The maximum shift of the decomposition exotherm of AN towards higher temperatures was obtained with calcium carbonate additives.

Earlier, the influence of Estonian limestone and dolomite from different deposits added to AN at the mole ratio of AN/(CaO + MgO) = 2:1 on the thermal behaviour of AN was studied using combined TG-DTA-EGA (FTIR) equipment [14].

I. Rudjak · T. Kaljuvee (✉) · A. Trikkel · V. Mikli
Department of Chemical and Materials Technology, Tallinn
University of Technology, Ehitajate tee 5,
19086 Tallinn, Estonia
e-mail: tiidu@staff.ttu.ee

The aim of the present research was to study the thermal behaviour of AN prills coated with limestone and dolomite powder and to calculate the kinetic parameters of decomposition reactions of the coated AN prills.

Experimental

Materials

Commercial fertilizer-grade AN (34.4% N) (Tserepovetski Azot Ltd, Russia) was under investigation. Six previously ground Estonian limestone and dolomite samples (<45 μm) were used as the coating material. Coating of AN prills was carried out on a plate granulator with diameter 0.30 m using saturated solution of AN as a binding agent. The mass of AN prills and coating material was calculated on the assumption of the mole ratio of $\text{AN}/(\text{CaO} + \text{MgO}) = 2:1$. SEM images of the cross-sections of an AN prill and the prill coated with Anelema dolomite powder (thickness 200–300 μm) are presented in Fig. 1.

The chemical composition and specific surface area (SSA) of the limestone and dolomite samples is presented in Table 1. In limestone samples the content of total CaO and MgO was in between 52.9–54.2 mass% and 1.1–2.8 mass%, and in dolomite samples in between 26.0–29.0 mass% and 24.3–26.6 mass%, respectively. More precise characterization of the limestone and dolomite samples used has been presented in [14].

Methods

The thermal behaviour of AN and its coated prills was studied using Setaram Labsys 2000 equipment coupled to Interspec 2020 Fourier Transform Infrared Spectrometer (FTIR) by a transfer line. The experiments were carried out under dynamic heating conditions up to 900 $^{\circ}\text{C}$ at the heating rate of 10 $^{\circ}\text{C min}^{-1}$ and for calculation of kinetic parameters, additionally, at the heating rates of 2, 5 and 20 $^{\circ}\text{C min}^{-1}$ in a stream of dry air (flow rate 120 mL min^{-1}). Standard 100 μL alumina crucibles were

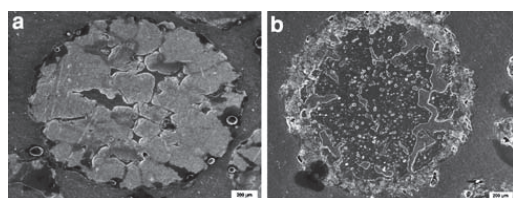


Fig. 1 SEM pictures of the cross-sections of neat AN prill (a) and AN prill coated with Anelema dolomite powder (b) (magnification $\times 10$)

used. A single prill was analyzed, the mass of AN prills was 15 ± 0.2 mg, the mass of coated prills varied between 24 and 26 mg.

FTIR measurements were recorded in the 4,000–600 cm^{-1} region with the resolution of 4 cm^{-1} and an average out of four scans was taken. To identify the gaseous compounds, the Bio-Rad (Sadler) KnowItAll search program and Gases and Vapours Database (code GS) were used.

The surface observations of the samples were carried out with a scanning electron microscope Jeol JSM-8404.

A model-free kinetic analysis approach based on the differential isoconversional method of Friedman [15] was used to calculate the kinetic parameters. After baseline correction and normalization, the TG signals were processed with the AKTS Advanced Thermokinetics software [16].

Results and discussion

Thermal analysis

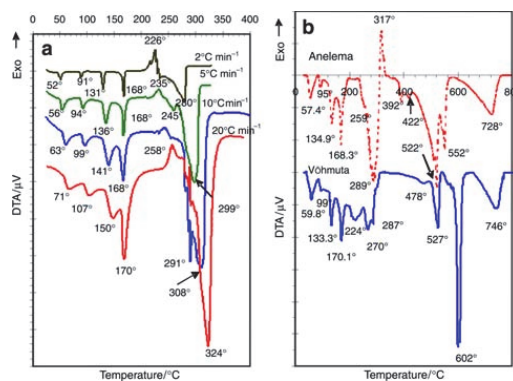
On the DTA curves of thermally treated AN prills four endotherms between 30 and 180 $^{\circ}\text{C}$ corresponding to the respective phase transformations can be observed (Fig. 2a). Depending on the heating rate, the first, $\text{AN}_{\text{IV}} \leftrightarrow \text{AN}_{\text{III}}$ transition with a minimum on DTA curve, was fixed in a temperature interval from 52 to 71 $^{\circ}\text{C}$. The principal transitions $\text{AN}_{\text{III}} \leftrightarrow \text{AN}_{\text{II}}$, $\text{AN}_{\text{II}} \leftrightarrow \text{AN}_{\text{I}}$ and $\text{AN}_{\text{I}} \leftrightarrow \text{AN}_{\text{melt}}$ with minimums on DTA curve occurred at temperatures from 91 to 107 $^{\circ}\text{C}$, 131 to 150 $^{\circ}\text{C}$ and 168 to 170 $^{\circ}\text{C}$. At higher temperatures these phase transitions were followed with a modest exoeffect and massive endoeffect with maximums and minimums on the DTA curve in between 226–258 $^{\circ}\text{C}$ and 280–324 $^{\circ}\text{C}$, respectively, corresponding to the decomposition of AN. Besides, the endoeffect has two shoulders between 259–290 $^{\circ}\text{C}$ and 273–307 $^{\circ}\text{C}$. The curves indicate a complicated multi-step character of the decomposition pathway of AN.

Differently, from the results with previously ground AN prills [14], when using whole prills, the temperature minimums on DTA curve for $\text{AN}_{\text{IV}} \leftrightarrow \text{AN}_{\text{III}} \leftrightarrow \text{AN}_{\text{II}} \leftrightarrow \text{AN}_{\text{I}}$ transitions were shifted at the heating rate of 10 $^{\circ}\text{C min}^{-1}$ 10–14 $^{\circ}\text{C}$ and for $\text{AN}_{\text{I}} \leftrightarrow \text{AN}_{\text{melt}}$ transition 5.2 $^{\circ}\text{C}$ towards higher temperatures, and the decomposition pathway of ground AN prills was accompanied also by a very intensive exoeffect on the DTA curve with maximum at 263 $^{\circ}\text{C}$.

The thermograms of AN prills coated with limestone or dolomite powder showed complicated but quite similar pathway of interactions as compared to thermal behaviour of AN blends with limestone or dolomite additives at the same mole ratio of $\text{AN}/(\text{CaO} + \text{MgO}) = 2:1$ [14]. For

Table 1 Chemical composition and specific surface area (SSA) of limestone and dolomite samples

Sample	Chemical composition/mass% ^a							BET SSA/m ² g ⁻¹
	CaO	MgO	CO ₂	I. R. ^b	Al ₂ O ₃	Fe ₂ O ₃	S _{sulphate}	
Karinu	52.92	2.76	38.98	0.80	1.72	0.08	0.04	0.74
Võhmuta	53.17	1.50	39.87	1.33	1.81	0.04	0.06	1.56
Vasalemma	54.22	1.14	40.45	0.75	1.50	0.09	0.09	0.89
Kurevere	29.04	24.40	41.87	3.17	0.64	0.21	0.09	1.70
Anelema	28.85	26.63	40.81	5.83	0.84	0.14	0.10	2.44
Anelema wastes	25.95	24.29	35.58	12.41	1.41	0.37	0.10	5.79

^a Per dry mass^b Insoluble residue in aqua regia**Fig. 2** DTA curves of neat AN prills at different heating rates (a) and AN prills coated with Anelema dolomite and Võhmuta limestone powder at the heating rate of 10 °C min⁻¹ (b)

example, on the DTA curves of AN prills coated with Võhmuta limestone or Anelema dolomite powder, a multi-peaked endotherm was fixed in the decomposition region of AN (190–340 °C). With the prills coated with Anelema dolomite, additionally, a modest exotherm with a maximum at 317 °C was fixed (Fig. 2b). These peaks characterize the interactions between AN and Mg, Ca-carbonates with the formation of nitrates. The total mass loss at heating of the AN prills coated with Võhmuta limestone and Anelema dolomite powder up to 340 °C was 35.4 and 56.2%, respectively, indicating that dolomite (CaCO₃·MgCO₃) reacts with AN less actively than limestone (CaCO₃).

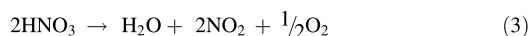
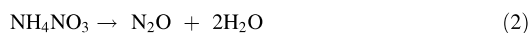
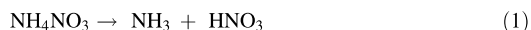
The subsequent endotherms on the DTA curve of AN prills coated with Võhmuta limestone powder with minimums at 527 and 602 °C (Fig. 2b) characterize, respectively, the melting and decomposition of previously formed Ca(NO₃)₂ [17]. The double-peak endotherms on the DTA curve of AN prills coated with Anelema dolomite powder with minimums at 392 and 422 °C, and at 522 and 552 °C (Fig. 2b) characterize the decomposition of previously formed Mg(NO₃)₂ and Ca(NO₃)₂, respectively [17, 18].

The last endotherms on DTA curves with minimums at 746 and 728 °C (Fig. 2b), describe the decomposition of residual carbonates.

The total mass loss at heating of the AN prills coated with Võhmuta limestone powder up to 610 and 770 °C was 65.1 and 71.7% and in the case of Anelema dolomite powder coating when heated up to 440, 560 and 770 °C, respectively, 59.1, 71.0 and 79.3%.

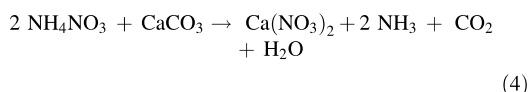
FTIR analysis

FTIR spectra of gaseous compounds evolved at thermal treatment of neat AN prills showed peaks characteristic to NH₃ (967 and 932 cm⁻¹), N₂O (2,235 and 2,215 cm⁻¹), NO₂ (1,630 and 1,595 cm⁻¹) and H₂O (bands in the broad ranges 3,900–3,500 and 1,900–1,300 cm⁻¹) having maximum intensity at 250, 280, 300 and 300 °C, respectively (Fig. 3a). The peaks characteristic to NO₂ and NH₃ were 1.5–2 times more intensive as compared to these obtained at thermal treatment of previously ground AN prills [14]. It is in a good correlation with the results presented in [19, 20]—the decomposition of AN, after dissociation into NH₃ and HNO₃ in the first step, can follow different pathways with the formation of N₂O at lower temperatures (<280 °C) and NO₂ at higher temperatures. Compactable AN prills follow preferably high-temperature route of AN decomposition. So, the decomposition pathway of AN at thermal treatment could be presented by the following simplified equations:

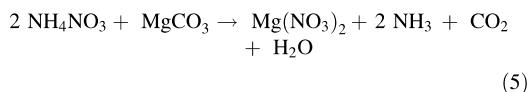


In the FTIR spectra of AN prills coated with limestone powder, the peaks characteristic to NH₃ and CO₂ (2,358 and 2,354 cm⁻¹) dominated in the temperature interval from 200 to 300 °C. The characteristic peaks for H₂O, NO₂ and N₂O were also present, but had lower intensity

(Fig. 3b). In the FTIR spectra of AN prills coated with dolomite powder, the peaks characteristic to NO_2 and, especially, to N_2O in the same temperature interval were presented more intensively (Fig. 3c). This indicates that at these temperatures the following interaction between AN and CaCO_3 with the formation of $\text{Ca}(\text{NO}_3)_2$ dominated:



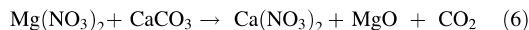
The reaction of AN with MgCO_3



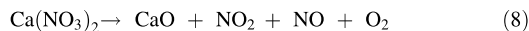
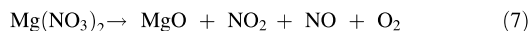
was not as complete as MgCO_3 is thermodynamically less reactive towards AN than CaCO_3 . In addition, using dolomite as the coating material, more AN decomposed with the formation of nitrous gases as compared to

limestone coating. Corresponding tendencies in FTIR spectra collected in the same temperature interval at thermal treatment of AN blends with limestone and dolomite additives were observed also in [14].

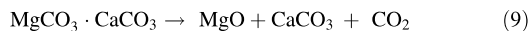
The second maximum on the absorbance profile of CO_2 at 390–400 °C at thermal treatment of AN prills coated with Anelema dolomite powder (Fig. 3c) points to the partial interaction of formed $\text{Mg}(\text{NO}_3)_2$ with CaCO_3 :



The peaks characteristic to NO_2 were fixed in FTIR spectra once again with maximum intensities at 400 and 540 °C when using Anelema dolomite coating (Fig. 3c) and with maximum intensity at 580 °C when using Vöhmata limestone coating (Fig. 3b). These are the temperatures of decomposition of Mg, Ca-nitrates formed at lower temperatures. The bands with maximum intensity at 540 °C when using dolomite and at 580 °C in the case of limestone, fixed in FTIR spectra in the 1,800–1,950 cm^{-1} region, also indicate the formation and emission of NO (Fig. 3b, c). The decomposition of Mg, Ca-nitrates can be presented by the following simplified equations:



The last maximum on the absorbance profile of CO_2 at 680 and 730 °C obtained at thermal treatment of AN prills coated, respectively, with Vöhmata limestone (Fig. 3b) and Anelema dolomite powder (Fig. 3c), is caused by the decomposition of residual carbonates:



Hereby, the results of EGA from the experiments with coated AN prills confirmed that the interactions between AN and carbonates contained in the coating materials used proceeded mostly by similar pathway as compared to AN blends with limestone and dolomite [14]—partially, or almost completely through the formation of $\text{Mg}(\text{NO}_3)_2$ and $\text{Ca}(\text{NO}_3)_2$ which decomposed thereupon in the temperature range of 360–620 °C.

Determination of kinetic parameters

The reaction rates and the kinetic parameters A and E for the decomposition of AN prills calculated using the differential isoconversional method of Friedman are presented in Fig. 4, and for AN prills coated with limestone or dolomite powder in Table 2. Here, step I presents data for low temperature region (depending on the heating rate between 150 and 350 °C) where interactions between AN and carbonates with the formation of Ca, Mg-nitrates take

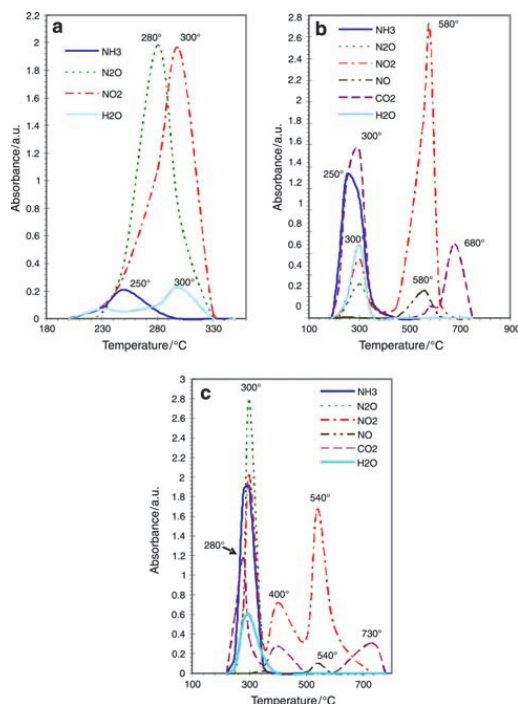


Fig. 3 Absorbance profiles of gaseous compounds evolved at thermal treatment of neat AN prill (a), AN prills coated with Vöhmata limestone (b) and Anelema dolomite (c) powder at the heating rate of $10 \text{ }^\circ\text{C min}^{-1}$

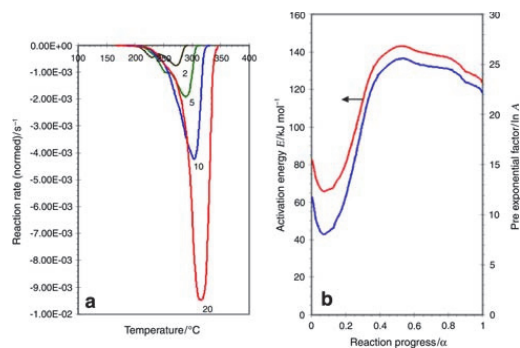


Fig. 4 Reaction rate dz/dt (DTG, normalized signals) as a function of the temperature for different heating rates (a), and activation energy E_a and pre-exponential factor A determined by Friedman analysis as a function of the reaction progress (b) for the decomposition of neat AN prills. (The value of the heating rate in $^{\circ}\text{C min}^{-1}$ are marked on the curves.)

place, but also unreacted AN, especially, in the case of dolomite coating decomposes. Step IIA presents data characterizing reactions occurring with $\text{Mg}(\text{NO}_3)_2$ in the temperature region from 310 to 450 $^{\circ}\text{C}$ and step IIB data characterizing decomposition of $\text{Ca}(\text{NO}_3)_2$ in the temperature region of 420–620 $^{\circ}\text{C}$. For AN prills coated with

limestone powder having poor content of MgO (Table 1) the step IIA is missing.

For neat AN prills the activation energy in the range of conversion (decomposition) level $0.1 < \alpha < 0.9$ was in between 66.7 and 142.7 kJ mole^{-1} (pre-exponential factor A from 4.0×10^3 to $1.2 \times 10^{11} \text{ s}^{-1}$) (Fig. 4b) varying at that more than this calculated in [14] in the case of powdered neat AN (E between 92.7 and 106.8 kJ mole^{-1}) indicating more complicated character of decomposition of AN in prills than in powdered form.

For AN prills coated with limestone and dolomite powder the value of activation energy in the same range of α (decomposition and interactions of AN with carbonates—step I) varied also in a wide range. For example, for AN prills coated with Vöhmata limestone powder from 82.8 to 119.6 kJ mole^{-1} (pre-exponential factor A in between 7.3×10^5 and $1.3 \times 10^{10} \text{ s}^{-1}$), with Kurevere dolomite powder from 111.3 to 154.8 kJ mole^{-1} (A in between 2.0×10^8 and $2.9 \times 10^{12} \text{ s}^{-1}$). For step IIA (interactions with Mg-nitrate) and IIB (decomposition of Ca-nitrate) the value of activation energy also varied in a great extent. For example, for AN prills coated with Kurevere dolomite powder from 185.2 to 344.7 kJ mole^{-1} (A in between 1.3×10^{12} and $2.8 \times 10^{24} \text{ s}^{-1}$) during step IIA and from 154.6 to 194.1 kJ mole^{-1} (A in between 5.9×10^7 and

Table 2 The activation energy E (kJ mole^{-1}) and pre-exponent factor $\ln A$ versus reaction progress α

Sample	α																	
	0.1		0.2		0.3		0.4		0.5		0.6		0.7		0.8		0.9	
	E	$\ln A$	E	$\ln A$	E	$\ln A$	E	$\ln A$	E	$\ln A$	E	$\ln A$	E	$\ln A$	E	$\ln A$	E	$\ln A$
<i>Step I:</i>																		
Neat AN	66.7	8.3	81.0	11.9	114.4	19.3	136.7	24.2	142.7	25.5	141.0	25.2	138.7	24.8	138.7	24.5	129.6	23.2
AN + Vöhmata	119.6	23.3	114.4	21.7	110.9	20.5	106.5	19.3	104.6	18.6	101.1	17.7	95.1	16.3	87.2	14.4	82.8	13.5
AN + Karinu	106.7	20.0	90.7	20.6	96.0	14.5	83.9	13.8	81.7	13.2	79.0	12.5	80.2	12.8	83.6	13.5	87.6	14.4
AN + Vasalemma	109.7	19.3	91.9	15.2	85.5	13.6	85.8	13.6	92.2	14.9	106.8	17.9	116.3	19.9	119.2	20.5	118.7	20.4
AN + Kurevere	111.3	19.1	118.8	20.9	131.5	23.7	154.8	28.7	153.3	28.2	152.6	28.0	144.9	26.2	133.9	23.8	131.4	23.2
AN + Anelema	107.2	18.1	101.5	16.9	97.9	16.1	97.9	16.2	97.9	16.2	99.6	16.6	101.7	17.1	103.9	17.5	107.2	18.2
AN + Anelema wastes	92.4	15.0	95.6	15.9	100.0	16.9	102.6	17.5	101.7	17.4	103.0	17.6	102.0	17.4	102.3	17.5	101.9	17.4
<i>Step II:</i>																		
AN + Vöhmata	124.8	11.6	120.4	10.7	206.9	23.5	247.0	29.5	255.3	30.8	230.2	27.5	223.7	26.8	219.9	26.4	206.6	24.7
AN + Karinu	170.3	17.9	205.1	23.1	200.8	22.6	170.0	18.4	156.6	16.7	173.1	19.3	178.3	20.2	182.8	21.0	191.3	22.4
AN + Vasalemma	192.8	22.3	194.0	22.3	192.1	21.7	197.0	22.3	219.5	25.9	229.6	27.7	218.0	26.3	223.5	27.2	228.1	28.1
AN + Kurevere, IIA	253.8	40.0	335.5	54.8	344.7	56.3	308.2	49.7	265.7	42.0	234.9	36.5	219.1	33.6	205.3	31.3	185.2	27.9
AN + Kurevere, IIB	160.3	18.7	154.6	18.0	158.9	18.9	165.4	19.8	169.0	20.3	168.1	20.0	155.9	17.9	172.1	20.3	194.1	23.8
AN + Anelema, IIA	246.1	39.3	292.5	47.7	321.1	52.8	316.3	51.9	297.4	48.4	285.7	46.2	283.4	47.9	172.1	20.3	194.1	23.8
AN + Anelema, IIB	177.4	20.9	153.8	17.3	145.8	16.3	164.8	19.3	175.0	20.9	174.2	20.6	163.0	18.8	123.6	12.9	135.5	14.9
AN + Anelema wastes, IIA	253.8	41.0	299.2	49.4	110.1	51.3	304.0	50.1	287.7	47.1	273.0	44.5	263.9	42.8	249.2	40.1	228.4	36.4
AN + Anelema wastes, IIB	160.3	18.7	154.6	18.0	158.9	18.8	165.4	19.3	169.0	20.3	168.1	20.0	155.9	17.9	172.1	20.3	194.1	23.8

$2.2 \times 10^{10} \text{ s}^{-1}$) during step IIB (Table 2). For AN prills coated with Vöhmata limestone powder the activation energy for step II varied from 120.4 to 255.3 kJ mole⁻¹ (A in between 4.4×10^4 and $2.4 \times 10^{13} \text{ s}^{-1}$).

The results obtained indicate the complex character of the decomposition of AN and the interactions occurring in the AN prills coated with limestone or dolomite powder, prove the formation (step I) and decomposition of nitrates (step II), and point to the visible dependence of the values of activation energy and pre-exponential factor on the reaction extent.

Conclusions

AN prills coated with limestone or dolomite powder follow at thermal treatment predominantly the same complicated but safe behaviour as AN blends with limestone or dolomite additives—interactions between AN and Ca, Mg-carbonates with the formation of Ca, Mg-nitrates excluding exothermic explosive decomposition of AN and the following decomposition of the formed nitrates at higher temperatures.

Acknowledgements This work was partly supported by the Estonian Ministry of Education and Research (SF0140082s08) and the Estonian Science Foundation (G7548).

References

1. International Fertilizer Industry Association's Public Statistics 2009. Fertilizer supply statistics. <http://www.fertilizer.org/ifa/statistics.asp>.
2. Keeping faith with AN. *Fertil Int.* 2004;401 July/August:6–9.
3. Dechy N, Bourdeaux T, Ayrault N, Kordek M-A, Le Coze J-C. First lessons of the Toulouse ammonium nitrate disaster, 21st September 2001, AZF plant, France. *J Hazard Mater.* 2004; 111:131–8.
4. Oxley JC, Smith JL, Rogers E, Yu M. Ammonium nitrate: thermal stability and explosivity modifiers. *Thermochim Acta.* 2002;384:23–45.
5. Olszak-Humienik M. On the thermal stability of some ammonium salts. *Thermochim Acta.* 2001;378:107–12.
6. Sun J, Sun Z, Wang Q, Ding H, Wang T, Jiang C. Catalytic effects of inorganic acids on the decomposition of ammonium nitrate. *J Hazard Mater.* 2005;127:204–10.
7. Remya Sudhakar AO, Mathew F. Thermal behaviour of CuO doped phase-stabilised ammonium nitrate. *Thermochim Acta.* 2006;451:5–9.
8. Wu HB, Chan CK. Effects of potassium nitrate on the solid phase transitions of ammonium nitrate particles. *Atm Environ.* 2008;42:313–22.
9. Skordilis CS, Pomonis PJ. The influence of Mn, Co and Cu cations on the thermal decomposition of NH₄NO₃ in pure form and supported on alumina. *Thermochim Acta.* 1993;216:137–46.
10. Kestilä E, Harju MEE, Valkonen J. Differential scanning calorimetric and Raman studies of phase transition V - IV of ammonium nitrate. *Thermochim Acta.* 1993;214:67–70.
11. Simões PN, Pedroso LM, Portugal AA, Campos JL. Study of the decomposition of phase stabilized ammonium nitrate (PSAN) by simultaneous thermal analysis: determination of kinetic parameters. *Thermochim Acta.* 1998;319:55–65.
12. Laurent B. Straight ammonium nitrate fertilizer granule-prill stabilization: theoretical possibilities. Proceedings of the International Industry Association Technical Conference, Chennai, India. http://www.fertilizer.org/ifa/Library/Conference_proceedings/Technical_conferences/2002_tech_laurent.pdf.
13. Lang AJ, Vyazovkin S. Phase and thermal stabilization of ammonium nitrate in the form of PVP-AN glass. *Mater Lett.* 2008;62:1757–60.
14. Kaljuvee T, Edro E, Kuusik R. Influence of lime-containing additives on the thermal behaviour of ammonium nitrate. *J Therm Anal Calorim.* 2008;92:215–21.
15. Friedman HL. Kinetics of thermal degradation of char-forming plastics from thermogravimetry. Application to a phenolic plastic. *J Polym Sci.* 1965;6C:183–95.
16. AKTS Software and SETARAM Instruments: a global solution for kinetic analysis and determination of the thermal stability of materials. Switzerland: AKTS AG; 2006. p. 88.
17. Madarász J, Varga PP, Pokol G. Evolved gas analyses (TG/DTA-MS and TG-FTIR) on dehydration and pyrolysis of magnesium nitrate hexahydrate in air and nitrogen. *J Anal Appl Pyrolysis.* 2007;79:475–8.
18. Ettarh C, Galwey AK. A kinetic and mechanistic study of the thermal decomposition of calcium nitrate. *Thermochim Acta.* 1996;93:203–19.
19. Brower KR, Oxley JC, Tewari M. Evidence for homolytic decomposition of ammonium nitrate at high temperature. *J Phys Chem.* 1989;93:4029–33.
20. Oxley JC, Kauchik SM, Gilson NS. Thermal decomposition of ammonium nitrate-based composites. *Thermochim Acta.* 1989; 153:269–86.

Paper IV

I. Klimova, T. Kaljuvee and R. Kuusik.

"Investigation of Limestone Powder Layering onto Ammonium Nitrate Prills in Disc Granulator."

Reprinted with permission from:

Journal of Materials Science and Engineering, vol. 5A, pp. 151-159, 2014.

Investigation of Limestone Powder Layering onto Ammonium Nitrate Prills in Disc Granulator

Irina Klimova, Tiit Kaljuvee and Rein Kuusik

Laboratory of Inorganic Materials, Tallinn University of Technology, Tallinn 19086, Estonia

Received: April 13, 2014 / Accepted: May 05, 2014 / Published: May 10, 2014.

Abstract: Covering ammonium nitrate with limestone powder aims to increase the thermal stability of fertilizer, to decrease its negative impact on the soil's acidity, and to increase the durability of fertilizer granules under compression. The process of the layering of limestone particles onto ammonium nitrate prills in disc granulator is considered for the first time. The effects of granulation variables such as granulation time, rotation speed and inclination of disc, ratios of liquid to solid material and powder to prills on the granules' growth and strength are shown. It was found that the optimum residence time of the granules in the tumbling layer is just a few minutes. Liquid saturation is the main factor affecting the particles packing to the covering layer. For example, the crush strength of the covered granules produced with a mass ratio of binder to the limestone powder of 10% and 20% differed from each other in two times. The maximum strength achieved exceeded the strength of initial ammonium nitrate prills in three times.

Key words: Ammonium nitrate, limestone, disc granulator.

Nomenclatures

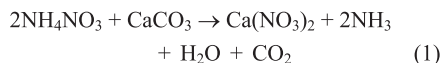
AN:	Ammonium nitrate
B/P:	Binder liquid to powder mass ratio (%)
P/S:	Powder to seed (AN prills) mass ratio (-)
P:	Powder feed mass (g)
D:	Disc's inner diameter (m)
CS:	Crush strength (N)
d_w :	Weight mean diameter (mm)
g:	Free-fall acceleration ($m \cdot s^{-2}$)
n:	Disc's rotation speed (rpm)
n_{cr} :	Critical speed (rpm)
t:	Time (min)
w_i :	Mass of fraction (g)
α :	Angle of disc inclination ($^\circ$)
η :	The effectiveness of powdered material consumption (%)
σ :	Standard deviation
σ/CS :	Coefficient of variation (-)

1. Introduction

There are several reasons to cover ammonium nitrate (AN) prills with powdered limestone: to decrease the

acidifying effect of fertilizer on soil, to increase the thermal stability of fertilizer by mixing it with an inert additive, and to strengthen the fertilizer's granules to prevent them cracking and caking.

The covering could be conducted in a disc granulator. This method allows to vary widely the content of nitrogen in fertilizer. The risks of ammonia loss and the formation of highly hygroscopic calcium nitrate via Eq. (1) are eliminated, because the mixture of AN prills and limestone powder in a granulator is not subjected to heating.



This is important because even the formation of a small amount of calcium nitrate significantly increases the hygroscopicity of the AN fertilizer and leads to its granules cracking and caking [1]. On the other hand, these phenomena are promoted by the AN solid phase transition IV \leftrightarrow III [2, 3], which occurs at close to ambient temperature (32-55 $^\circ\text{C}$), because it involves the significant reorganization in AN crystalline lattice

Corresponding author: Irina Klimova, MSc., research fields: ammoniumnitrate-based fertilizers and granulation. E-mail: irina.klimova@ttu.ee.

and density. Our previous works [4-6] show that the temperature of this phase transition in blends of AN and powdered limestone shifts a few degrees towards a higher temperature, and in case of limestone content of $\geq 20\%$, the AN solid phase transition IV \leftrightarrow II (which occurs at about 50 °C and involves a much smaller change in substance density) takes place instead of the IV \leftrightarrow III and III \leftrightarrow II solid phase transitions in the temperature range of 30-80 °C. Furthermore, the thermal behaviour of AN prills covered with limestone does not differ significantly from the thermal behaviour of blends of AN and powdered limestone.

In this work, we investigated the layering of powdered limestone onto AN prills in a disc granulator. The model of granule growth through an auto-layering mechanism where the feed particles were divided into two components, layering fines and coarse seeds, is described by Kapur and Runkana [7]. Past research on the fundamentals of seeded granulation provided a basic understanding of the kinetics of granule growth [8-11] and a formal description of the mechanisms of granule formation [11]. However, these works are concerned with high-shear and drum granulation. Disc granulation is rarely the subject of laboratory studies [12-14].

This study aimed to examine the effect of the variables of a disc granulation process: such as granulation time (t), binder to powder (B/P) and powder to seeds (AN prills) (P/S) mass ratios, and variables of equipment such as rotation speed (n) and angle of inclination of the disc (α): on granules' growth (the layering of powdered limestone onto AN prills) and strength.

2. Materials and Methods

For greater clarity, the close-cut fraction (2.00-2.24 mm) of commercial fertilizer-grade AN prills (34.4% N; TsrepovetskiAzot Ltd., Russia) was sieved and used as seeds in experiments. Limestone (mined from Karinu deposit, Estonia) grounded to a particle size $< 160 \mu\text{m}$ (the specific surface area = $1.93 \text{ m}^2 \cdot \text{g}^{-1}$) in a ball mill was used for layering onto the AN prill. The

mineral composition of limestone is as follows: 93.4% calcite, 6.3% dolomite, and 0.3% quartz. The chemical composition expressed in CaO, MgO, and CO₂ is 52.9, 2.8, and 38.98 wt%, respectively. The limestone is relatively clean, with the content of 0.08% Fe₂O₃ and 0.04% sulphur. To prevent the dissolution of AN prills during the granulation process, the saturated solution of AN (47.3 wt%, density = $1.086 \text{ g} \cdot \text{cm}^{-3}$) was used as a binder liquid.

Experiments were carried out on a disc granulator equipped with a scraper bar and a pin to remove excessive build-up on the disc walls and to provide better mixing of tumbling mass. The disc diameter was 0.5 m, and the rim height was 0.1 m.

A certain quantity of powder was added continuously at a predefined rate to the 100 g of seeds tumbling on the disc. The binder was sprayed at the predefined rate onto the tumbling mass, using a pulveriser, positioned to ensure good distribution of the binder over the tumbling material. Addition of the powder and the binder was disrupted 1 min before the end of the process. The sample was rotated for a predefined length of time, after which the produced granules were left to dry for 3 h in an oven at 60 °C.

To observe the effect of the selected variables on the layering effectiveness and on the crush strength of the produced granules, a set of experiments designed to study one factor at a time was carried out. Process parameters that were applied in individual trials are shown in Table 1.

After drying, each sample was divided into fractions on a set of sieves with the aperture sizes of 1.0, 2.0, 2.5, 3.0, 4.0, and 5.0. The weight mean diameter (d_w) of granules(2.0-5.0 mm) in each sample was calculated as follows:

Table 1 The plan of experiments.

Variable studied	t	n	α	B/P	P/S
t (min)	2-16	23	45	15; 20	1.5
n (rpm)	4	19-28	45	15	1.0
α (°)	4	23	30-45	15	1.0
B/P (%); P/S (-)	4	23	45	10-21	0.5-2.0

$$d_w = \sum_{i=1}^{k-1} \left[\frac{w_i \times d_i}{w_t} \right] \quad (2)$$

where, k is the number of sieves with aperture size between 5.0 and 2.0 mm, w_i is the mass of granules that remained on each sieve, w_t is the total mass of 2.0-5.0 mm fraction, and d_i is the mean diameter of aperture size of the collecting sieve and the one above.

Granules with sizes ranging from 3.0 to 4.0 mm from each set of experiments were tested for crush strength by applying a slowly increasing pressure (0.10 mms^{-1}) on the individual granule placed on a scale.

The change of slope and the peak of the load-displacement curve on Fig. 1a indicate the crack and the full breakdown, respectively, of neat AN prill. The typical load-displacement curve of AN prills covered with limestone powder (Fig. 1b and 2) has two peaks: the first one corresponds to the crack of granules' covering layer and the second one to the full breakdown of granules.

The average strength (CS) and the coefficient of its variation (σ/CS), that is, the ratio of standard deviation (σ) and mean value, for at least 30 granules for each set of experiments were calculated.

The total porosity of the granules was measured by the mercury intrusion porosimetry (PoreMaster PV007130; Quatachrome Instruments). The surface observations of the cross section of granules were carried out with a scanning electron microscope (SEM; Jeol JMS-8404).

3. Results and Discussion

3.1 Granules' Growth

Particles of granulate could be divided into three groups according to their nature: nonlayered powder (0-1.0 mm), fragments of the broken seeds (1.0-2.0 mm), and AN prills fully or partly covered with limestone powder (2.0-5.0 mm). The structure of covered granules is shown on Fig. 2.

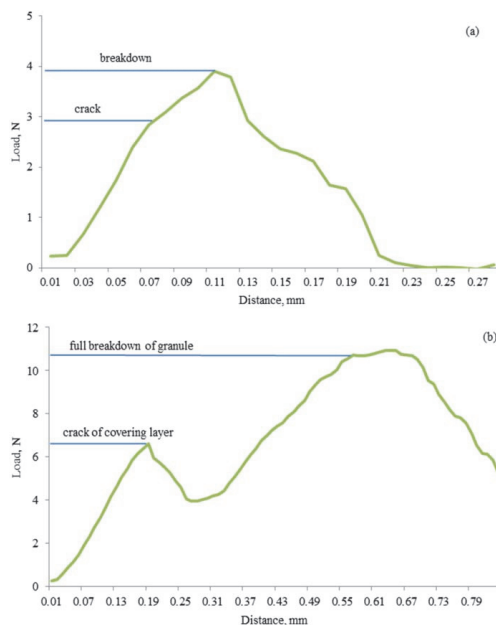


Fig. 1 Force-displacement curve for (a) AN prill and (b) AN prill covered with limestone powder.

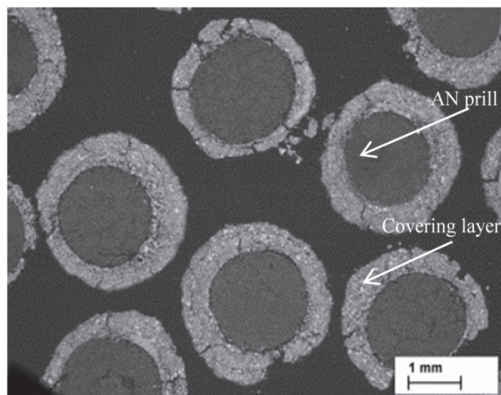


Fig. 2 SEM pictures of the cross sections of granules in the size range of 2.5-3.0 mm produced at 4 min.

Tumbling of AN prills leads to their attrition and breaking, because they are enough fragile particles (AN prill's strength, measured as the load under which granule cracks, is on the level of 3.0 N). The breaking of AN prills should be suppressed, as it leads to the serious nitrogen losses during granulation (the nitrogen content of fraction 1.0-2.0 mm is 19.4%).

3.1.1 The Effect of Granulation Time

Fig. 3 shows the size distribution of particles of granulate as a function of granulation time. By increasing time from 2 to 16 minutes, the mass fraction of broken seeds (1.0-2.0 mm) does not change and stays at the level of 4%-5%. This indicates that breaking of seeds takes place only in the initiation stage of the granulation process, when the mass ratio of powdered material to AN prills is low. The granules containing inclusions of broken seeds in the covering layer were not found on the SEM pictures of cross sections of granules produced at different granulation durations. The yield of covered granules, produced at 4 minutes, was upwards 80% and does not change with the increase in granulation duration, as well as mean granule size, which almost does not increase after the fourth minute of granulation (Fig. 4). It seems that 4 min is the optimum granulation time regarding granule growth through powder layering. These results are consistent with the results obtained by other researchers [10, 11] in the sense that optimum granulation time is quite short, just a few minutes.

3.1.2 The Effect of the Rotation Speed and the Inclination angle of the Disc

Fig. 5 shows the cumulative size distribution of granulate particles obtained at different disc rotation speeds. By increasing the disc rotation speed from 19 to 28 rpm, the mass fraction of covered granules larger than 2.0 mm increases from 57% to 82%; at the same time, the mass fraction of granules larger than 3.0 mm decreases from 27% to 18% with increase in disc rotation speed from 23 to 28 rpm, indicating the breakage of the thicker covering layer. The mass fractions of nonlayered powder (0-1.0 mm) and broken seeds (1.0-2.0 mm) decrease from 28% and 15% to 13% and 4%, respectively, with increase in disc rotation speed from 19 to 28 rpm. The sample produced at the disc rotation speed of 23 rpm has the largest mean size of covered granules, i.e. the largest mean thickness of covering.

The effect of inclination angle of disc on the

effectiveness of powder layering is shown in Fig. 6. An increase in the disc angle of inclination from 30° to 45° results in the 12% increase in the yield of covered granules.

A key operating parameter for a disc granulator is critical speed (the speed at which a granule is just held stationary on the rim of the disc by centripetal force alone) [15], which can be calculated by Eq. (3).

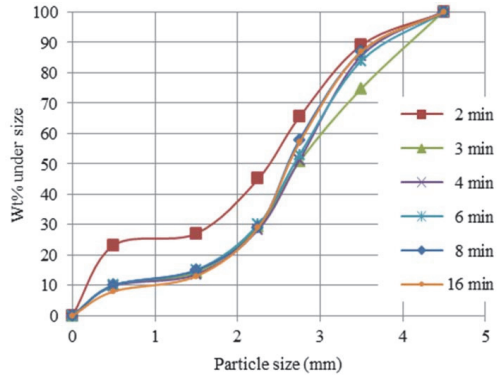


Fig. 3 Effect of granulation time on the size distribution of granulate particles.

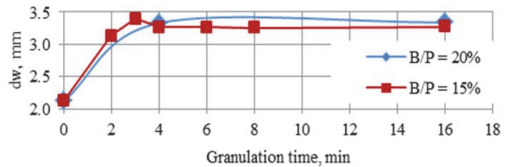


Fig. 4 Effect of granulation time on the weight mean diameter of covered granules in the size range of 2-5 mm.

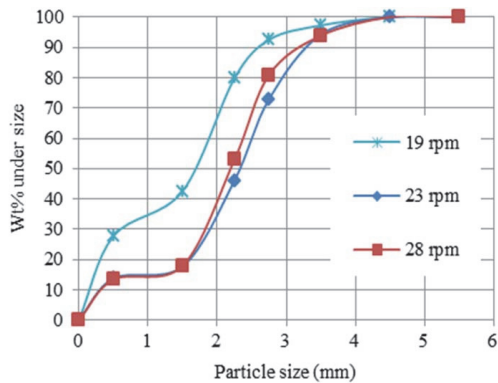


Fig. 5 Effect of disc rotation speed on the size distribution of granulate particles .

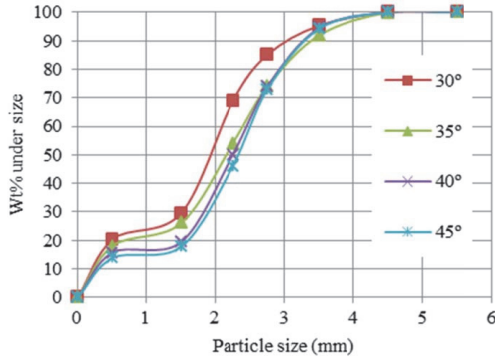


Fig. 6 Effect of disc angle of inclination on the size distribution of granulate particles.

$$n_{cr} = \sqrt{\frac{g \sin \alpha}{2\pi^2 D}}, \quad (3)$$

where, g is free-fall acceleration, α is the inclination angle of the disc to the horizontal plane, and D is inner diameter of the disc.

Generalizing the results obtained, it seems that the effectiveness of powder layering increases with the increase of disc rotation speed at a particular angle of inclination until the optimal n/n_{cr} ratio is obtained. Further increase of this ratio does not result in yield increase (Table 2). At that, the rotation speed of 23 rpm and 45° of discs inclination ($n/n_{cr}=0.46$) are the optimal parameters for granulation regarding the yield of covered granules.

3.1.3 The Effect of the P/S and B/P Ratios

Figs. 7 and 8 demonstrate the size distribution of granulate particles produced at different B/P and P/S ratios. The quantity of mass fraction of broken seeds (1.0-2.0 mm) decreases from 6% to 2% with the increase of B/P from 11% to 20%, and P/S, from 0.5 to 2.0. Increasing the intensity of feeding of powder particles and binder liquid, it is possible to suppress the breakage of AN prills tumbling on the disc. The mass fraction of 0-1.0 mm (nonlayered feed) decreases with the increase of B/P and P/S ratios. The effectiveness of powdered material consumption (Eq. (4)) as a function of P/S and B/P is shown in Fig. 12.

$$\eta = \left(1 - \frac{w_1}{P}\right) \times 100 \quad (4)$$

where, w_1 is the mass of particles smaller than 1.0 mm and P is the mass of powder feed.

The effectiveness of powder layering increases with an increase in the quantity of the powder and the binder liquid. For example, at the B/P of 15%, a quick increase occurred in the layered powder quantity from 67 to 91wt% between the P/S of 0.5 and of the 2.0 (Fig. 9). The most obvious effect of B/P on the layering of powder can be seen on granules with the size range of 2.0-2.5 mm. The characteristic feature of such granules prepared with a low amount of binder is their regular

Table 2 Effect of disc rotation speed and angle of inclination on the strength of granules' covering layer.

n (rpm)	α (°)	n_{cr} (rpm)	n/n_{cr}	CS (N)	σ	σ/CS	Yield (%)
19	45	50.30	0.38	5.62	1.10	0.20	57
23	45	50.30	0.46	6.78	1.32	0.19	82
23	40	47.28	0.48	6.59	1.28	0.19	81
23	35	45.28	0.51	6.20	1.20	0.19	74
23	30	42.28	0.54	6.04	1.15	0.19	70
28	45	50.30	0.56	6.82	1.35	0.20	82
28	30	42.28	0.66	6.81	1.31	0.19	82

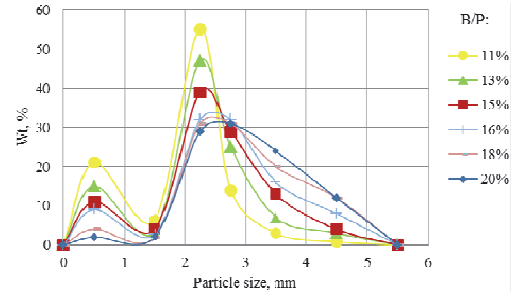


Fig. 7 The differential size distribution of granulates obtained at different B/P ratios (P/S = 0.5).

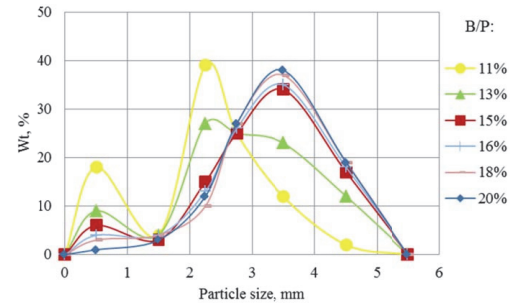


Fig. 8 The differential size distribution of granulates obtained at different B/P ratios (P/S = 2.0).

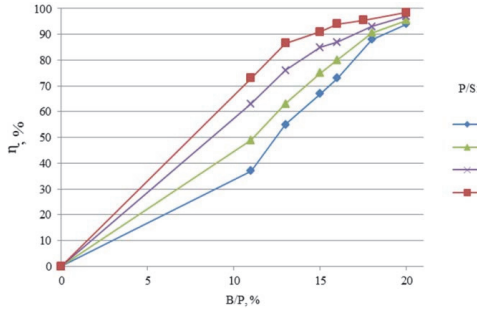


Fig. 9 The effectiveness of powder consumption.

covering layer (Fig. 10a). The layering of powder particles improves with the increase in the amount of feed powder and binder liquid. As shown on Fig. 10b, the covering of granules in the size range of 2.0-2.5 mm produced with a B/P of 18% and a P/S of 2.0 is fully formed. Independently of used P/S and B/P ratios, produced granules in the size range of 2.5-5.0 mm have a well-formed covering layer (Fig. 2).

The size distribution of covered granules (fraction 2.0-5.0 mm) almost does not change with an increase of B/P ratio from 15% to 20% (Figs. 8 and 9). The growth and breakage of the covering layer reached equilibrium. Further increase of this parameter leads to the over wetting of tumbling mass.

3.2 Granules' Strength

Fig. 11 shows the dispersion of load needed for full breakdown of covered granules produced at different granulation process variables (Table 1). Granule full strength exceeds the strength of pure AN prills three times and is independent of studied variables. In contrast, the strength of granules' covering layer (Fig. 1, first peak) depends on the process variables.

3.2.1 The Effect of Granulation Time

The effect of granulation time on the mean strength of the covering layer of produced granules is shown in Fig. 12. The most durable layer was obtained in 3 to 4 min of granulation. Further increase in granulation time reduces the strength of the covering layer. This fact confirms that the process of powder particle layering and the process of destruction of the covering

layer reach equilibrium on the fourth minute. An increase in the quantity of defects in the granule's covering layer leads to a decrease in its strength. In case of the binder liquid amount being enough for granule maximum saturation ($B/P = 20\%$), the decrease in strength is less obvious, but the coefficient of variation

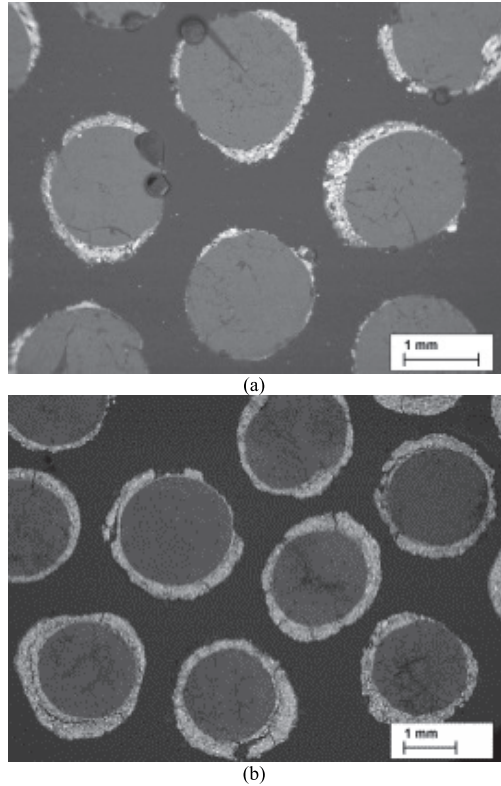


Fig. 10 SEM pictures of the cross sections of granules in the size range of 2.0-2.5 mm produced (a) with $B/P = 11\%$ and $P/S = 0.5$ and (b) with $B/P = 18\%$ and $P/S = 2.0$.

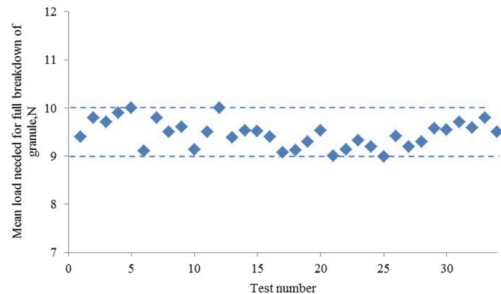


Fig. 11 Load needed for full breakdown of covered granule.

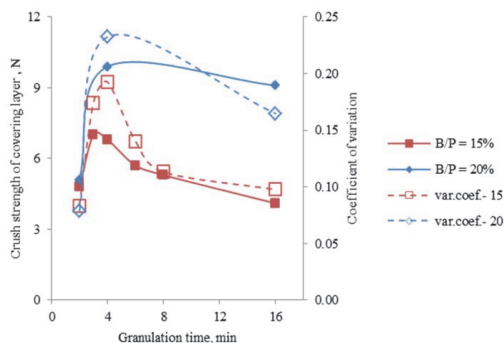


Fig. 12 Effect of granulation time on the strength of granules' covering layer.

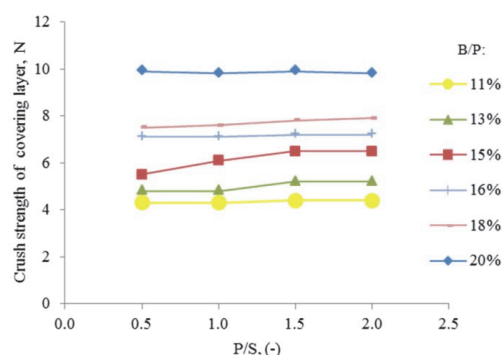


Fig. 13 Effect of B/P and P/S on the strength of granules' covering layer.

of strength decreases from 0.23 until 0.16, with an increase in granulation time from 4 to 16 min. This indicates that by increasing the residence time of granules in the tumbling layer, the narrower strength distribution of granules' covering layer could be obtained.

3.2.2 The Effect of the Rotation Speed and the Inclination Angle of the Disc

Increasing the rotation speed from 19 to 23 rpm (Table 2, $\alpha = 45^\circ$) results in an increase of the strength of granules' covering layer, but further increase of rotation speed does not make any effect. Increasing the angle of disc inclination from 30° to 45° (Table 2, $n = 23$ rpm) also results in the slight increase in the strength of the covering layer, but an increase of inclination angle in the desired range at a higher rotation speed does not result in the change in strength (Table 2, $n =$

28 rpm).

The crush strength of the covering layer increases with the increase of disc rotation speed to critical speed ratio (n/n_{cr}) from 0.38 to 0.46 rpm (Table 2). As shown in Shæfer and Mathiesen [16], the probability of successful coalescence and densification rate of particles increases with the increase in collision velocity of particles. Greater consolidation leads to lower porosity and hence higher strength [10]. The obtained correlation between the mean crushing strength of the covering layer and the porosity of covered granules is in agreement with this, i.e., granules' lower porosity matches with granules' higher strength. The results of granule strength at higher ratios of rotation speed to critical speed (0.46-0.66) suggest that the maximum strength of the covering layer for used B/P ratio has been achieved.

3.2.3 The Effect of the P/S and B/P Ratios

As shown in Walker et al. [17], the major parameter that has an influence on granulation mechanism and on granules' properties is liquid saturation. The granulation with high liquid-to-solid phase ratios and, therefore, high fractional saturation produces granules with more binder liquid in bonds between particles. These lead to the formation of large and strong crystal bridges and therefore serve to decrease porosity and increase the strength of granules. The results show that the strength of the covering layer of granules is independent of the P/S ratio, but it increases from 4.3 to 9.9 N at the increase of the B/P ratio from 11% to 20% (Fig. 13). As it was mentioned above, further increase of this parameter leads to the over wetting of tumbling mass. The maximum strength of granules is achieved with this. The load-displacement curve of such granules has only one peak, corresponding to the full granule breakdown in one step.

4. Conclusions

Prospects for the strengthening of AN prills by forming a covering layer on their surface have been proven. The optimal parameters for covering AN prills

with limestone powder in a disc granulator were elaborated.

The full strength of covered granules exceeds the strength of pure AN prills three times and is almost 10N per granule, as well as it is independent of studied variables. The strength of granules' covering layer could be improved on the process variables. The major parameter that has an influence on granulation mechanism and on granules' properties is liquid saturation. The maximum strength of the covering layer of granules achieved in experiments was 9.9 N; such granules were produced at the *B/P* ratio of 20%.

The effectiveness of powder layering increases with the increase in the mass ratios of binder to powder and powder to seeds (AN prills). Seed breaking could be suppressed with the increase of *B/P* and *P/S* ratios. In addition, in the interval of the binder-to-powder feed ratio of 11%-20%, more liquid was used in the granulation, and a stronger covering layer on the seed granule (AN prill) was produced. Tumbling mass reaches saturation in case of a *B/P* ratio higher than 20%, and further binder addition leads to the over-wetting of tumbling mass. At the binder-to-powder feed ratio of 15%-20%, satisfactory compact and homogeneously covered granules in the range of 2.0-5.0 mm were obtained, the yield of which was 85%-97%. Higher quantity of powder and binder liquid in the granulation process improves powder particle packing.

The optimum residence time of granules in the tumbling layer is short enough, just 4 min. The maximum yield of covered granules and the maximum strength of granules' covering layer was obtained at this granulation time.

Increasing the disc rotation speed to critical speed ratio (n/n_{cr}) has an effect on the effectiveness of powder layering and on the crush strength of covering layer, until the optimum ratio is achieved. Disc rotation speed of 23 rpm and 45° of disc inclination are the optimal parameters for disc granulator used regarding strength and the yield of produced granules.

Acknowledgments

This work was partially supported by the graduate school "Functional Materials and Technologies" and received funding from the European Social Fund in Estonia (project No. 1.2.0401.09-0079) and from the Estonian Ministry of Education and Research (grant No. SF0140082s08).

References

- [1] R. Latham, P.R. Geissler, Hygroscopicity of complex fertilizers: Effect of calcium nitrate and water concentrations on the critical relative humidity of ammonium nitrate-limestone, *Journal of Agricultural and Food Chemistry* 16 (3) (1968) 384-387.
- [2] A. Lafci, K. Guruz, H. Yucel, Investigation of factors affecting caking tendency of calcium ammonium nitrate fertilizer and coating experiments, *Fertilizer Research* 18 (1988) 63-70.
- [3] H.B. Wu, M.N. Chan, C.K. Chan, FTIR characterization of polymorphic transformation of ammonium nitrate, *Aerosol Science and Technology* 41 (2007) 581-588.
- [4] T. Kaljuvee, E. Edro, R. Kuusik, Influence of lime-containing additives on the thermal behaviour of ammonium nitrate, *Journal of Thermal Analysis and Calorimetry* 92 (2008/1) 215-221.
- [5] T. Kaljuvee, I. Rudjak, E. Edro, A. Trikkel, Heating rate effect on the thermal behavior of ammonium nitrate and its blends with limestone and dolomite, *Journal of Thermal Analysis and Calorimetry* 97 (1) (2009) 215-221.
- [6] I. Rudjak, T. Kaljuvee, A. Trikkel, V. Mikli, Thermal behaviour of ammonium nitrate prills coated with limestone and dolomite powder, *Journal of Thermal Analysis and Calorimetry* 99 (3) (2010) 749-754.
- [7] P.C. Kapur, V. Runkana, Balling and granulation kinetics revisited, *International Journal of Mineral Processing* 72 (2003) 417-427.
- [8] N. Rahmanian, M. Ghadiri, X. Jia, Seeded granulation, *Powder Technology* 206 (2011) 53-62.
- [9] N. Rahmanian, M. Ghadiri, X. Jia, F. Stepanek, Characterization of granule structure and strength made in a high shear granulator, *Powder Technology* 192 (2) (2009) 184-194.
- [10] N. Rahmanian, A. Naji, M. Ghadiri, Effects of process parameters on granules properties produced in a high shear granulator, *Chemical Engineering Research and Design* 89 (2011) 512-518.
- [11] V.S. Sastry, P. Dontula, C. Hosten, Investigation of the layering mechanism of agglomerate growth during drum

- pelletization, *Powder Technology* 130 (2003) 231-237.
- [12] F. Delwel, F.A. Veer, Continuous granulation of sodium triphosphate in a pan granulator, *Industrial and Engineering Chemistry Process Design and Development*, 17 (1978) 261-265.
- [13] A. Heim, R. Kaźmierczak, A. Obraniak, The effect of equipment and process parameters on torque during disc granulation of bentonite, *Physicochemical Problems of Mineral Processing* 38 (2004) 157-166.
- [14] T. Gluba, Investigation of continuous disc granulation process, *CHEMIK* 66 (5) (2012) 360-369.
- [15] J. Litster, B. Ennis, L. Liu, *The Science and Engineering of Granulation Processes* edited by Chapter 8, p. 180.
- [16] T. Schæfer, C. Mathiesen, Melt pelletization in a high shear mixer. VIII. Effects of binder viscosity, *International Journal of Pharmaceutics* 139 (1996) 125-243.
- [17] G.M. Walker, H.E.M.N. Moursy, C.R. Holland, M.N. Ahmad, Effect of process parameters on the crush strength of granularfertiliser, *Powder Technology* 132 (2003) 81-84.

APPENDIX B: CURRICULUM VITAE

ELULOOKIRJELDUS

1. Isikuandmed

Ees- ja perekonnanimi Irina Klimova
Sünniaeg ja -koht 04.03.1984 Tallinn
Kodakondsus Eesti

2. Kontaktandmed

Aadress Madala 11-28, 10315, Tallinn
Telefon +372 58144576
E-posti aadress irina.klimova@mail.ee

3. Hariduskäik

Õppeasutus (nimetus lõpetamise ajal)	Lõpetamise aeg	Haridus (eriala/ kraad)
Tallinna Tehnikaülikool	2008 –...	Keemia- ja materjalitehnoloogia, doktoriõpe
Tallinna Tehnikaülikool	2008	Keemia- ja keskkonnakaitsetehnoloogia/ Tehnikateaduste magistrikraad
Tallinna Tehnikaülikool	2006	Keemia- ja keskkonnakaitsetehnoloogia/ bakalaureusekraad
Maardu Gümnaasium	2002	Keskharidus

4. Keelteoskus (alg-, kesk- või kõrgtase)

Keel	Tase
Vene keel	Emakeel
Eesti keel	Kõrgtase
Inglise keel	Kõrgtase
Soome keel	Algtase

5. Täiendusõpe

Õppimise aeg	Täiendusõppe läbiviija nimetus
2013 (2 päeva)	Granulation course (Sheffield, Inglismaa) – 6th International Granulation Workshop
2012-2013	Doktorikool „Funktsionaalsed materjalid ja tehnoloogiad“ (Tartu Ülikool ja Tallinna Tehnikaülikool)
2009 (6 päeva)	IRCELYON (Lyon, Prantsusmaa) – Summer School of Calorimetry. Calorimetry and thermal methods in catalysis
2009 (3 päeva)	Tallinna Tehnikaülikool (Eesti) – MathCAD
2009 (10 päeva)	Audentes (Eesti) – inglise keelelaager
2008-2010	Doktorikool „Funktsionaalsed materjalid ja tehnoloogiad“ (Tartu Ülikool ja Tallinna Tehnikaülikool)
2008 (12 tundi)	Tallinna Tehnikaülikool (Eesti) – Pedagoogika ja õppemetoodika: Õppe-/ ainekava kavandamine ja hindamine
2008 (24 tundi)	Tallinna Tehnikaülikool (Eesti) – Pedagoogika ja õppemetoodika: sotsiaalsed ja kommunikatiivsed oskused
2005 (3 päeva)	OÜ Keskkonnauuringute Keskus (Eesti) – veeproovivõtja 20-tunnise koolituskursus

6. Teenistuskäik

Töötamise aeg	Tööandja nimetus	Ametikoht
2014 - ...	Interchemie werken De Adelaar Eesti AS	keemialabori juhataja
2007 - 2014	TTÜ Anorgaaniliste materjalide teaduslaboratoorium (Eesti)	insener
2008, suvi	Lappeenranta University of Technology (Soome), department of chemical engineering	insener
2006, suvi	Saybolt Eesti AS (Eesti)	keemik
2006, suvi	Norfolier Baltic AS (Eesti)	laborant
2005, suvi	AS Silikaat (Eesti)	laborant
2005, suvi	OÜ Eesti Geoloogiakeskus (Eesti)	keemik
2004, suvi	AS Veda-pak (klaastehas, Venemaa)	keemik

7. Kaitstud lõputööd

Magistritöö: *Ca²⁺-ioonide leostuvus põlevkivituhkadest.* Tallinna Tehnikaülikool, 2008. Juhendaja: Rein Kuusik

8. Teadustöö põhisuunad

Ammooniumnitraatvætise modifitseerimine

9. Teised uurimisprojektid

SF0140082s08 Karbonaat- ja fosfaatpõhiste anorgaaniliste süsteemide keemia ja rakendused (2008 – 2013)

SF0142518s03 Anorgaaniliste mitmekomponentsete süsteemide keemia ja rakendused (2003 – 2007)

Lep7017 Põlevkivituhk kaltsiumkarbonaadi toormena (2007 – 2008)

ETF7379 Süsinikdioksiidi mineraliseerimisprotsesside modelleerimine (2008 – 2011)

APPENDIX B: CURRICULUM VITAE

CURRICULUM VITAE

1. Personal data

Name Irina Klimova
Date and place of birth 04.03.1984, Tallinn

2. Contact information

Address Madala 11-28, 10315, Tallinn, Estonia
Phone +372 58144576
E-mail irina.klimova@mail.ee

3. Education

Educational institution	Graduation year	Education (Field of study/ degree)
Tallinn University of Technology	2008 –...	Chemical and Materials Technology, PhD studies
Tallinn University of Technology	2008	Chemical and Environmental technologies/ M. Sc. in Chemical Engineering
Tallinn University of Technology	2006	Chemical and Environmental technologies/ B. Sc. in Chemical Engineering
Maardu Gymnasium	2002	Secondary school education

4. Language competence/ skills

Language	Level
Russian	Native language
Estonian	Good
English	Good
Finnish	Basic skills

5. Special Courses

Period	Educational or other organization
2013 (2 days)	Granulation course (Sheffield, UK) – 6th International Granulation Workshop
2012-2013	Graduate school “Functional Materials and Processes” (University of Tartu and Tallinn University of Technology)
2009 (6 days)	IRCELYON (Lyon, France) – Summer School of Calorimetry. Calorimetry and thermal methods in catalysis
2009 (3 days)	Tallinn University of Technology (Estonia) - MathCAD
2009 (10 days)	Audentes (Estonia) – English language summer school
2008-2010	Graduate school “Functional Materials and Processes” (University of Tartu and Tallinn University of Technology)
2008 (36 hours)	Tallinn University of Technology (Estonia) - Teaching and learning methods.
2005 (3 days)	Estonian Environmental Research Centre (Estonia) – Course of water sample collection

6. Professional Employment

Period	Organization	Position
2014 -	Interchemie werken De Adelaar Eesti AS	Manager of Chemical Laboratory
2007 - 2014	Tallinn University of Technology, Laboratory of Inorganic Materials (Estonia)	Engineer
2008, summer	Lappeenranta University of Technology, Laboratory of Separation Technology (Finland)	Engineer
2006, summer	Saybolt Core Laboratories (Estonia)	Chemist
2006, summer	Norfolier Baltic AS (Estonia)	Laboratory assistant
2005, summer	AS Silikaat (Estonia)	Laboratory assistant
2005, summer	OÜ Geological Survey of Estonia (Estonia)	Chemist
2004, summer	AS Veda-pak (glass factory, Russia)	Chemist

7. Defended theses

M. Sc. Thesis: Ca-ions leaching from oil shale ashes. Tallinn University of Technology, 2008. Supervisor: Rein Kuusik

8. Main areas of scientific work/ Current research topics

Modification of ammonium nitrate fertilizer

9. Other research projects

SF0140082s08 Chemistry and applications of carbonate-phosphate-based inorganic systems (2008 – 2013)

SF0142518s03 Chemistry and applications of inorganic multicomponent systems (2003 – 2007)

ETF7379 Modeling of carbon dioxide mineralization processes (2008 – 2011)

Lep7017 PCC from oil shale ash (2007 – 2008)

**DISSERTATIONS DEFENDED AT
TALLINN UNIVERSITY OF TECHNOLOGY ON
CHEMISTRY AND CHEMICAL ENGINEERING**

1. **Endel Piiraja**. Oxidation and Destruction of Polyethylene. 1993.
2. **Meili Rei**. Lihatehnoloogia teaduslikud alused. Fundamentals of Food Technology. 1995.
3. **Meeme Põldme**. Phase Transformations in Hydrothermal Sintering Processing of Phosphate Rock. 1995.
4. **Kaia Tõnsuaadu**. Thermophosphates from Kovdor and Siilinjärvi Apatites. 1995.
5. **Anu Hamburg**. The Influence of Food Processing and Storage on the N-Nitrosamines Formation and Content in Some Estonian Foodstuffs. 1995.
6. **Ruth Kuldvee**. Computerized Sampling in Ion Chromatography and in Capillary Electrophoresis. 1999.
7. **Külliki Varvas**. Enzymatic Oxidation of Arachidonic Acid in the Coral *Gersemia fruticosa*. 1999.
8. **Marina Kudrjašova**. Application of Factor Analysis to Thermochromatography and Promotion Studies. 2000.
9. **Viia Lepane**. Characterization of Aquatic Humic Substances by Size Exclusion Chromatography and Capillary Electrophoresis. 2001.
10. **Andres Trikkel**. Estonian Calcareous Rocks and Oil Shale Ash as Sorbents for SO₂. 2001.
11. **Marina Kritševskaja**. Photocatalytic Oxidation of Organic Pollutants in Aqueous and Gaseous Phases. 2003.
12. **Inna Kamenev**. Aerobic Bio-Oxidation with Ozonation in Recalcitrant Wastewater Treatment. 2003.
13. **Janek Reinik**. Methods for Purification of Xylidine-Polluted Water. 2003.
14. **Andres Krumme**. Crystallisation Behaviour of High Density Polyethylene Blends with Bimodal Molar Mass Distribution. 2003.
15. **Anna Goi**. Advanced Oxidation Processes for Water Purification and Soil Remediation. 2005.
16. **Pille Meier**. Influence of Aqueous Solutions of Organic Substances on Structure and Properties of Pinewood (*Pinus sylvestris*). 2007.
17. **Kristjan Kruusement**. Water Conversion of Oil Shales and Biomass. 2007.
18. **Niina Kulik**. The Application of Fenton-Based Processes for Wastewater and Soil Treatment. 2008.
19. **Raul Järviste**. The Study of the Changes of Diesel Fuel Properties a its Long Term Storage. 2008.

20. **Mai Uibu.** Abatement of CO₂ Emissions in Estonian Oil Shale-Based Power Production. 2008.
21. **Valeri Gorkunov.** Calcium-Aluminothermal Production of Niobium and Utilization of Wastes. 2008.
22. **Elina Portjanskaja.** Photocatalytic Oxidation of Natural Polymers in Aqueous Solutions. 2009.
23. **Karin Reinhold.** Workplace Assessment: Determination of Hazards Profile using a Flexible Risk Assessment Method. 2009.
24. **Natalja Savest.** Solvent Swelling of Estonian Oil Shales: Low Temperature Thermochemical Conversion Caused Changes in Swelling. 2010.
25. **Triin Märtson.** Methodology and Equipment for Optical Studies of Fast Crystallizing Polymers. 2010.
26. **Deniss Klauson.** Aqueous Photocatalytic Oxidation of Non-Biodegradable Pollutants. 2010.
27. **Oliver Järvik.** Intensification of Activated Sludge Process – the Impact of Ozone and Activated Carbon. 2011.
28. **Triinu Poltimäe.** Thermal Analysis of Crystallization Behaviour of Polyethylene Copolymers and Their Blends. 2011.
29. **Mariliis Sihtmäe.** (Eco)toxicological Information on REACH-Relevant Chemicals: Contribution of Alternative Methods to *in vivo* Approaches. 2011.
30. **Olga Velts.** Oil Shale Ash as a Source of Calcium for Calcium Carbonate: Process Feasibility, Mechanism and Modeling. 2011.
31. **Svetlana Jõks.** Gas-Phase Photocatalytic Oxidation of Organic Air Pollutants. 2012.
32. **Aleksandr Dulov.** Advanced Oxidation Processes for the Treatment of Water and Wastewater Contaminated with Refractory Organic Compounds. 2012.
33. **Aleksei Zaidentsal.** Investigation of Estonian Oil Shale Thermo-bituminization in Open and Closed System. 2012.
34. **Dmitri Šumigin.** Composites of Low-Density Polyethylene and Poly(Lactic Acid) With Cellulose and Its Derivatives. 2014.
35. **Aleksandr Käkinen.** The Role of Physico-chemical Properties and Test Environment on Biological Effects of Copper and Silver Nanoparticles. 2014.
36. **Ada Traumann.** Improvement of Work Environment through Modelling the Prevention of Health Risks Focusing on Indoor Pollutants. 2014.
37. **Marika Viisimaa.** Peroxygen Compounds and New Integrated Processes for Chlorinated Hydrocarbons Degradation in Contaminated Soil. 2014.
38. **Olga Budarnaja.** Visible-light-sensitive Photocatalysts for Oxidation of Organic Pollutants and Hydrogen Generation. 2014.
39. **Jelena Hruljova.** Role of Specifically Interacting Solvents in Solvent Swelling of Kukersite Oil Shale Kerogen. 2014.